Functional analyses of the conserved Cysteine-rich with EGF-like domains (Creld) protein family in *Mus musculus*

Dissertation

zur

Erlangung des Doktorgrades (Dr. rer. nat.)

der

Mathematisch-Naturwissenschaftlichen Fakultät

der

Rheinischen Friedrich-Wilhelms-Universität Bonn

vorgelegt von

Elvira Mass

aus

Semipalatinsk

Bonn

August, 2013

Angefertigt mit Genehmigung der Mathematisch-Naturwissenschaftlichen Fakultät der Rheinischen Friedrich-Wilhelms-Universität Bonn

1. Gutachter: Prof. Dr. rer. nat. M. Hoch
2. Gutachter: Prof. Dr. med. J. L. Schultze

Tag der Promotion: 20.12.2013
Erscheinungsjahr: 2014

Danksagung

Zuallererst möchte ich mich bei meinem Doktorvater Prof. Michael Hoch bedanken, unter dessen Leitung und Betreuung ich meine Arbeit am LIMES Institut machen durfte.

Ein ganz besonderer Dank gilt Dagmar Wachten, die immer mit Rat und Tat an meiner Seite war und mir meinen Enthusiasmus für die Wissenschaft wiedergegeben hat.

Mein Dank geht an Nina Moderau und Rüdiger Bader für die seelische und wissenschaftliche Unterstützung.

Ich danke Anna Aschenbrenner für die wissenschaftlichen und nicht so wissenschaftlichen Diskussionen, ganz besonders an den Wochenenden.

I would like to thank Disha Varma for supporting me in so many different ways as a friend and colleague.

Ich danke Melanie Thielisch, die mir den Laboralltag mit ihrem Humor versüßt (D'Embryo) und mir wissenschaftlich immer zur Seite steht.

Ich bedanke mich bei Birgit Stümpges, die mir einen guten Start in die Wissenschaft ermöglicht hat.

Heidrun Schneider-Klinkosch danke ich für die unglaublich guten Zeiten in ihrem Büro.

Ich danke André Völzmann, der mir in Zeiten der Not mit seinen grafischen Zeichnungen ausgeholfen hat.

Ich danke Tom Wegner, der alle meine Computer und Festplatten gerettet hat.

Vielen Dank geht an Joachim Degen, der mit von Anfang an unterstützend zur Seite gestanden hat.

Ich möchte mich auch bei all meinen Kollegen für eine tolle Zeit, es wurde wirklich nie langweilig…

Ganz besonderer Dank gilt Svetlin Mladenov, der mir als Nicht-Wissenschaftler so viel Verständnis entgegengebracht hat und im letzten Jahr der Fels in der Brandung war.

Meiner Familie, besonders meinen Eltern danke ich vom ganzen Herzen. Ohne ihre Unterstützung hätte ich mein Ziel nicht erreichen können.

Abbreviations

A	Adenine
Amp	Ampicillin
Aqua bidest	double distilled water
bp	base pair
C	Cytosine
cDNA	complement DNA
CreId	Cysteine-rich with EGF-like domains
DMSO	Dimethylsulfoxide
DNA	Desoxyribonucleic acid
E.coli	*Escherichia coli*
EDTA	Ethylene diamine tetraacetic acid
e.g.	exempli gratia (latin); for example
EGTA	Ethylene glycol tetraacetic acid
et al.	et aliter
Fig	Figure
g	gram
G	Guanine
h	hours
HA	*hemagglutinin*
HEPES	2-[4-(2-hydroxyethyl)piperazin-1-yl]ethanesulfonic acid
HRP	Horderadish peroxidase
kb	kilo base
IF	Immunofluorescence
IgG	Immunoglobulin G
l	liter
LB	Luria-Bertani medium
µ	micro
m	milli
M	Molarity
min	minute
mRNA	messenger RNA
o/n	over night
PBS	*Phosphate buffered saline*
PCR	Polymerase-chain-reaction
pH	decimal logarithm of the reciprocal of the hydrogen ion activity, in a solution
qRT-PCR	Quantitative real time polymerase-chain-reaction
RIPA	radio immunoprecipitation assay
RNA	ribonucleic acid
rpm	rounds per minute
RT	room temperature

T	Thymine
Tab	table
TAE	Tris-acetate-EDTA
TEMED	N,N,N’,N’-Tetramethylethane-1,2-diamine
U	Unit
UV	ultraviolet
WB	Western blot

Table of contents

1 Introduction

1.1 The Creld protein-family

Cysteine-Rich with EGF-Like Domains (*Creld)* genes are evolutionarily conserved and encode proteins that are highly similar in their domain structure (Fig. 1-1). In mammals, two members of the Creld family were identified: *Creld1* and *Creld2*. The genome of *Drosophila melanogaster* encodes only one Creld1-like protein (*dCRELD*)[1]. The orthologs of Creld1 contain an N-terminal signal peptide, a unique WE domain, one or two arrays of epidermal growth factor (EGF)-like and Ca^{2+} binding EGF-like (cbEGF-like) domains, and one or two C-terminal type III transmembrane domains. The WE domain is rich in tryptophan (W) and glutamic acid (E) residues and contains the nonapeptide (GG(N/D)TAWEE(E/K)), which is highly conserved in all members of the Creld protein family[1]. The function of the WE domain has not been identified so far, but it has been proposed to play a role in protein interaction[1].

Proteins possessing EGF-like domains are functionally diverse and include cell adhesion proteins, extracellular matrix components, transmembrane proteins, growth factors, and signaling proteins[2]. The function of these domains can vary within one protein family, like in the selectin protein-family[3]. They contain one EGF-like domain facing the extracellular matrix, which is important for cell adhesion, ligand recognition[4,5], and dendritic cell maturation[6]. Similarly, proteins containing cbEGF-like domains are also functionally diverse. They are involved in blood coagulation, the complement system, fibrinolysis, are part of the extracellular matrix (e.g. fibrillin), and function as cell surface receptors (e.g. Notch receptor and low density lipoprotein receptor). Binding of Ca^{2+} to the cbEGF-like domain stabilizes the protein and induces a conformational change needed for protein activity[7].

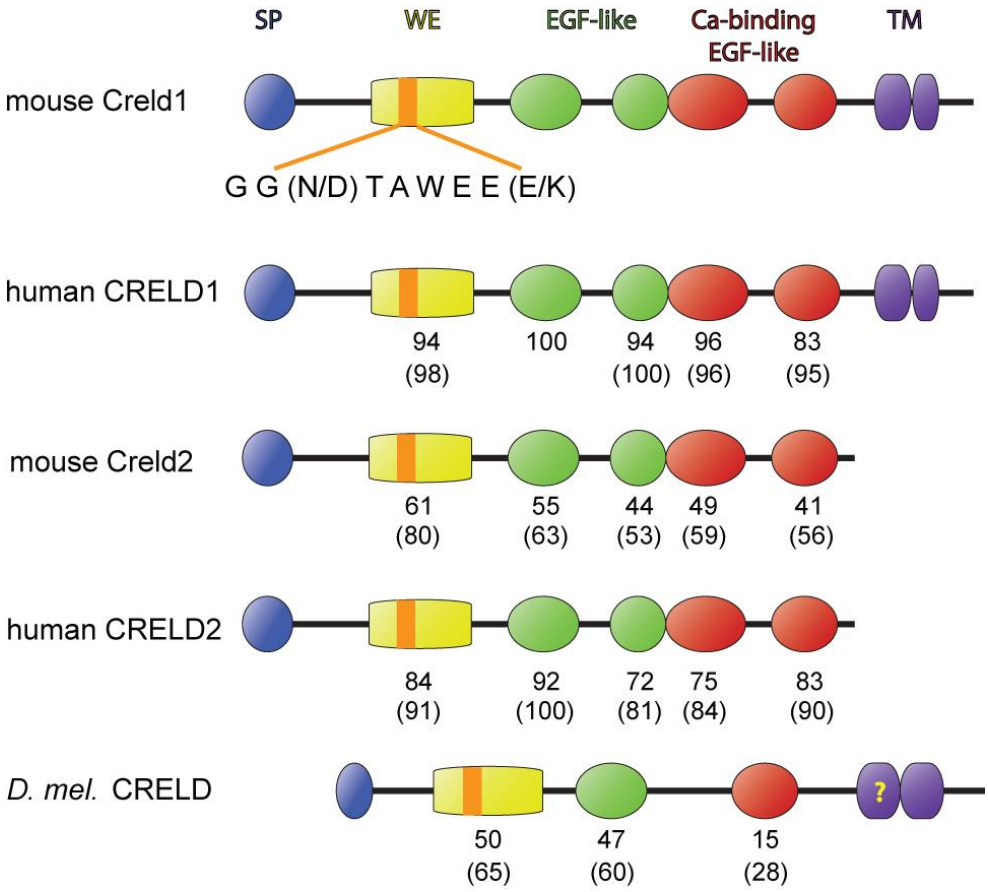

Fig. 1-1 Predicted primary protein structure of the murine, human, and *Drosophila melanogaster* (*D. mel*) Creld proteins. Each protein has a signal peptide (SP) at the N terminus (blue), a WE domain (yellow) possessing a highly conserved nonapeptide (orange), one or two epidermal growth factor (EGF)-like (green), and one or two calcium-binding EGF-like domains (cbEGF red). There are two transmembrane domains in mammalian Creld1 proteins, and one or two in *D. mel*, depending on the prediction tool that was used. Creld2 proteins do not possess transmembrane domains. Numbers indicate identity of each domain; numbers in brackets indicate similarity to the domains of murine Creld1. Human CRELD2 was compared to mouse Creld2.

Based on bioinformatic analysis of the protein sequence, it has been suggested that Creld1 proteins act as membrane-tethered cell adhesion molecules[1]. Nevertheless, experimental verification of Creld1 being localized at the plasma membrane is lacking.

Creld2, however, does not possess any transmembrane regions, but is otherwise very similar to Creld1 in its domain structure (Fig. 1-1). It has been shown that Creld2 localizes to the endoplasmic reticulum (ER) and the Golgi apparatus[8,9] from where it is secreted[10].

1.2 Creld1 – a risk gene factor for AVSD

First insights into the physiological function of human CRELD1 were revealed when *CRELD1* was identified as a risk gene factor for atrioventricular septal defects (AVSD)[11–16]. AVSD is a common cardiovascular malformation that occurs in 3.5 of 10000 births[1]. The formation of the atrioventricular septa and valves is required for the generation of the four chambers known as atria and ventricles. The heart valves are located within the chambers and regulate the blood flow through the heart by opening and closing during each contraction.

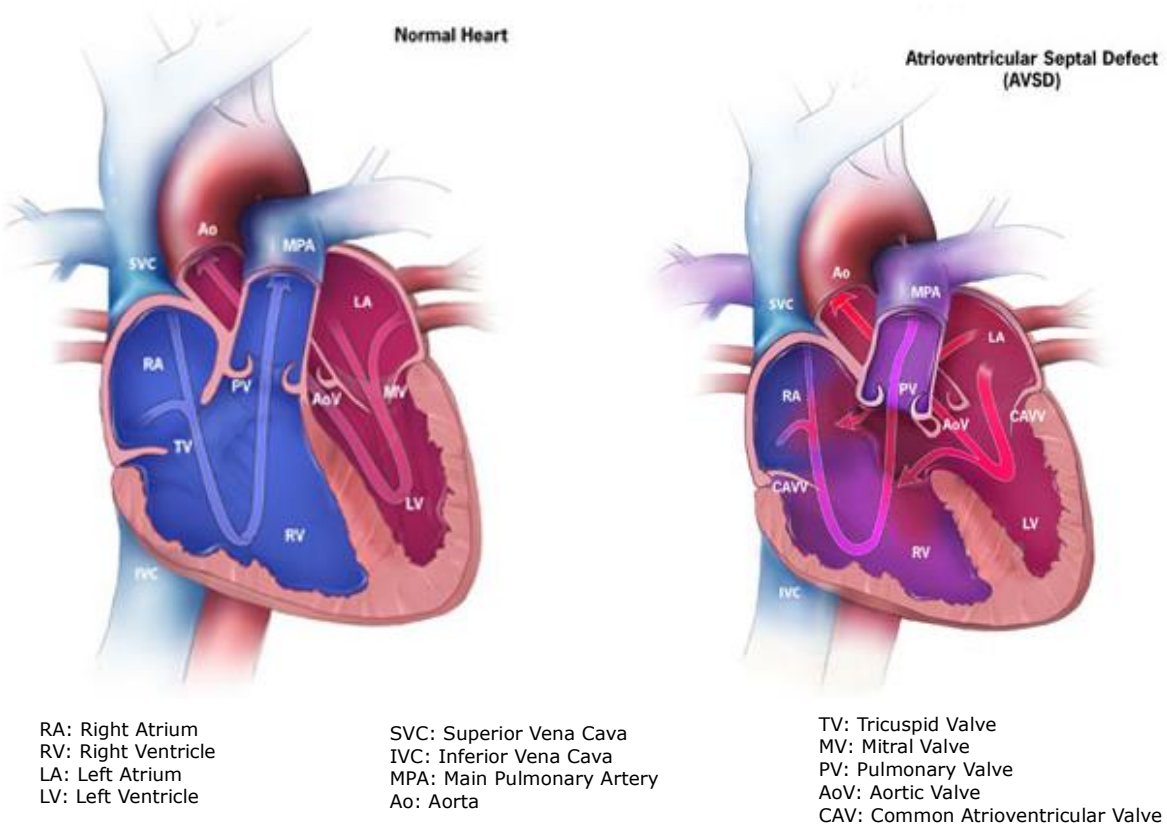

RA: Right Atrium
RV: Right Ventricle
LA: Left Atrium
LV: Left Ventricle

SVC: Superior Vena Cava
IVC: Inferior Vena Cava
MPA: Main Pulmonary Artery
Ao: Aorta

TV: Tricuspid Valve
MV: Mitral Valve
PV: Pulmonary Valve
AoV: Aortic Valve
CAV: Common Atrioventricular Valve

Fig. 1-2 Graphic illustration of a normal heart and a heart with AVSD. While septa and valves enable the unidirectional blood flow in a normally developed heart, the oxygen rich and oxygen poor blood of an AVSD heart is mixed. Pictures are provided by the Centers for Disease Control and Prevention, National Center on Birth Defects and Developmental Disabilities.

1.3 Atrioventricular cushion formation

The heart is the first organ to be developed during embryogenesis. A primitive heart tube is formed at day 8 of embryonic development (E8.0). The formation of the murine heart valves is initiated around E9.0 (Fig. 1-3). From E9.0 to E10.5, endocardial cells within the atrioventricular (AV) canal region of the developing heart tube respond to signals released from the underlying myocardium (Fig. 1-4). These endocardial cells then delaminate into the cardiac jelly, an extensive extracellular matrix located between the endocardium and the myocardium of the heart tube, where they undergo endocardial-mesenchymal transformation (EMT) and proliferation[17]. The cellularized cushions act as precursors of AV and outflow tract (OFT) valves and septa, which are required to facilitate unidirectional blood flow in the heart[18,19]. In a subsequent remodeling process, the AV cushions (AVC) elongate and mature into a highly organized, trilaminar architecture characteristic for mature cardiac valves[17,19–25].

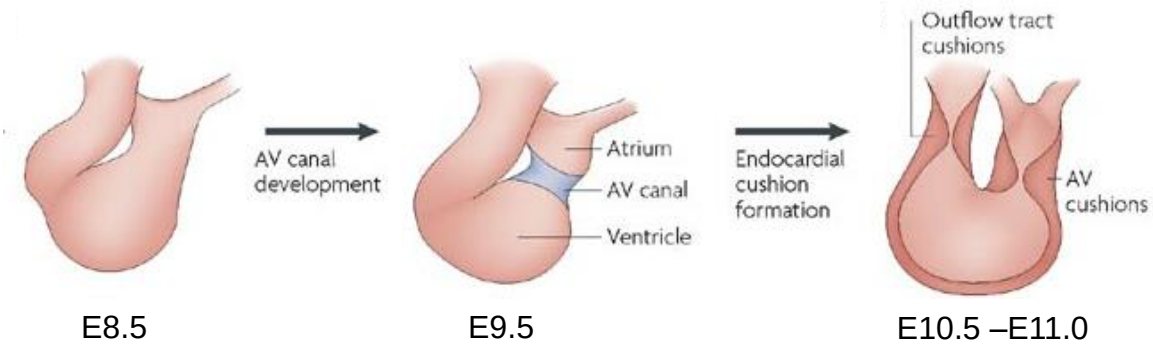

Fig. 1-3 Formation of endocardial cushions. At embryonic day (E)8.5 of development, the murine heart consists of a looping tube. AV canal development, which is initiated around E9.0, creates a boundary between the presumptive atrial and ventricular regions of the heart tube. Signaling and transformation processes between E9.5 and E10.5 lead to the formation of the AV and outflow tract (OFT) cushions - the precursors of the four major heart valves. The formation of OFT cushions is initiated between E10.5 and E11.0. Figure and figure caption are adapted from High & Epstein[107].

A key regulatory pathway for the initiation of heart-valve morphogenesis is calcineurin/nuclear factor of activated T-cells (NFAT) signaling, which is activated by growth factor receptors such as vascular endothelial growth factor (VEGF) receptors and ion channels[26]. Activation of growth factor receptors and channels elevates the intracellular Ca^{2+} concentration and consequently, activates calcineurin, a Ca^{2+}/calmodulin-dependent serine/threonine phosphatase composed of regulatory (calcineurin B) and catalytic (calcineurin A) subunits[27]. Activated calcineurin dephosphorylates cytoplasmic NFAT proteins, whereby nuclear localization signals are exposed and NFAT proteins translocate into the nucleus[28,29]. Once in the nucleus, they cooperate with other family members as well as with other unrelated transcription factors to bind DNA and regulate target gene expression[29,30].

During heart valve formation, calcineurin/NFAT signaling is required at multiple stages (Fig. 1-4). At E9.5, calcineurin/NFATc2/c3/c4 signaling represses VEGF transcription in the myocardium that underlies the area of the endocardium where the prospective AVC will form[31]. This repression of VEGF is essential for endocardial cells to transform into mesenchymal cells. At E10.5, calcineurin/NFATc1 signaling is fundamental for proliferation of endocardial cushion cells. After proliferation of endocardial and mesenchymal cells, EMT needs to be terminated, which is controlled by an increase of VEGF expression in the AVC field[32,33]. Subsequently, calcineurin/NFATc1 signaling is counteracted by regulator of calcineurin 1 (Rcan1) through a negative feedback loop[17,34,35]. Rcan1 inhibits the nuclear translocation of NFATc1 by competing for the binding site on calcineurin and inhibiting the phosphatase activity[36,37]. Thereby proliferation of the endocardium is abolished.

After the formation of the AVC, further remodeling into valvular and septal tissues is initiated. However, the signaling events that occur after EMT in the endocardial cushion are ill-defined[35].

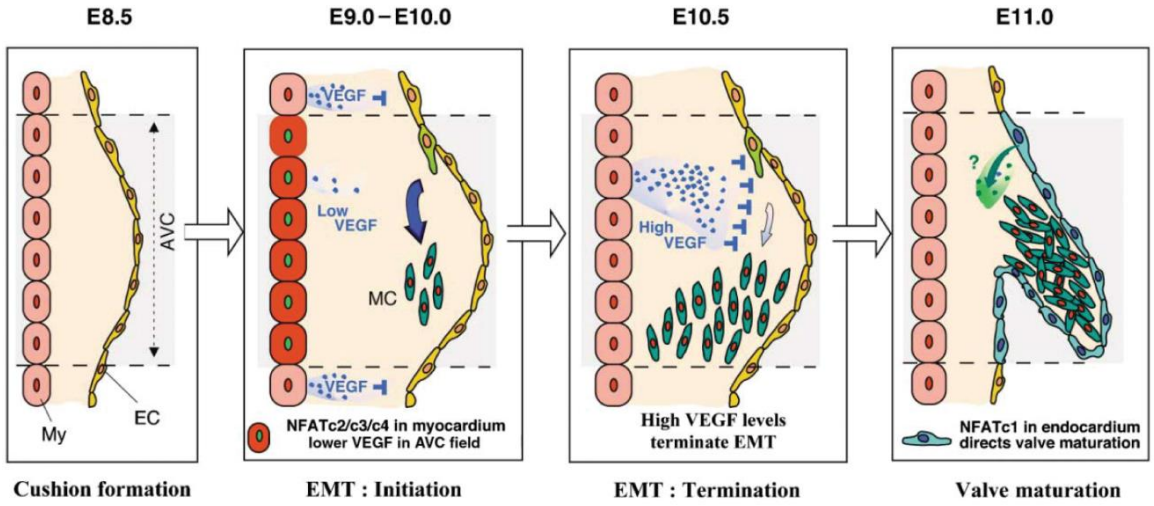

Fig. 1-4 Calcineurin/NFAT signaling in the atrioventricular cushion (AVC). Between E9.0 and E10.0, endocardial cells undergo endocardial-mesenchymal transformation (EMT). In a dose-dependent manner VEGF controls EMT in the AVC field: minimal levels at E9.0 are required for EMT, while high levels at E10.5 terminate EMT. By preventing VEGF expression from reaching excessive levels at E9.0, NFATc2, c3, and c4 in the myocardium allow EMT to proceed. VEGF in the adjacent regions outside the AVC field might suppress EMT. From E11.0 on, NFATc1 in the endocardium controls valve maturation, but the signals remain to be determined. EC: endocardium, My: myocardium; MC: mesenchymal cells. Figure and figure caption are adapted from Lambrechts & Carmeliet[31].

1.4 The endoplasmic reticulum stress response

Promoter analyses of the mouse *Creld2* gene revealed an ER-stress response element (ERSE) that is activated by the activating transcription factor 6 (ATF6). Hence, Creld2 expression can be induced by ER stress[9,38].

ER stress is evoked in the ER upon accumulation of misfolded proteins during protein synthesis. Newly synthesized proteins enter the ER to be post-translationally folded and modified. If there is an elevated protein synthesis or failure of protein folding, transport or degradation, the cells make use of the unfolded-protein response (UPR) to reduce the ER stress[39–41]. The mammalian UPR consists of three axes, with ATF6, double-stranded RNA-activated protein kinase (PKR)–like ER kinase (PERK), and inositol requiring enzyme 1 (IRE1) being the proximal sensors of the ER (Fig. 1-5). All three are maintained in an inactive state by the ER chaperone glucose-regulated protein 78 (GRP78). When ER stress occurs, GRP78 dissociates from ATF6, PERK and IRE1, thereby activating an ER stress gene-expression program[40,42]. The combined action restores ER function by blocking further protein entrance, enhancing the folding capacity and initiating degradation of protein aggregates[43].

1.4.1 The PERK axis

PERK is a type I transmembrane protein with an ER-luminal domain that binds to GRP78 in resting cells[44] and a cytoplasmic domain with kinase activity[45,46]. PERK is activated when GRP78 dissociates and subsequently undergoes oligomerization and autophosphorylation[44]. In turn, phosphorylated PERK phosphorylates eukaryotic translation initiation factor 2α (eIF2α), causing inactivation and an arrest of mRNA translation[47]. However, some genes, including the transcription factor ATF4, are not dependent on eIF2a, thus, are more efficiently translated. ATF4 translocates to the nucleus, where it activates a set of UPR genes, including *growth-arrest DNA damage gene 34* (*GADD34*) and *C/EBP homologous protein* (*CHOP*). GADD34 negatively feedbacks PERK by dephosphorylation of eIF2α. CHOP is a pro-apoptotic factor, which is fully activated when ER stress conditions persist[48,49].

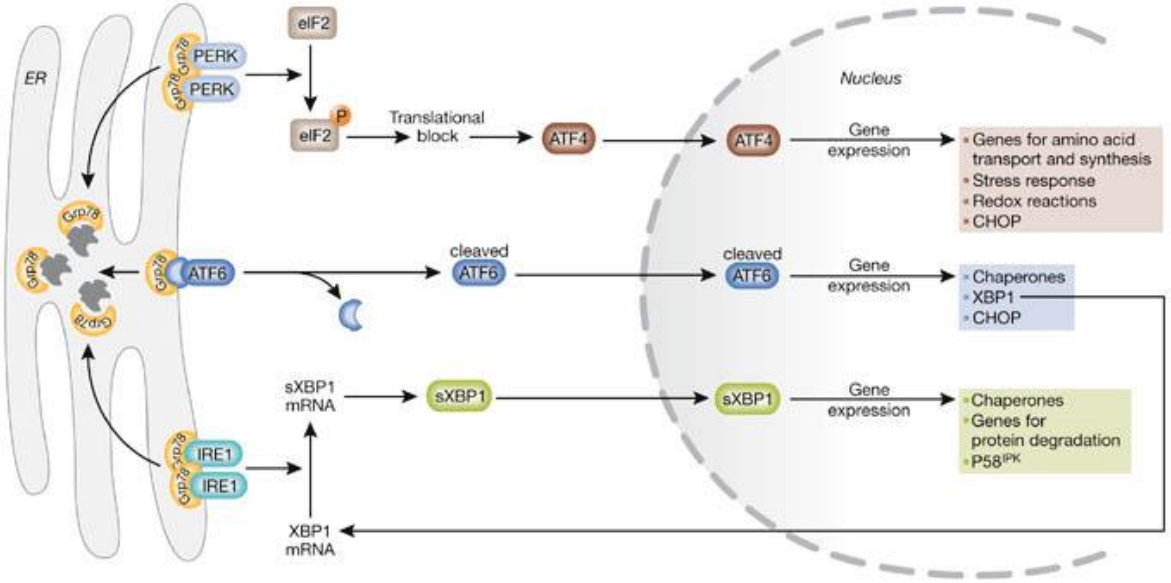

Fig. 1-5 The unfolded protein response. Upon aggregation of unfolded proteins, GRP78 dissociates from the three endoplasmic reticulum (ER) stress receptors, pancreatic ER kinase (PKR)-like ER kinase (PERK), activating transcription factor 6 (ATF6), and inositol-requiring enzyme 1 (IRE1), allowing their activation. The activation of the receptors occurs sequentially, with PERK being the first, rapidly followed by ATF6, and IRE1 being last. Activated PERK blocks general protein synthesis by phosphorylating eukaryotic initiation factor 2α (eIF2α). ATF4 is more efficiently translated due to internal ribosomal entry sites, therefore being independent of eIF2α. ATF4 translocates to the nucleus and induces the transcription of genes required to restore ER homeostasis. ATF6 is activated by limited proteolysis after its translocation from the ER to the Golgi apparatus. Active ATF6 regulates the expression of ER chaperones and X box-binding protein 1 (XBP1). To be active, XBP1 undergoes mRNA splicing, which is carried out by IRE1. Spliced XBP1 protein (sXBP1) translocates to the nucleus and controls the transcription of chaperones, the PERK-inhibitor $P58^{IPK}$, as well as genes involved in protein degradation. CHOP: C/EBP homologous protein. Figure and figure caption are adapted from Szegezdi et al.[43].

1.4.2 The ATF6 axis

ATF6 is a type II transmembrane protein with a bZIP motif in the cytosolic domain[50]. The ER-luminal domain contains Golgi-localization sequences that are exposed upon GRP78 dissociation. After translocation to the Golgi, ATF6 is sequentially cleaved by site-1 protease (S1P) and S2P, thereby releasing the cytoplasmic domain[51,52]. The truncated protein translocates to the nucleus and

acts as transcription factor, binds to ER-stress response elements (ERSE)[50,53], and induces transcription of numerous genes, including GRP78, CHOP, and X-box binding protein 1 (XBP1)[53,54].

1.4.3 The IRE1 axis

IRE1 is a type I transmembrane protein with an ER-luminal domain that resembles that of PERK. The cytoplasmic domain contains a serine/threonine kinase and an endoribonuclease domain[55,56]. When GRP78 is sequestered, IRE1 oligomerizes and trans-phosphorylates other IRE1 proteins in the complex. Activated IRE1 cleaves the mRNA of XBP1 (sXBP1) by a unique splicing mechanism[57,58]. The sXBP1 protein translocates to the nucleus and activates many genes important for protein secretion and degradation, as well as the PERK-inhibitor p58^{IPK} [58].

1.5 Aim of the thesis

The Creld protein family has been described a few years ago. However, the function *in vivo* is ill defined. I investigated the physiological role of Creld1 and Creld2 by generating and analyzing knockout mouse models for both genes.

2 Material

2.1 General materials

2.1.1 Consumables

Consumables	Company
1.5 / 2 ml reaction tubes	Eppendorf
Cell strainer	BD Falcon
Cover slips	VWR
Electroporation cuvette 0.4 cm	Biorad
Embedding cassettes	Simport
General laboratory equipment	Faust, Schütt
Glass plates 16 x 18 cm for SE 600 unit	Hoefer
Microscope slides	VWR
Native Gel chamber (standard dual cooled vertical unit SE 600)	Serva electrophoresis
nitrocellulose membrane	Hybond N^+, Amersham
Novex 4-12 % Bis-Tris Gel	Invitrogen
Paraffin	Medim-Plast
PCR reaction tubes	Sarstedt
Plastic wares	Greiner
Sephadex G50 columns	GE Healthcare
Superfrost Plus adhesive microscope slides	Thermo scientific
Syringe	Inject disposable 5 ml BBraun
X-ray films	Fuji MedicalX-Ray Film Super RX
Tissue-Tek	Sakura

2.1.2 Equipment

Equipment	Company
Autoclave	H+P Varioklav Dampfsterilisator EP-2
Bacteria incubator	Innova 44 New Brunswick scientific
Balances	Sartorius BL 150 S; Sartorius B211 D
Binocular	Zeiss Stemi 2000
Blotting equipment	Biometra Whatman Fastblot B43
Centrifuges	5415R/5424 Eppendorf; Avanti J-26 XP Beckman Coulter; Biofuge primo R Heraeus; Rotina 420R
Confocal microscope	Zeiss LSM710
Cryostat	Leica
Dehydration carrousel	Leica TP 1020
Developer machine	Curix 60 AGFA
Electro pipette	Accu Jet
Electroporator	Biorad Gene Pulser Xcell
Flow cytometer	BD Biosciences LSR II
Fluorescence microscope	Zeiss AxioCam MRm; Olympus SZX 12
Gel documentation	BioRad
Gradient maker	Hoefer SG15
Homogenizer	Precellys Peqlab
Incubators / shaker	Biostep Dark Hood DH-40/50 (Benda) Heiz Thermo Mixer MHR13 HCL (Memmert), Innova 44 New Brunswick Scientific
Microtome	Leica RM2255
Microwave	Panasonic
PCR machine	C1000 Thermal Cycler BioRad
Photometer	Nano Drop 2000 PeqLab
Plate reader	Fluostar Omega (BMG Labtech)
RealTime PCR machine	iCycler BioRad
Rotating disc	Rotator SB3 Stuart
Ultrasonic apparatus	Bandelin SONOPLUS HD2070
UV cross linker	Stratalinker 2400 Stratagene
Voltage source	Power Pac 3000 BioRad
Vortexer	Vortex Genie2
Water bath	Julabo SW22

2.2 Standards und Kits

Name	Company
Nucleic Acid & Protein Purification, NucleoBond, PC 100	Macherey & Nagel
BCA Protein Assay	Pierce
ECL Western Blotting Substrate	Pierce
iQ™ SYBR Green Supermix	Biorad
QuantiTect, Reverse Transcription Kit	Qiagen
Ready-to-use System for fast Purification of Nucleic Acids, NucleoSpin, Extract II	Macherey & Nagel
Nucleic Acid & Protein Purification, NucleoSpin, RNAII	Macherey & Nagel
NucleoSpin RNA/Protein	Macherey & Nagel
Dual-Glo Luciferase Assay System	Promega
PCR Nucleotide Mix	Roche
NucleoSpin RNA XS	Macherey & Nagel
DAPI-Fluoromount G	Biozol
Immunoprecipitation Starter Pack	GE Healthcare
NucleoSpin Plasmid QuickPure	Macherey & Nagel
2-Log DNA ladder, 1 kb DNA ladder	NEB
Native gel protein marker (45 – 545 kDa)	Sigma
Precision Plus Protein All Blue Standards	Biorad
Nova Red	Vector Laboratories, CA
Flow cytometry ompensation beads	Invitrogen
Multiprime DNA labeling kit	GE Healthcare

2.3 Buffers

Unless otherwise noted, all buffers and solutions were made with double distilled water (aqua bidest). At solutions that were not kept at room temperature a storage temperature indicated. Percent indications correspond to mass per volume. At the solutions, which were made as concentrated stock solution, the concentration factor is indicated.

Buffer	**composition**
Agarose	1 % agarose in TAE
Ammonium persulfate (APS)	10 % APS
Ampicillin (-20 °C) (1000x)	50 mg/ml
Blocking solution	5 % milk powder (Roth) in TBST (1x)
EDTA	0.5 M EDTA (pH 8.0)
EGTA	0.5 M EGTA (pH 8.0)
Fixation solution	4 % Paraformaldehyde (PFA) in PBS (Histofix, Roth)
KHM buffer	110 mM KOAc, 2 mM $MgCl_2$, 20 mM Hepes (pH 7.2)
Laird buffer	0.1 M Tris (pH 8.0), 0.2 % SDS, 0.2 M NaCl, 5 mM EDTA
Loading buffer (10x)	Lysis buffer 20 mM Tris/HCl (pH 7.5), 200 mM NaCl, 20 mM EDTA, 2 % SDS
Lysozyme (-20 °C)	10 mg/ml in TE-buffer
Native gel running buffer (50x)	250 mM Tris, 1,92 M glycine
Native gel sample buffer (3x)	30 % Glycerol, 6 % Native running buffer, 0.1% Bromphenolblue
Non-denaturating lysis buffer	2 mM EDTA, 10% glycerol, 1 % Nonidet P-40, 137 mM NaCl, 20 mM Tris·HCl (pH 8.0)
PBS (20x)	2.6 M NaCl, 140 mM Na_2HPO_4, 60 mM NaH_2PO_4

Buffer	composition
	(pH 7.0)
PBT	0.1 % Tween 20 in PBS (1x)
Proteinase K stock solution (-20 °C)	20 mg/ml in DEPC
Red blood cells lysis buffer	155 mM NH_4Cl, 12 mM $NaHCO_3$, 0.1 mM EDTA
RIPA buffer	150 mM NaCl, 1 % IPEGAL CA-630, 0.5 % Sodium Deoxycholate (DOC), 0.1 % SDS, 50 mM Tris/HCl (pH 8.0)
SDS	10 % SDS
SDS-PAGE loading buffer (5x)	100 mM Tris, 3% SDS, 10% Glycerol, 0.1% Bromphenolblue, 2 % β-Mercaptoethanol (pH 6.8)
SDS-PAGE running buffer (10x)	250 mM Tris/HCl, 1.92 M Glycine, 1 % SDS
Sodium acetate	3 M NaAc, with acetic acid to pH 6.0
Sodiumactetate (10x)	100 mM $C_2H_3NaO_2$
SSC (20x)	3 M NaCl, 0.3 M $Na_3C_6H_5O_7$ (trisodium citrate)
TAE buffer	40 mM Tris-Acetate (pH 8.0), 1 mM EDTA
TBST	0.01 M Tris/HCl (pH 7.5), 0.15 M NaCl, 0.05 % Tween 20
TE-buffer	10 mM Tris/HCl (pH 8.0), 1 mM EDTA
Transferring buffer (4 °C)	25 mM Tris, 150 mM Glycine, 10 % Methanol
Oil-Red-O stock stain	0.5 % Oil-Red-O in isopropanol

2.4 Enzymes

Enzyme	Company
Digitonin (5 %, 4°C)	Invitrogen
Eosin	Merck
GoTaq Polymerase	Promega
Hematoxylin	Merck
Neuraminidase	NEB
O-glycosidase	NEB
Phusion Hot Start Polymerase	Thermo scientific
PNGase F	NEB
Proteinase K	Sigma Aldrich
Restriction endonucleases	NEB
RNase A	Sigma Aldrich
Shrimp Alkaline Phosphatase (SAP)	Roche
T4 DNA Ligase	Roche
Trypsin	Sigma

2.5 Solutions and chemicals

Enzyme/chemical	Company
Acetic acid	Roth
Colcemid	Sigma
Complete protease inhibitors	Roche
Cyclosporin A	Sigma
Digitonin (4 °C)	Sigma
Entallan	Merck
Eosin	Merck
Ethanol	Roth
Giemsa solution	Sigma
Hematoxylin	Merck
Ionomycin	Tocris Bioscience

Enzyme/chemical	Company
Isopropanol	Roth
Methanol	Roth
Phorbol myristate acetate (PMA)	Sigma
QuickHyb	Stratagene
Thapsigargin	Sigma
Trypsin	Invitrogen
Xylol	Roth
G418	Invitrogen

2.6 Bacterial Strains

Name	Genotype	Origin
DH5α	F- *end*A1 *deo*R (φ80*lacZ*ΔM15) *rec*A1 *gyr*A (Nal^r) *thi*-1 *hsd*R17 (r_K^-, m_K^+) *sup*E44 *rel*A1 Δ(*lac*ZYA-*arg*F)U169	Stratagene

2.7 Media

2.7.1 Media for bacterial cultures

The bacteria were cultivated in the following media. All media were autoclaved for 20 min at 120 °C.

Name	Composition
LB-medium	10 g NaCl, 10 g tryptophan, 5 g yeast extract ad 1 l aqua bidest (pH 7.0)
LB-ampicillin medium	LB-medium with 50 µg/ml ampicillin
LB-kanamycin medium	LB-medium with 25 µg/ml kanamycin
LB-ampicillin agar	LB-medium with 20 g agar and 50 µg/ml ampicillin
LB-kanamycin agar	LB-medium with 20 g agar and 25 µg/ml kanamycin

2.7.2 Media for cell cultures

All solutions were purchased from Invitrogen.

Cell line	Composition
NIH3T3, HEK239	10 % FBS, 1 % Penicillin/Streptomycin in DMEM
Jurkat E6.1	10 % FBS, 1 % Penicillin/Streptomycin in RPMI

Metafectene pro and Opti-MEM are used for transfection.

2.7.3 Media and buffer for ES-cell culture

If not other noted, all media were purchased from Invitrogen and Sigma. LIF was provided by AG Magin.

Medium	Composition
Culture medium	1 % L-glutamine, 1 % non-essential-amino-acids, 1 % Sodium-pyruvate, 1 % Penicillin/Streptomycin, 10 % ES-FCS, 0.1 % β-Mercaptoethanol, 0.1 % LIF in GMEM (Invitrogen)
Freezing medium (2x)	10 % FCS, 20 % DMSO (Merck) in culture medium
β-Mercaptoethanol	0.1 mM β-Mercaptoethanol in ES-H_2O, sterile
Gelatin	1 % in ES-H_2O, autoclaved, mixed, then autoclaved again
Gelatin working solution	0.1 % Gelatin
ES-trypsin	10 % Chicken serum, 5 % of 2.5 % trypsin, 6.33 mM EDTA in ES-PBS (pH 8.0, autoclaved), ad ES-PBS
HBS buffer	2 % Hepes buffer, 0.1 % Glucose, ad ES-PBS
Lysis buffer (clone PCR)	1x PCR buffer, 0.2 mg/ml Proteinase K
Lysis buffer (genomic DNA)	50 mM NaCl, 20 mM TrisHCl (pH 8.0), 100 mM EDTA, 2 mM $CaCl_2$, 0.5 % SDS

2.8 Primer

2.8.1 qRT-PCR Primer

Primer name	fw primer (5’ – 3’)	rev primer (5’ – 3’)
Acox1	GCC CAA CTG TGA CTT CCA TC	GCC AGG ACT ATC GCA TGA TT
Aldoa	CAA CGG TCA CAG CAC TTC GTC G	CAG GGC TCG ACC ATA GGA GAA AG
Atf6	GGC GGC TAA GTC CTC TTC TC	TGC CCT GAA AAC ATC TCA CC
C/ebpα	TGGACAAGAACAGCAACGAG	TCA CTG GTC AAC TCC AGC AC
Car9	CGA TTG AGG CTT CCT TCC CTG C	TAG CTA ACT CTA TCT TTG GTC CCA CTT C
Chop	TCA CCT CCT GTC TGT CTC TCC	TAC CCT CAG TCC CCT CCT C
Cpt1a	GCT GGG CTA CTC AGA GGA TG	CAC TGT AGC CTG GTG GGT TT
Creld1	AGG AGC TGG TGG AAA ACT GG	TTC AGG GAA TCG GAA CAG AG
Creld2	GGC TAC ACC AAG GAG AGT GG	GGA CAC ACG CAC ACG AAG
Dgat2	AGG CCC TAT TTG GCT ACG TT	GAT GCC TCC AGA CAT CAG GT
Dscr1(e1)/Rcan1	TGC GAG ATG GAG GAG GTG	ACT GGA AGG TGG TGT CCT TG
Epo	GAA AAT GTC ACG ATG GGT TGT GCA GA	GGC CTG TTC TTC CAC CTC CAT TCT TT
EpoR	CTC CAC CAC AGA CAA CCA TCA CG	CTC ATT CTG GTC CTC ATC TCG CTG
Errα	GCAGGGCAGTGGGAAGCTA	CCT CTT GAA GAA GGC TTT GCA
Fabp1	CCA TGA CTG GGG AAA AAG TC	GCC TTT GAA AGT TGT CAC CAT
Fasn	GCT GCT GTT GGA AGT CAG C	AGT GTT CGT TCC TCG GAG TG
G6pc	TCT GTC CCG GAT CTA CCT	GAA AGT TTC AGC CAC AGC

Primer name	fw primer (5’ – 3’)	rev primer (5’ – 3’)
	TG	AA
Gadd34	ACGATCGCTTTTGGCAAC	GACATGCTGGGGTCTTGG
Gck	GTG AGG TCG GCA TGA TTG T	TCC ACC AGC TCC ACA TTC T
Grp78	CGA CAA GCA ACC AAA GAT G	CCA GGT CAA ACA CAA GGA TG
Hk1	GCC ATT GAA ACG GGA TGG GAA CTC	GTT GGC TGA TCG GAA GGA GAC G
Hprt	TCC CAG CGT CGT GAT TAG CGA TGA	AAT GTG ATG GCC TCC CAT CTC CTT CAT GAC AT
Ldha	GCG GTT CCG TTA CCT GAT GGG A	TTG TGA ACC TCC TTC CAC TGC TCC
Lipc	ACA AGG CGT GGG AAC AGA	TGG CTT CTT TAA TGG CTT GC
Ndufs1	CGG CCT TGG GAA ACA AGA	ATG TTA CTT CCC ACT GCA TCC A
Nfatc1	CTC TGG AGA GCC CTA GAA TTG	CGC AGA AGT TTC CTT TCC TG
Pck1	GGA GTA CCC ATT GAG GGT ATC AT	GCT GAG GGC TTC ATA GAC AAG
Pcx	TCC GTG TCC GAG GTG TAA A	CAG GAA CTG CTG GTT GTT GA
Pparα	CAC GCA TGT GAA GGC TGT AA	CAG CTC CGA TCA CAC TTG TC
Ppia	GCG TCT CCT TCG AGC TGT T	RAA GTC ACC ACC CTG GCA
Srebp1	GGT TTT GAA CGA CAT CGA AGA	CGG GAA GTC ACT GTC TTG GT
Srebp2	ACC TAG ACC TCG CCA AAG GT	GCA CGG ATA AGC AGG TTT GT
sXbp1	TGC TGA GTC CGC AGC AGG	GTC CAG AAT GCC CAA CAG G
Vegfa	CAC AGC AGA TGT GAA TGC AG	TTT ACA CGT CTG CGG ATC TT

2.8.2 Primer for cloning

Primer name	Sequence
3‘ UTR-pA fw-eGFP	5‘-GAG CTG TAC AAG TGA CGG GCA TCC GGA TTC
3‘ UTR-pA rev-int.SpeI	5‘-AGG TAC AAA CTG ACT AGT GGT AAT GCC C
3’HR fw-int.SpeI	5‘-TTA CCA CTA GTC AGT TTG TAC C
3’HR rev-NotI	5‘-ATA GTT TAG CGG CCG CTT TGC CTA CCA GAT GAG G
5‘HR 1b rev-ATG-eGFP	5‘-GCC CTT GCT CAC CAT GGC GGG AGG GCT GC
5‘HR1b fw-5’HR1a-NdeI	5‘-GTC CCC ACA ATT CAT ATG AAC TCA AAG GCC GTC ACG CG
5’HR1a fw-SacI	5‘-CGA GCT CTT AAA GGC CTG CGC CAC C
5’HR1a rev-5’HR1b-NdeI	5‘-GGC CTT TGA GTT CAT ATG AAT TGT GGG GAC ACA GGG AG
Cre2 5extern fw	5’-TTT CTC CAG GAA GAC TTC AGA GGG
Cre2 5extern rev	5’-TAC AGC AGG CTG GAT GGA GCA GG
Cre2_5'extern fw	5‘-AAG ATG GAA GGA CTG GGA GGC CG
Cre2_5'extern rev	5‘-TAC AGC AGG CTG GAT GGA GCA GG
eGFP fw-5’HR1b	5‘-GGC AGC CCT CCC GCC ATG GTG AGC AAG GGC
eGFP rev-STOP-3’UTR	5‘-TCC GGA TGC CCG TCA CTT GTA CAG CTC GTC CAT G
mCre1-flagCT-HindIII fw	5‘-CCC AAG CTT ATG GCT CCA CTG CCC CC
mCre1-flagCT-XbaI rev	5‘-GCT CTA GAT TAC TTA TCG TCG TCA TCC TTG TAA TCT CTA CCC TTG ATG AAG CCC TCC
mCre2-flagNT- HindIII fw	5‘-CCC AAG CTT ATG GAT TAC AAG GAT GAC GAC GAT AAG CAC CTG CTG CTT GCA GCC
mCre2-flagNT- XbaI rev	5‘-GCT CTA GAT CAC AAA TCC TCA CGG GAG G
mCreId1- P162A-soe fw	5’-CAG GCC CTC TCT GTG CCC

Primer name	Sequence
mCreld1- R107H-soe fw	5‘-GC CAC CAC CTG CTC GAG
mCreld1_rev_KpnI_pMJGreen	5’-GGG GTA CCA TTC TAC CCT TGA TGA AGC CCT C
mCreld1delTM-Flag-XbaI rev	5‘-TCT AGA TTA CTT ATC GTC GTC ATC CTT GTA ATC TTC ATC CTC CGT CAT CTC CG
mCreld1delTM-RFP-KpnI-rev	5‘-GGT ACC ATT TCA TCC TCC GTC ATC TCC G
mCreld1-E414K-soe fw	5‘-CCG TGT GCT GAA GGG CTT C
mCreld1-E414K-soe rev	5’-GAA GCC CTT CAG CAC ACG G
mCreld1-P162A-soe rev	5‘-G GGC ACA GAG AGG GCC TG
mCreld1-R107H-soe rev	5’-CTC GAG CAG GTG GTG GC
mCreld1-R329C-soe fw	5‘-GGAG GGA GGC TAC TGC TGT GTC
mCreld1-R329C-soe rev	5’-GAC ACA GCA GTA GCC TCC CTC C
mCreld1-T311I-soe fw	5‘-GTG GAT GAG TGT GAG ATT GTG G
mCreld1-T311I-soe rev	5‘-CCA CAA TCT CAC ACT CAT CCA C
mCreld1-ΔcbEGF- soe fw	5‘-CAC CTC AAG TGT GTA AAG GAG CAG GTC CCG GAG
mCreld1-ΔcbEGF- soe rev	5‘-CGG GAC CTG CTC CTT TAC ACA CTT GAG GTG ATG CAG GG
mCreld1-ΔEGF- soe fw	5‘-CTG AAG CTC TGC TGC GAC ATC GAT GAG TGT GGT ACA GAG C
mCreld1-ΔEGF- soe rev	5‘-ACA CTC ATC GAT GTC GCA GCA GAG CTT CAG GGA ATC
mCreld1-ΔTAWEE- soe fw	5’-CAT CCG GGA CAA CTT CGG GAA GTT GTC CAA ATA CAA AGA CAG TGA GAC C
mCreld1-ΔTAWEE- soe rev	5‘-GGT CTC ACT GTC TTT GTA TTT GGA CAA CTT CCC GAA GTT GTC CCG GAT G

2.8.3 Genotyping primer

Primer	Sequence
neo_fw	5'-GGC TAT GAC TGG GCA CAA CAG
neo_rev	5'-TTT CTC GGC AGG AGC AAG GTG
gt_fw	5'-CCA TCC GCC TTT CTC TCG GA
gt_rev	5'-GAG ATG GGA CCA GGC CCC
gt_lacZ	5'-GTC TGT CCT AGC TTC CTC ACT G
gt2_fw	5'-CAT CTA TCT CCC TTT GAG TCC G
gt2_rev	5'-GTC ACC AGG AAC AGG ACG TG
neo2_fw	5'-CCC AGG GCT CGC AGC C
ES_fw	5'-TTC CCC GAA AAG TGC C
ES_rev	5'-ACA GTG GCC AGC G

2.9 Plasmids

Plasmid	Plasmid source
CFP-CD3δ	H. Lorenz, National Institutes of Health, Maryland
Creld1E414K -RFP	E. Mass
Creld1E414K-Flag	E. Mass
Creld1-GFP	E. Mass
Creld1P162A-Flag	E. Mass
Creld1P162A-RFP	E. Mass
Creld1R107H-Flag	E. Mass
Creld1R107H-RFP	E. Mass
Creld1R329C-Flag	E. Mass
Creld1R329C-RFP	E. Mass
Creld1-RFP	E. Mass

Plasmid	Plasmid source
Creld1T311I -RFP	E. Mass
Creld1T311I-Flag	E. Mass
Creld1ΔcbEGF-Flag	E. Mass
Creld1ΔcbEGF-RFP	E. Mass
Creld1ΔEGF-Flag	E. Mass
Creld1ΔEGF-RFP	E. Mass
Creld1ΔTM-Flag	E. Mass
Creld1ΔTM-RFP	E. Mass
Creld1ΔWE-Flag	E. Mass
Creld1ΔWE-RFP	E. Mass
Creld2KO targeting vector	E. Mass
NFATc1-GFP	E. Olson, University of Texas Southwestern Medical Center, Dallas
NFATc1-HA	D. Wachten, Bonn (Caesar)
pcDNA3.1(+)	AG Hoch (T. Krsmanovic)
pGL3-NFAT-luc	Addgene (plasmid 17870)
pMJ-Green	AG Willecke, Bonn
pRFP-N1	AG Lang, Bonn
psiCHECK-1	Promega
YFP-PrP	H. Lorenz, National Institutes of Health, Maryland

2.10 Antibodies

2.10.1 Primary antibodies

antibody	company	species	Method (conc.)
actin	Novus Biologicals	mou	WB (1:5000)
B220 APC-Cy7	Biolegend	rat IgG2a, κ	FACS (1:100)
Calcineurin B	Sigma	mou	IF (1:100)
CD11b BV650	Biolegend	rat IgG2b, κ	FACS (1:100)
CD11c PE	Biolegend	armenian hamster IgG	FACS (1:100)
CD4 BV510	Biolegend	rat IgG2a, κ	FACS (1:100)
CD8a Pacific blue	Biolegend	rat IgG2a, κ	FACS (1:100)
Creld1	Abnova	mou	IHC (1:100), WB (1:500)
Creld2	Santa cruz	rab	IF (1:100), IHC (1:100), WB (1:750)
DSCR1	Sigma	rab	WB (1:500)
HA	Roche	rat	IF (1:200), WB (1:5000)
hCreld1 #1 WLSERSDRVLEGFIKGR	PLS	gp	IF (1:50 - 1:100)
KDEL	abcam	mou	IF (1:500)
MF-20	DSHB	mou	IF (1:200)
NFATc1	Santa cruz	mou	IF (1:200)
NKp46 PerCP-Cy5.5	Biolegend	rat IgG2a, κ	FACS (1:100)
p-Histone3	Santa cruz	rab	IF (1:400)
PP2B1/2 (CnB)	Santa cruz	rab	IF (1:100), WB (1:200)

2.10.2 Secondary antibodies

Name	Species	Source	Concentration
α-guinea pig-HRP	donkey	Santa Cruz	1:15000 WB
α-rabbit-HRP	donkey	Santa Cruz	1:15000 WB
α-mouse-HRP	donkey	Santa Cruz	1:15000 WB
α-rat-HRP	donkey	Santa Cruz	1:15000 WB
normal rabbit IgG	donkey	Santa Cruz	Co-IP
α-mouse-Cy3	donkey	Dianova	1:100 IF
α-guinea pig-Cy3	donkey	Dianova	1:100 IF
α-rabbit-Cy3	donkey	Dianova	1:100 IF
α-guinea pig-Alexa 488	donkey	Molecular Probes	1:100 IF
α-rabbit-Alexa 488	donkey	Molecular Probes	1:100 IF
α-guinea pig-Alexa 633	donkey	Molecular Probes	1:100 IF

3 Methods

3.1 Isolation and purification of DNA and RNA

3.1.1 Isolation of tail tip DNA

The tail tips of mice were incubated in 400 µl Laird buffer at 55 °C in a water bath o/n. After centrifugation at 13200 rpm the supernatant was transferred into a new tube with 500 µl isopropanol. DNA was precipitated by centrifugation at 13200 rpm for 10 min. Subsequently, the DNA was washed with 500 µl of 70 % ethanol, and the pellet was air dried and resuspended in 100 µl aqua bidest.

3.1.2 Isolation of plasmid DNA

For analytical preparation, 2 ml LB medium containing the appropriate antibiotic were inoculated with a single colony of transformed bacteria and were incubated o/n at 37 °C with vigorous shaking. The culture was centrifuged for 3 min at 13200 rpm, resuspended in 400 µl TELT buffer with lysozyme (100 µg/ml) and RNase A (10 µg/ml) and boiled for 5 min in a thermal cycler. After cooling down on ice genomic DNA and debris were pelleted by centrifugation at 13200 rpm for 15 min. The pellet was removed with a tip. 400 µl isopropanol was added to the supernatant and the plasmid DNA was pelleted by further centrifugation at 13200 rpm for 30 min. The pellet was washed once with 1 ml of 70% ethanol, then air dried and resuspended in 50 µl aqua bidest.

For preparation of bigger amounts or highly pure plasmid DNA, Macherey & Nagel Nucleospin Plasmid kits (mini, midi or maxi) were used according to manufacturers' specifications.

3.1.3 Gel electrophoresis for separation of DNA fragments

For separation of DNA fragments, 1 % agarose gels were used. The agarose was diluted in 1x TAE buffer and boiled until it was completely dissolved. Afterwards it was cooled down to 60 °C and Syber-Safe was mixed in a dilution of 1:10000 into the fluid agarose. The gel was placed in a chamber with 1x TAE. Probes were diluted 1:10 with 10-fold DNA loading buffer and loaded into the pockets of the gel.

3.1.4 Cleanup of DNA fragments

Macherey & Nagel Nucleospin extract II kit was used according to manufacturers' instructions for cleanup of DNA fragments after enzymatic reactions or gel electrophoresis. DNA fragments were eluted in an appropriate volume of autoclaved aqua bidest and stored at -20 °C.

3.1.5 Photometric determination of DNA and RNA concentration

The concentration of DNA and RNA was measured with a Nanodrop system using 1 µl aqua bidest as blank and 1 µl of the probe for the measurement.

3.1.6 Isolation of RNA

Isolation of RNA was performed using the Macherey & Nagel Nucleospin RNA II kit. For embryonic hearts the NucleoSpin RNA XS was used. In case of the simultaneous preparation of proteins, the Nucleospin RNA II Column flow through was used for protein precipitation, according to the manufacturer' instructions.

3.1.7 Reverse transcription of RNA into cDNA

cDNA was reverse transcribed using Qiagen QuantiTect reverse transcription kit including rDNaseI treatment following the manufacturers protocol. 500 ng of total RNA was used in a 10 µl reaction and filled up to 50 µl with aqua bidest after cDNA synthesis.

3.2 Cloning of DNA fragments

3.2.1 Enzymatic digestion

NEB restriction endonucleases and buffers were used for enzymatic digestions of DNA. In a total volume of 20 µl 1-2 µg of DNA were digested, including 2 µl of the appropriate 10x buffer and 3-5 enzymatic units per µg of DNA. After the DNA was incubated for 2-4 h, the fragments were separated by gel electrophoresis and finally cleaned up using Macherey & Nagel Nucleospin extract II kit. For double digestion with two different enzymes one common buffer according to manufacturers' recommendation was used.

3.2.2 Vector preparation

Vectors were digested with appropriate endonucleases as described above. To avoid re-ligation cut vectors were dephosphorylated by shrimp alkaline phosphatase. For the dephosphorylation reaction, 2 µl of 10x Roche dephosphorylation buffer and one enzymatic unit of shripms alkaline phosphatase was used in a 20 µl reaction. The samples were incubated at 37 °C for 10 min and phosphatase was inactivated by heating the sample to 65 °C for 15 min.

3.2.3 Ligation

For optimal results, the amount of insert DNA should be around three to six times higher as compared to the vector DNA. The ligation reaction was done o/n at 18 °C in a total volume of 10 µl, including 1 µl 10x ligation buffer and 1 µl T4 DNA ligase.

3.2.4 Sequencing DNA

Sequencing was performed by SeqLab. The DNA was prepared according to the requirements of the company.

3.3 Preparation of electrocompetent bacteria and recombineering

Bacteria containing a BAC (BMQ 440p13) that contained the wildtype locus of Creld2, was made electrocompetent by inoculating one BAC colony in 5 ml LB^{Amp} medium o/n at 37°C and 250 rpm. The next day, 1 ml of this preculture was inoculated in 100 ml fresh, prewarmed LB selection medium and incubated under the same conditions until an OD_{600nm} = 0.6-0.8 is reached. From now on, the suspension was always kept on ice. All centrifugation steps lasted 10 min and were performed at 4°C. The culture was transferred to two 50 ml falcon tubes and centrifuged consecutively at 2900 g, 4000 g, 5750 g, and 7250 g. The supernatant was discarded after each centrifugation step and the pellet resuspended in 40 ml 10% glycerol solution. After the centrifugation at 7250 g, the pellets from both 50 ml falcon tubes were combined and resuspended in 40 ml 10% glycerol solution. After another centrifugation (9000 g), the pellet was resuspended in 150 µl 50% glycerol solution, portioned in aliquots. (Adapted from Diploma thesis of A. Aschenbrenner). One of the aliquots was used to transform the bacteria with the mini-phage λ in order to make the bacteria recombination-competent. The selection of mini-phage λ positive bacteria was done with kanamycin-containing agar plates.

These bacteria were subsequently made electrocompetent again like described above, with the difference, that the recombination-competent strain was maintained at 32 °C. To activate recombination functions, the culture was incubated at 42 °C for 15 min, and then cooled in ice water for 20 min before proceeding with the first centrifugation steps.

After the bacteria were electrocompetent, they were transformed with the linearized retrieval vector containing sequences of 500 bp on each end that encompassed the 5’ homology arm. Selection was done with ampicillin. Clones of this last step were screened for the vector that was subsequently used for homologous recombination of the Creld2 locus in ES-cells.

3.4 PCR techniques

3.4.1 Cloning PCR

For cloning of DNA fragments the Phusion Hot Start High-Fidelity DNA Polymerase was taken to ascertain high specificity and proof reading. PCR reactions were set up as proposed by the manufacturers' manual. The samples were mixed in a 0.2 ml PCR-tube:

Component	Volume / 20 µl reaction	Final concentration
H_2O	13.4 µl	
5x Phusion HF buffer	4 µl	1x
10 mM dNTPs	0.4 µl	200 µM each
Forward primer	1 µl	0.5 µM
Reverse primer	1 µl	0.5 µM
Template DNA	1 µl	1 pg – 5 ng
Phusion Hot Start DNA Polymerase (2 U/µl)	0.2 µl	0.02 U/µl

Program:

Cycle step	Temperature	Time	Number of cycles
Initial denaturation	98 °C	30 s	1
Denaturation Annealing Extension	98 °C 60-74 °C 72 °C	10 s 30 s 60 s	25-35
Final extension	72 °C 4 °C	5-10 min hold	1

After the PCR program the DNA fragments were purified by gel electrophoresis, cut out of the gel and cleaned up.

3.4.2 Genotyping PCR

For genotyping the GoTaq polymerase was used. Primer concentration was 100 pmol/µl.

Component	Volume / 20 µl reaction (*Creld1KO*)	Volume / 20 µl reaction (*Creld2KO*)
H_2O	13.4 µl	13.5 µl
5x Green GoTaq reaction buffer	4 µl	4 µl
10 mM dNTPs	0.2 µl	0.2 µl
Forward primer	0.1 µl (gt_fw or neo_fw)	0.1 µl (gt2_fw or neo2_fw)
Reverse primer	0.1 µl each (gt_rev, gt_lacZ or neo_rev	0.1 µl (gt2_rev)
Template DNA	2 µl	2 µl
GoTaq DNA Polymerase (5 U/µl)	0.1 µl	0.1 µl

Program:

Cycle step	Temperature	Time	Number of cycles
Initial denaturation	95 °C	30 s	1
Denaturation Annealing Extension	95 °C 58 °C 72 °C	20 s 20 s 20 s	35
Final extension	72 °C 4 °C	5 min hold	1

3.4.3 qRT-PCR

Primers for qRT-PCR were designed by using Universal Probe Library - Roche Applied Science.

qRT-PCR primers		
Condition	*Range*	*Optimum*
Primer length	18-25 bp	20 bp
Product lenght	75-150 bp	120 bp
Melting temperature	57-61 °C	59 °C
% GC (of total)	40-60	50

Primers were synthesized by Invitrogen without 5' and 3' modifications, desalted and shipped lyophilized. Before use, primers were resuspended in aqua bidest to a final concentration of 20 pmol/µl.

Primers for qRT-PCR were tested for efficiency before use. Efficiency tests include dilution of template cDNA from 1:1 up to 1:125. Primers used for real-time PCR showed at least 80% efficiency up to a dilution of 1:25. All primers were optimized and used at an annealing temperature of 59 °C. The appearance of primer dimer was further ruled out by melt curve analysis.

All qRT-PCR experiments were done with BioRad I-cycler and IQ5 optical system using SYBR-Green to detect amplification after each PCR cycle. Reactions were performed as duplicates or triplicates in 96-well plates and a total volume of 15 µl. Gene expression studies were analyzed with BioRad IQ5 optical system software. Expression is always shown relative to a control condition and relative to an internal expression control, which were PPIA and HPRT in all the experiments. For the gene studies of different animals the control condition was set to 1. Data were calculated according to the delta-delta-CT method.

Real-time PCR reactions were set up as follows:

Component	**Volume / 15 µl reaction**
Template cDNA	0.75 µl
Forward primer	0.375 µl (5 pmol/µl)
Reverse primer	0.375 µl (5 pmol/µl)
2x SYBR-Green Supermix	7.5 µl
Aqua bidest	6 µl

Program:

Cycle step	Temperature	Time	Number of cycles
Denaturation and polymerase initiation	95 °C	5 min	1
Denaturation Annealing Extension	95 °C 59 °C 72 °C	30 s 20 s 20 s	40
Melt curve	55 °C to 95 °C (+0.5 °C increase per cycle)	30 s	81

3.5 Biochemical Methods

3.5.1 Protein extraction

For total protein extracts, 5×10^6 cells, one to two embryos (E10.5) or 1-5 mg tissue was lysed in 200 - 500 µl of cold RIPA buffer with complete protease inhibitors by ultrasonication (3x 30 sec, on ice) or using the Precellys homogenizer. The homogenate was centrifuged at 13200 rpm for 15 min at 4 °C. The supernatant was transferred to a fresh 1.5 ml tube and stored at -80 °C.

For performing an SDS-PAGE, gel loading buffer was added to the lysates, resulting in 1x concentration, samples were boiled for 5 min and centrifuged shortly at room temperature.

3.5.2 Measurement of protein concentration using BCA-test

To determine the concentration of protein extracts the BCA Protein Assay kit was used. Reactions and standard curves were carried out as described in manufacturer's manual. Blank value determination was done with 950 µl working solution with 50 µl aqua bidest. After 30 min incubation at 37 °C, protein concentrations were measured at 562 nm.

3.5.3 Gel electrophoresis and transfer of proteins

3.5.3.1 SDS-PAGE and native PAGE

Proteins can be separated using polyacrylamide gels. To efficiently separate proteins of different sizes, acrylamide can be used in different concentrations, which results in different pore sizes. SDS-PAGE was carried out when denaturating conditions were required to separate proteins according to their size. Basic native PAGE was used to analyze the composition of oligomeric proteins in their native state. In this thesis, concentration of the resolving gels varied from 10 % to 15 %. Electrophoresis was carried out at 80 - 120 V.

Composition separating layer	**SDS-acrylamide gel (5 ml, 12 %)**	**Native gel (12 ml, 12.5 %)**
H_2O	1.9 ml	4 ml
30 % acrylamide mix	1.7 ml	5 ml
1 M Tris pH 8.8	1.3 ml	3 ml
SDS (10 % stock)	50 µl	---
APS	50 µl	84 µl
TEMED	3 µl	7 µl

Composition stacking layer	**SDS-acrylamide gel (1 ml, 5 %)**	**Native gel (7 ml, 4.3 %)**
H_2O	0.68 ml	5 ml
30 % acrylamide mix	0.17 ml	1 ml
1.5 M Tris pH 6.8	0.13 ml	1 ml
SDS (10 % stock)	10 µl	---
APS	10 µl	40 µl
TEMED	1 µl	8 µl

For the mobility shift assay of Ca^{2+} binding proteins the final concentration of EGTA was 1 mM and of $CaCl_2$ 50 µM for all gels and the running buffer.

3.5.3.2 Western Blot

For antibody detection, separated proteins by SDS-PAGE were transferred to a PVDF membrane. The membrane was activated with methanol for 1 min and equilibrated in transfer buffer. It was placed on the gel and layered in between of a stack of whatman paper and two foam pads, which were equilibrated in transfer buffer as well. The membrane was oriented to the anode, whereas the gel was oriented to the cathode. In addition to the holder, an ice-block was placed into the tank blotting apparatus and the tank was filled with transfer buffer. Electro blotting was carried out for 1 h at 100 V. The transfer efficiency of total protein was checked by Ponceau S staining, which was washed out with aqua bidest.

3.5.3.3 Antibody binding and ECL detection

After the transfer of proteins to the membrane, incubation with 5 % milk powder in TBST was carried out for at least 1 h. Primary antibodies in TBST with 5 % milk powder were added to the membrane, followed by o/n incubation at 4 °C. After that, the membrane was washed 3 times for 5-10 min in TBST before incubation with the second antibody, which lasted 1h. After several washing steps, the chemoluminescence produced by the HRP-coupled secondary antibody could be detected on an X-Ray film after the ECL substrate was poured on the membrane. X-ray films were developed in a Curix60 developer.

3.5.4 Co-Immunoprecipitation

For immunoprecipitation, lysates were prepared in cold non-denaturating lysis. Co-immunoprecipitation assays were performed using the immunoprecipitation starter pack. Protein A Sepharose 4 Fast Flow beads and Protein G Sepharose 4 Fast Flow beads were washed three times with an equal volume of lysis buffer. The Sepharose beads were pelleted by centrifugation at 12,000 x g for 30 sec and the supernatant was discarded. Protein lysates were prehybridized with 100 µl of Sepharose beads in order to pre-clear the lysate of proteins binding unspecifically to the beads. 2-5 µg of the antibody of interest or the

same amount of the corresponding IgG normal, respectively, as well as 200-500 µg of total protein were incubated for 1 h at 4 °C with rotation in a final volume of 250-500 µl. The antibody conjugate was immunoprecipitated with 100 µl of either Protein G or Protein A Sepharose beads for 1-3 h at 4 °C with rotation. Unbound proteins were removed by washing four times with 500 µl of lysis buffer. Immunoprecipitated proteins bound to the Sepharose beads were eluted by adding 30 µl 1x gel loading buffer and boiling for 5 min. The eluate was centrifuged at 12,000×g for 30 sec, and the supernatant containing the coimmunoprecipitated proteins was used for SDS-PAGE followed by Western-blot analyses.

3.5.5 Phosphorylation analysis of NFATc1

Cells were transfected with NFATc1-HA alone or together with Creld1-Flag for 16-22 hrs. For cyclosporine A experiments, cells were pre-treated for at least 30 min before transfection. After harvesting the cells, they were lysed by a Precellys homogenizer. Protein lysates were loaded on a Novex 4-12% Bis-Tris Gel.

3.6 Histochemistry

Embryos or organs were fixed for one to three days, in 4% Paraformaldehyde at 4 °C. Dehydration was performed using increasing percentages of ethanol (60 %, 70 %, 80 %, 90 %, 96 %, 100 %) and xylol, followed by embedding in paraffin.

For immunohistochemical stainings sections were deparaffinized and endogenous peroxidase activity was blocked using 1.2% of H_2O_2 in methanol. Then, sections were cooked three times 5 min in citrate buffer (10 mM, pH 6) in a microwave and treated 15 min with trypsin for antigen retrieval. To block unspecific binding sites, sections were prehybridized of with 5% BSA and 10 % donkey serum in PBS for 1 h followed by incubation with the primary antibody (in 5 % BSA in PBS) over night at 4 °C. As secondary antibody, HRP-conjugated antibody was incubated for 1 h at room temperature (1:100). Nova Red was used for color development and hematoxylin solution was used for

counter staining of nuclei.
For immunofluorescence sections were deparaffinized and rehydrated, followed by antigen retrieval. For antigen retrieval of Creld2 stained sections, the slides were incubated for 45 min at 85 °C instead of cooking them. For immunocytoshemisty, cells were fixed with 4 % paraformaldehyde and permeabilized with PBT. After prehybridization, sections and cells, respectively, were incubated o/n at 4 °C with primary antibodies. Primary antibodies were detected with fluorescent-labeled antibodies conjugated with Alexa488, Alexa546 or Alexa633. Sections and cells were mounted in DAPI-Fluoromount G.

3.7 Cell culture

Cells were cultured in DMEM or RPMI containing 10 % Fetal Calf Serum and 1 % Penicillin/Streptomycin. Transfection of NIH3T3 and HEK239 cells was performed using Metafectene pro and Opti-MEM. Transfection of Jurkat T cells was performed by electroporation.

3.7.1 Live cell imaging

Cells were grown in 8-well chamber slides. NFATc1-GFP and Creld1-RFP constructs were transfected with Metafectene pro for 16-22 hrs. Cells were treated with 0.1 µM thapsigargin or 1 µM cyclosporine A that were added simultaneously with the transfection solution.

3.7.2 Fluorescent protease protection (FPP) assay

YFP-PrP and CFP-CD3δ vectors were kindly provided by Holger Lorenz. Assay was performed as published earlier[59]. Working solution for trypsin was 4 mM and for digitonin was 100 µM.

3.7.3 Luciferase assay

HEK239 cells were transfected with pGL3-NFAT-luc[60], the psiCHECK-1 (Promega) and the FLAG-tagged Creld1 contructs. Concentrations were as follows: phorbol myristate acetate (PMA): 20 ng/ml, ionomycin: 1 µM, cyclosporine A: 1 µM. HEK293 cells were incubated for 5 h in DMEM + 10 % FCS. Assay was performed with the Dual-Glow Luciferase Assay system and the luminescence was detected using the Fluostar Omega. For analysis, firefly activity (NFAT-luc) was normalized to the renilla activity (psiCHECK1). Data sets were normalized to ctrl+DMSO and expressed as relative luciferase activity (%).

3.7.4 Flow cytometry

3.7.4.1 Primary cell culture

Splenic and thymic primary cell cultures were isolated from freshly sacrificed mice. Spleen and thymus were dissected and put into 4 ml ice-cold PBS. Organs were smashed with the blunt end of a 5 ml syringe plunger and strained through a 100 µm strainer to obtain single cells. Splenic cells were centrifuged for 5 min at 500 g and then incubated with red blood cell lysis buffer for 2 min. Lysis was stopped by addition of PBS. Cells were centrifuged again and resuspended in 4 ml PBS.

3.7.4.2 Antibody staining and FACS

1 ml each of thymic or splenic cell culture was added to two fluorescence activated cell sorting (FACS) tubes. One tube of each genotype served as unstained control. The staining of the antibodies was done at 4 °C for 30 min in a total volume of 100 µl. Staining of compensation beads with single antibodies was done simultaneously to the antibody incubation. Compensation ensures the integrity of the experimental data. Fluorescence acquisition was performed with a flow cytometer.

3.7.5 Homologous recombination in ES-cell culture

3.7.5.1 ES-cell culture

HM-1 embryonic stem (ES)-cells were kindly provided by AG Magin. HM-1 cells grew feeder independent on 0.1 % gelatin coated surfaces. Medium was changed every 24 hours. To maintain the culture, cells were split 1:4 – 1:6. For growing clones, cells were resuspended with a 1 ml pipette from 48-well to 6-well. Centrifugation steps were done for 5 min at 800 rpm.

Trypsinization:

Dish	0.1% gelatin	Medium/ end volume	PBS	Trypsin	Medium for stopping trypsinization
48-Well	100 µl	0.5 ml	0.5 ml	100 µl	0.5 ml
24-Well	250 µl	1.5 ml	1.0 ml	250 µl	1.0 ml
12-Well	500 µl	2.5 ml	2.0 ml	400 µl	1.0 ml
6-Well	1 ml	5-7 ml	3.0 ml	1.0 ml	4.0 ml
T 25	3 ml	7.0 ml	3-5 ml	1.5 ml	5.0 ml
T 75	6 ml	25-35 ml	7-10 ml	3.0 ml	7.0 ml
10 cm	6 ml	10 ml			

3.7.5.2 ES-cell transfection

HM-1 cells were grown confluent in a T75-flask, trypsinized and resuspended in HBS buffer. Cells were counted and diluted so that the cell number was 30 Mio. per 0.8 ml. 200-350 µg DNA was mixed with HM-1 cell and transferred into a cuvette. Cells were electroporated at 0.8 kV and 3µF. Cells were diluted in 20 ml culture medium and split on 10 cm dishes:

Dish #	x ml of cells	~ cell number
1-4	0.5	750000
5-16	1.0	1.5 Mio
17-20	1.5	2.2 Mio
21 Control	0.1	150000
22 Control	0.05	75000

Selection with G418 containing media was started 24 hours after transfection. Medium was changed every 2-3 days. Cells on control dish #21 were kept in culture medium without G418. Selection was stopped when clones grew big enough to be picked.

3.7.5.3 Picking of ES-cell clones and PCR

Approximately 2 weeks after electroporation ES-cell clones can be picked. This was done mechanically with a 200 µl pipet by scratching the clone off the dish with simultaneous sucking of the cells into the tip. Each clone was transferred into a 48-well dish. Clones were split every three to five days into a bigger dish. During the step from the 48-well to the 24-well dish a part of the cells was used for a PCR reaction. Therefor cells were pelleted and resuspended in lysis buffer and incubated at 55 °C o/n in a water bath. For the PCR 10 µl of lysed cells were added to the reaction tube.

Component	**Volume / 20 µl reaction**
H_2O	5.5 µl
5x Green GoTaq reaction buffer	4 µl
10 mM dNTPs	0.2 µl
Forward primer	0.1 µl
Reverse primer	0.1 µl
ES cell DNA	10 µl
GoTaq DNA Polymerase (5 U/µl)	0.1 µl

Program:

Cycle step	**Temperature**	**Time**	**Number of cycles**
Initial denaturation	95 °C	30 s	1
Denaturation Annealing Extension	95 °C 58 °C 72 °C	20 s 20 s 2 min	35
Final extension	72 °C 4 °C	5 min hold	1

3.7.5.4 Karyotyping

PCR-positive ES-cells were grown up to a T25 flask. Cells were incubated with 2 µg/ml colcemid for 1 hour in the incubator. Cells were washed, trypsinized and pelleted. The pellet was resuspended in 1 ml 0.56% KCl and incubated for 10 min. Cells were centrifuged and resuspended twice in ice-cold methanol/acetic acid (3 vol + 1 vol). After the third centrifugation step, cells were dropped on slides from a height of 10 – 30 cm. Thereby, nuclei burst and are visible under the microscope. Slides were air-dried and stained with Giemsa. Chromosomes of at least 10 cells per clone were counted. The genome of *Mus musculus* comprises of 40 chromosomes.

3.7.5.5 Isolation of ES-cell DNA

For Southern blot analyses, big amounts of genomic ES-cell DNA are needed. Therefore, cells were grown confluent in T25 flasks, washed twice with PBS and lysed in 1.5 ml lysis buffer containing 1 mg/ml Proteinase K and 200 µg/ml RNase. Cells were kept for 2-3 days in a water bath at 55 °C. DNA was precipitated with isopropanol, washed twice with 70 % ethanol, air-dried and resuspended in aqua bidest.

3.7.5.6 Southern blot

DNA of PCR-positive ES cell clones was digested by incubation with restriction endonucleases (700 ng DNA per digest). This mixture was separated according to length by agarose gel electrophoresis (0.7% agarose, maxi gel, 200V) and the resulting band pattern was documented next to a fluorescent ruler. Then, the gel was depurinated for 10 min in 0.25 M HCl washed briefly with water, and denatured for 30 min in 1.5 M NaCl + 0.5 M NaOH. The DNA was subsequently transferred onto a nitrocellulose membrane. After the blotting, the membrane was washed briefly in 2x SSC and air-dried. The DNA was immobilized on the membrane by UV crosslinking. The probes were labeled with ^{32}P using the Multiprime-DNA labeling system according to manufacturers' instructions.

Probes were purified through Sephadex G50 columns and denatured by boiling

for 5 min. The membrane was prehybridized in 10 ml QuickHyb for 1 hour at 68 °C. Subsequently, the single-stranded probe was added to the QuickHyb solution and the membrane was incubated further for 90 min at 68 °C. The membrane was washed with SSC containing 0.1% SDS in a 68°C water bath, starting with a 2x solution and lowering the concentration to 0.1x. The radioactivity of the washing solution and the membrane itself was monitored with the Geiger-Müller counter after each washing step until the signal from the membrane was reduced to 200 to 300 cpm.
The membrane was placed in a developing cassette with an intensifying screen in-between two x-ray films and incubated o/n at -80°C. Films were developed in a Curix60 developer.

3.8 Work with Mus musculus

3.8.1 Animal housing

Mice were kept under standard SPF housing conditions with a 12 h dark/light cycle and with food and water *ad libitum*. Genotyping was performed using isolated DNA obtained from tail tips. *Creld1KO* mouse line as ordered from KOMP (project ID: VG12264).
Primers for detection of the neomycin cassette of *Creld1KO*$^{w/neo}$ were neo_fw and neo_rev; transgenic band 275 bp. Primers for *Creld1KO* were gt_fw, gt_rev and gt_lacZ; transgenic band 403 bp, wildtype band 484 bp.
Primers for detection of the neomycin cassette of *Creld2KO*$^{w/neo}$ were neo2_fw and gt2_rev; transgenic band 189 bp. Primers for *Creld2KO* were gt2_fw and gt2_rev; transgenic band 374 bp, wildtype band 253 bp.

3.8.2 Endothelial-to-mesenchymal transformation (EMT) assay

The EMT was performed as described elsewhere[61].Briefly, heart explants of E9.5 embryos were placed on collagen, where they were allowed to adhere before adding media. Migrating mesenchymal cells were counted after 48 hours.

3.8.3 Stainings

3.8.3.1 H&E

Organs were fixed for one to three days, in 4% Paraformaldehyde at 4 °C. Dehydration was performed using increasing percentages of ethanol (60 %, 70 %, 80 %, 90 %, 96 %, 100 %) and xylol, followed by embedding in paraffin. Sections were deparaffinized and rehydrated. Staining with eosin was performed for 3 min. Sections were washed briefly in VE water and then transferred to the hematoxylin solution for 1 min. After a washing step in VE water, the samples were washed with running tap water. Slides were dehydrated and mounted with Entallan.

3.8.3.2 Oil-Red-O

Organs were mounted in Tissue-Tek, cut with the cryostat (6-14 µm) and fixed in 4 % PFA. After a washing step with running tap water (1 min) the slides were rinsed in 60 % isopropanol. The staining was performed with a freshly prepared Oil-Red-O working solution (filtered solution of 30 ml of the stock stain and 20 ml of aqua bidest) for 15 min. Slides were rinsed with 60 % isopropanol and lightly stained with hematoxylin. After a last washing step the slides were mounted in Fluoromount.

4 Results

4.1 Creld1

4.1.1 Creld1 expression pattern and subcellular localization

According to its primary structure, Creld1 has been proposed as a cell adhesion protein, with its functional domains facing the extracellular space[1]. The subcellular localization of Creld1 was examined by immunoflourescent staining using a mouse fibroblast cell-line (NIH3T3). Endogenously expressed Creld1, detected with a Creld1-specific antibody, co-localized with a marker for the endoplasmic reticulum (ER, Fig. 4-1a). The heterologously expressed protein showed a similar localization (Fig. 4-1b).

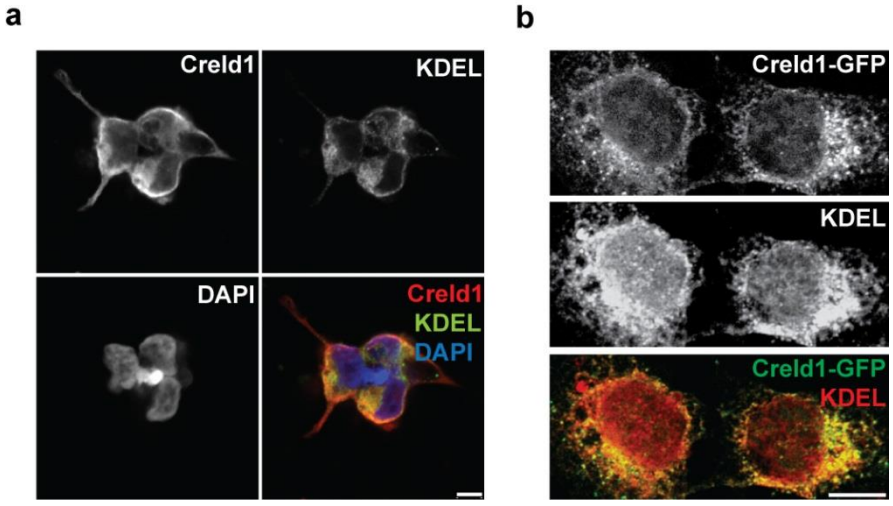

Fig. 4-1 Creld1 is localized at the ER. (**a**) Endogenous expression of Creld1 in NIH3T3 cells detected with an Creld1-specific antibody (red). Overlapping signals (yellow) with the ER marker KDEL (green) indicate localization at the ER. Scale bar indicates 20 µm. (**b**) Creld1 tagged with green fluorescent protein (GFP, green) also co-localizes with the ER marker KDEL (red) in NIH3T3 cells. Scale bar indicates 20 µm.

To further elucidate the cellular localization of Creld1, a fluorescence protease protection (FPP) assay was performed (Fig. 4-2). This assay was designed to determine the topology and localization of transmembrane proteins by using the restricted proteolytic digestibility of GFP-tagged proteins[62]. First, it was tested whether Creld1 indeed is a membrane protein at the ER. Therefore, the ER resident CD3δ protein tagged with a cyan fluorescent protein (CFP) with the fluorophore facing the cytosolic side of the ER was used as a control. Images were taken before and after permeabilization of the plasma membrane with digitonin and treatment with trypsin. The fluorescence of CD3δ-CFP was readily diminished after incubation with digitonin and trypsin (Fig. 4-2a). Similarly, the fluorescence of RFP fused to the C terminus of Creld1 decreased after treatment with digitonin and trypsin, indicating that the C terminus of Creld1 faces the cytosolic site (Fig. 4-2a). Next, it was tested whether the C terminus of Creld1 is facing the extracellular space (Fig. 4-2b), as has been proposed by Rupp et al.[1]. As a control, cells were transfected with YFP-PrP, a fusion between the GPI-anchored prion protein (PrP) and the yellow fluorescent protein (YFP)[62].

Here, the YFP is facing the extracellular space. After treatment with trypsin, the distinctive fluorescence at the cell surface disappeared (Fig. 4-2b). In contrast, cells expressing Creld1 with a green fluorescent protein (GFP) attached to its C terminus showed no change in fluorescence after trypsin treatment (Fig. 4-2b), indicating that the C terminus is not accessible from the extracellular side.

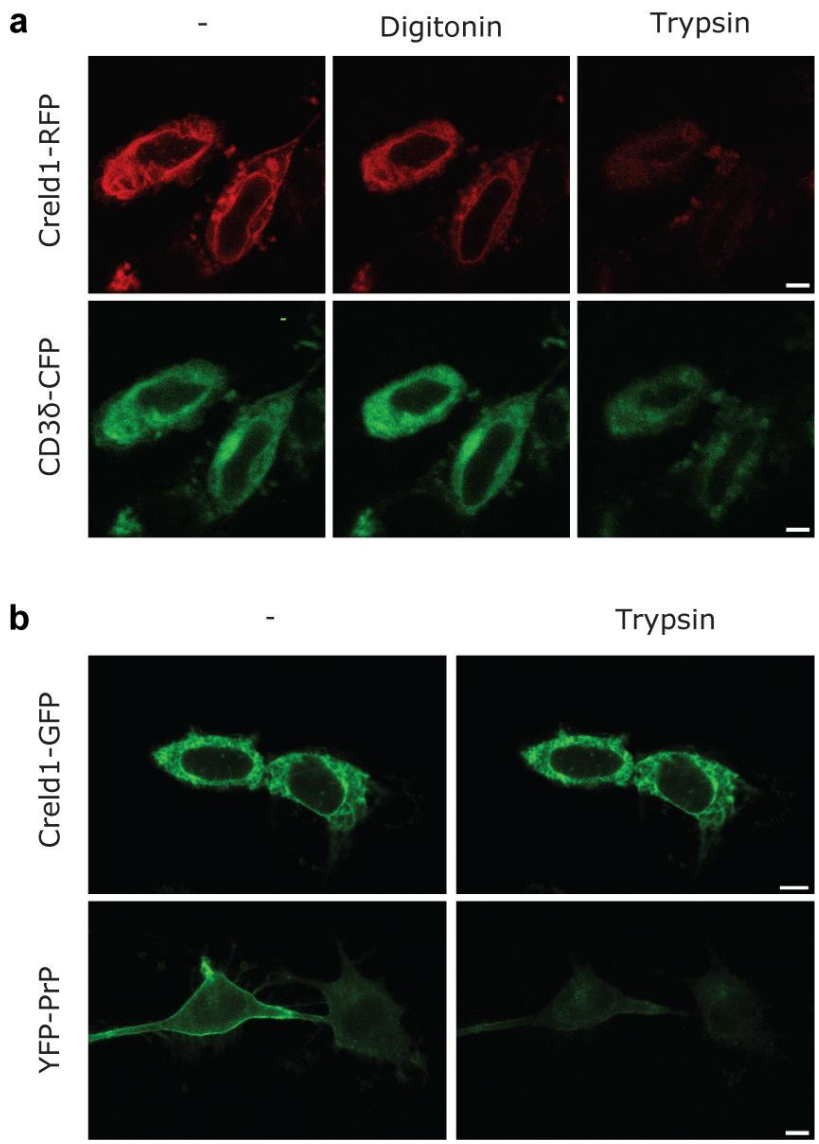

Fig. 4-2 Fluorescence protease protection assay. (**a**) NIH3T3 cells expressing Creld1-RFP or CD3δ-cyan fluorescent protein (CFP), an ER transmembrane protein with CFP located at the cytosolic site, were treated first with 100 µM digitonin and subsequently with 4 mM trypsin. The fluorescence was diminished for both constructs, indicating that the C terminus of Creld1 is facing the cytosol. Pictures were taken 1 min after treatment with digitonin and trypsin, respectively. (**b**) NIH3T3 cells expressing Creld1-GFP or yellow fluorescent protein (YFP)-PrP, a plasma membrane protein with an extracellular YFP-tag, were treated with trypsin for 1 min. Only the YFP-signal is lost, indicating that the C terminus of Creld1 is not located outside the cell. Scale bars indicate 10 µm.

Taken together, these data support the view that Creld1 is localized at the ER, with the C and N terminus facing the cytoplasm (Fig. 4-3).

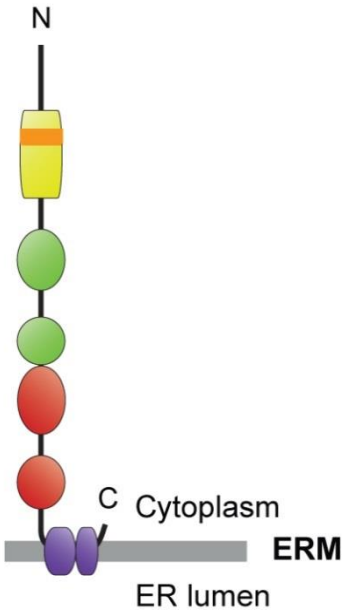

Fig. 4-3 Assumed membrane topology of Creld1. Its N and C termini are facing the cytoplasm. Domains are indicated as in Fig. 1-1a.

4.1.2 Non-conditional *Creld1KO* mouse

The non-conditional *Creld1* knock-out mouse (*Creld1KO*) was obtained from the Knock-Out Mouse Project (KOMP) Repository. The *Creld1* locus consists of ten exons. All exons were replaced with a lacZ and a floxed neomycin resistance-cassette (neoR) by homologous recombination using a BAC-based targeting vector (Fig. 4-4a). Integration of the vector and deletion of the neomycin cassette was confirmed by PCR (Fig. 4-4b). Absence of the Creld1 protein in homozygous *Creld1KO* embryos was confirmed by Western blot using a Creld1 specific antibody (Fig. 4-4c).

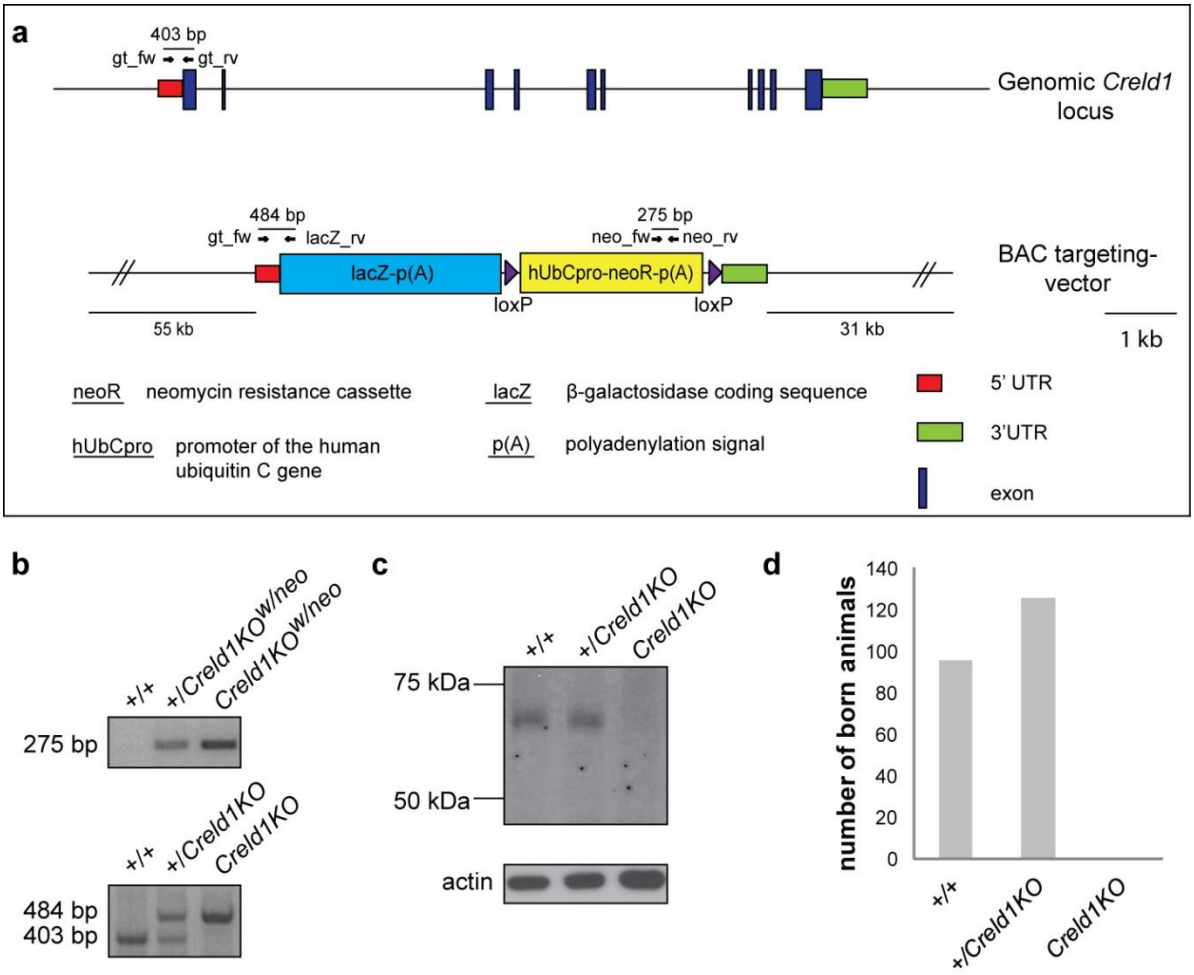

Fig. 4-4 Non-conditional *Creld1KO*. (a) Murine genomic Creld1 locus was replaced with a lacZ cassette and a floxed neoR by homologous recombination using a BAC targeting vector. Primers used for genotyping PCR are indicated **(b)** PCR analysis of wildtype (+/+), heterozygous (+/*Creld1KO*), and homozygous knockout (*Creld1KO*) animals. Mice with neoR in the *Creld1* locus are referred to as w/neo. **(c)** Western-blot analysis of +/+, +/*Creld1KO,* and *Creld1KO* total lysates from E10.5 embryos using an anti-Creld1 specific antibody. **(d)** Animals born from heterozygous matings. No *Creld1KO* mice were observed indicating embryonic lethality. UTR: untranslated region.

4.1.3 Phenotype analysis of *Creld1KO* mouse

Matings of heterozygous *Creld1KO* mice resulted only in wildtype and heterozygous pups (Fig. 4-4d). Isolation of embryos at different developmental stages revealed that *Creld1KO* mice die between E11.0 and E11.5 (Fig. 4-5a, b). *Creld1KO* and wildtype embryos develop similarly until E10.5. However, *Creld1KO* have a strong developmental delay at E11.0 (Fig. 4-7b, c) and at E11.5 they are already dead and start to be degraded (Fig. 4-5a).

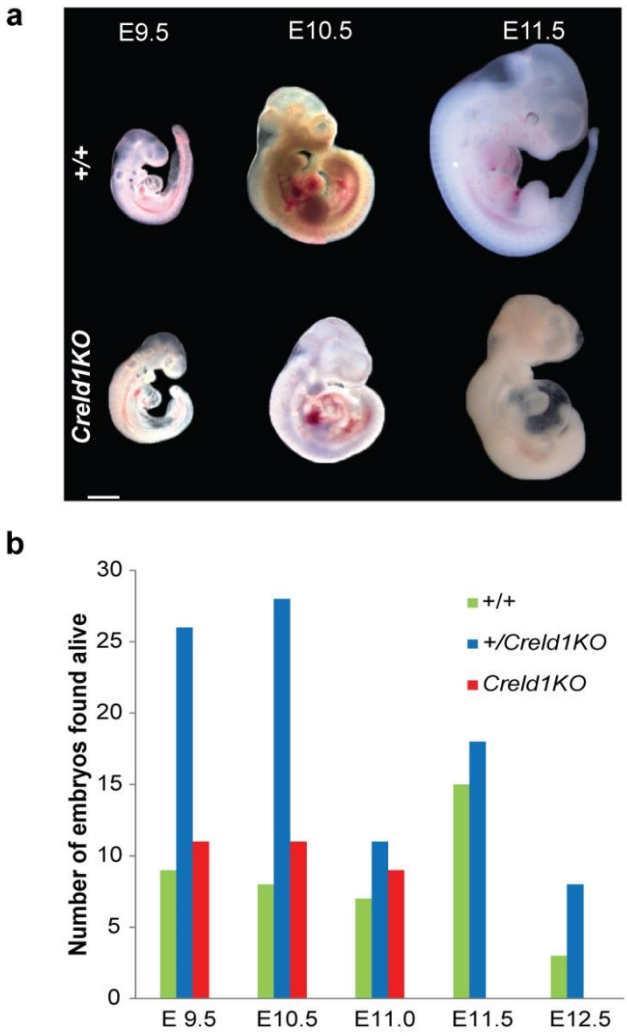

Fig. 4-5 Development of wildtype (+/+) and *Creld1KO* embryos between E9.5 and E11.5. (a) Development of *Creld1KO* embryos is delayed. At E11.5, they are already dead and start to be degraded. Scale bar indicates 1 mm. **(b)** Survival rates of wildtype, heterozygous, and homozygous embryonic mice at different stages of development. Lethality occurs between E11.0 and E11.5.

hCRELD1 has been described to be a risk factor for AVSD patients[11,12]. *Creld1* is highly expressed in the embryonic heart. At E9.5, Creld1 is expressed in the myocardium (Fig. 4-6). At E10.5 and E11.5, expression is also detected also in the endocardium (Fig. 4-6b, c).

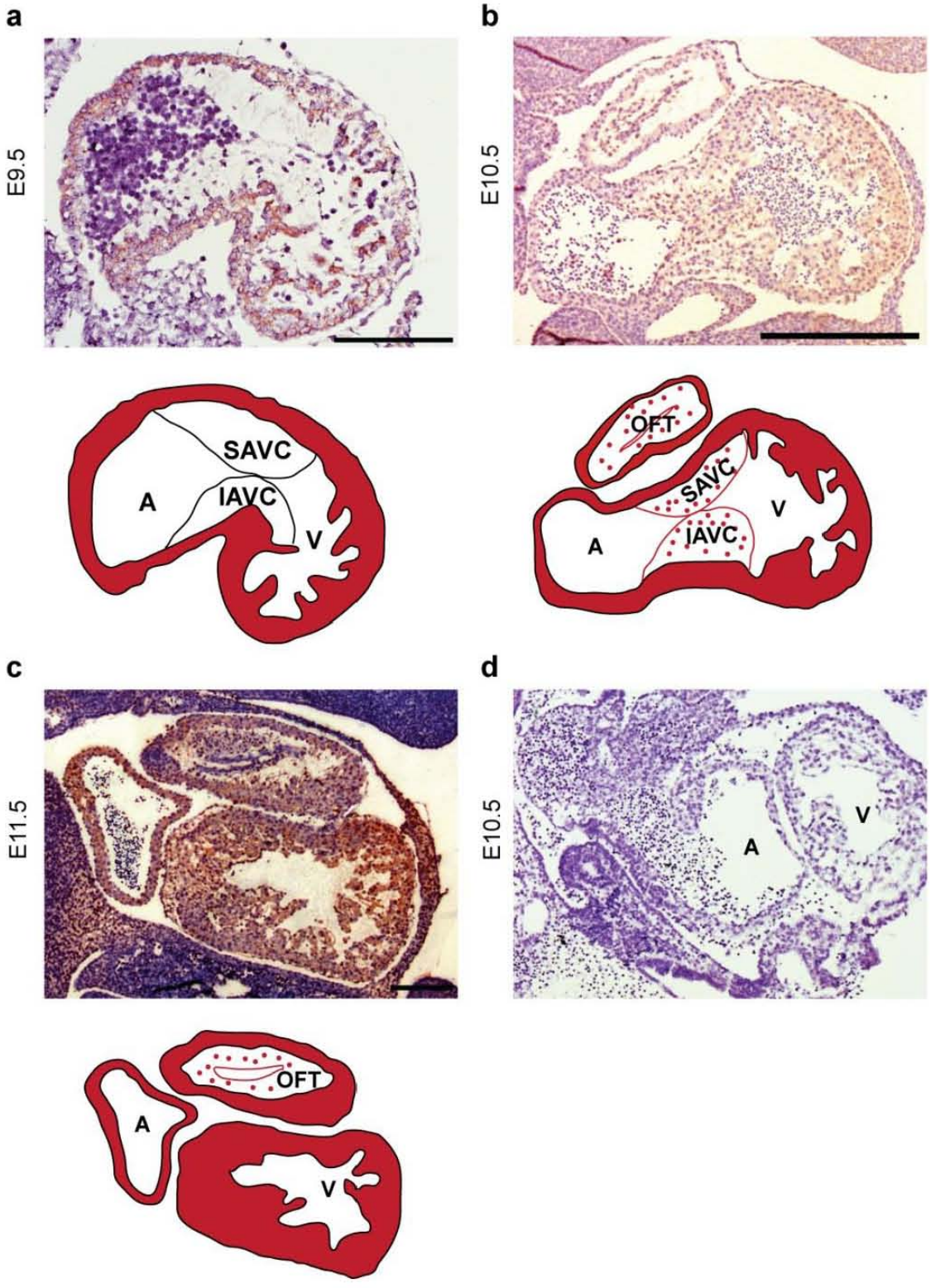

Fig. 4-6 Creld1 protein expression in the embryonic heart at E9.5 (a) E10.5 (b), and E11.5 (c). (a-c) Stained regions are depicted in red in the diagrams under the respective picture. At E9.5, Creld1 is exclusively expressed in cardiomyocytes. At E10.5 and E11.5, Creld1 is also observed in the atrioventricular and outflow tract cushions as well as in the endocardium. **(d)** Creld1 staining of a *Creld1KO* heart at E10.5. Scale bars indicate 200 µm. A: atrium, IAVC: inferior atrioventricular cushion, OFT: outflow tract, SAVC: superior atrioventricular cushion, V: ventricle.

Thus, *Creld1KO* embryos were analyzed for a defect in heart development. First, the heart beat frequency was examined. At E10.5, *Creld1KO* hearts beat significantly slower than wildtype hearts (Fig. 4-7a). As a consequence at E11.0, blood flow in the amnion sac was absent and blood clots in the head and tail region were observed (Fig. 4-7b). Furthermore, blood cells accumulated around the heart and the pericardial sac was immensely dilated (Fig. 4-7b).

Moreover, the development of *Creld1KO* hearts arrested at E11.0: whereas wildtype hearts already showed the typical four-chambered heart with two atria and two ventricles, *Creld1KO* hearts still displayed the shape of a tube with one common atrium and the immature left and right ventricle (Fig. 4-7c).

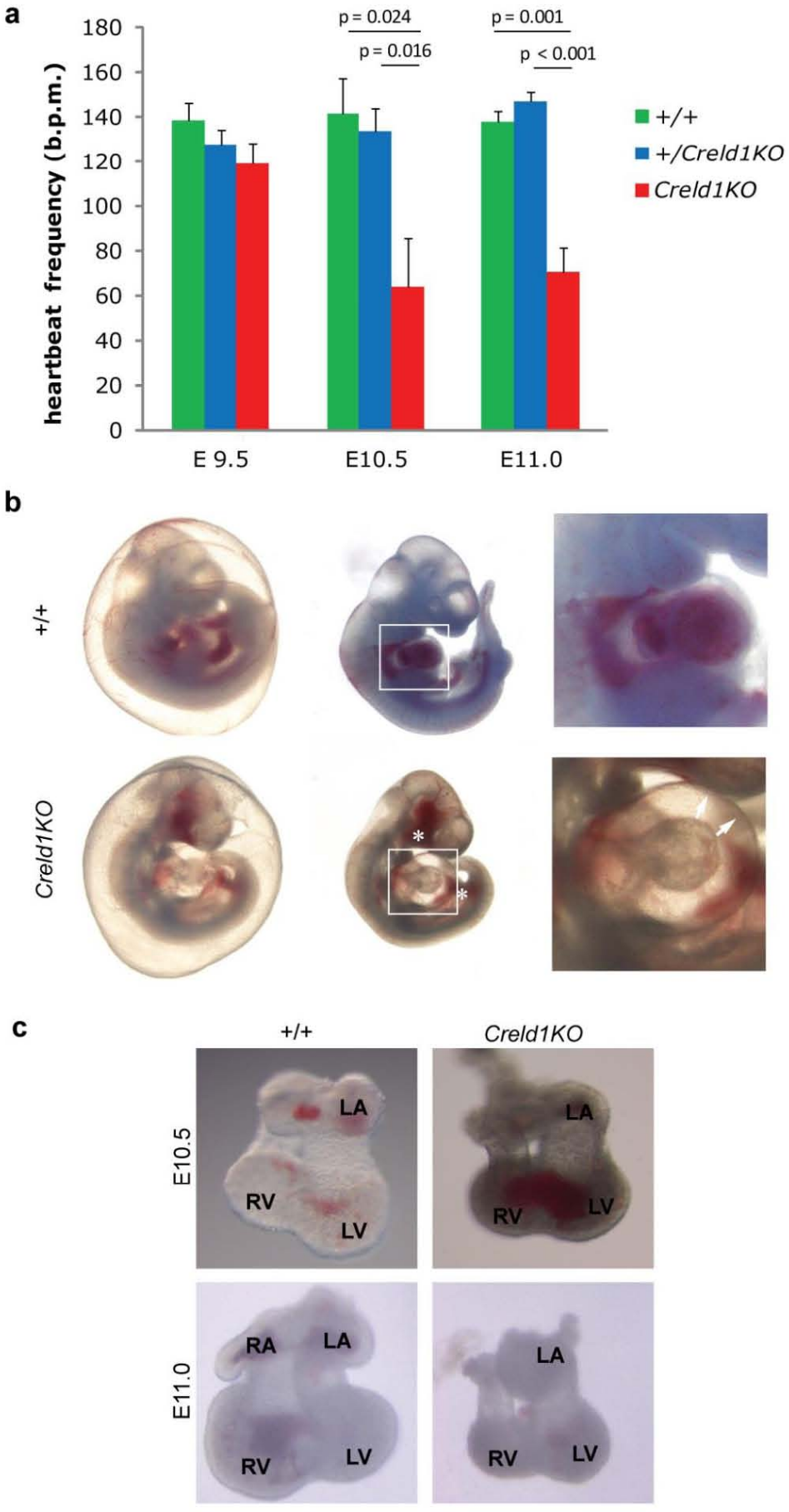
a
heartbeat frequency (b.p.m.)
180
160
140
120
100
80
60
40
20
0
p = 0.024
p = 0.016
p = 0.001
p < 0.001
+/+
+/Creld1KO
Creld1KO
E 9.5
E10.5
E11.0
b
+/+
Creld1KO
c
+/+
Creld1KO
E10.5
E11.0
LA
RV
LV
RA

Fig. 4-7 Heart-development defects in *Creld1KO* embryos. (a) Heartbeat frequency of wildtype (+/+), heterozygous *(+/Creld1KO*), and homozygous (*Creld1KO*) hearts. Hearts from *Creld1KO* embryos isolated at E10.5 and E11.0 beat significantly slower than +/+ or *+/Creld1KO* hearts. **(b)** Defects in *Creld1KO* embryos at E11.0. *Creld1KO* embryos are smaller, the amniotic sac is not supplied with blood, and the embryos develop blood clots, as seen in the head region, and sometimes in the tail region (asterisks). A detailed view of the heart region (indicated as a white box) shows a dilation of the pericardial sac (arrows) as well as blood cells that are located in the lumen between the sac and the heart. **(c)** *Creld1KO* hearts show an arrest in development at E10.5. Whereas hearts of wildtype embryos form two atria and two ventricles, *Creld1KO* hearts remain in a tubular form with only one atrium and the immature ventricle.

To further investigate the defect in cardiac development, E10.5 *Creld1KO* embryos were analyzed for hypoxia due to the decreased heart rate. Indeed, the expression of several marker genes for hypoxia[63] was upregulated (Tab. 4-1).

Tab. 4-1 Expression level of hypoxia marker genes in E10.5 *Creld1KO* embryos. Gene expression-levels in whole embryos were analyzed by qRT-PCR. Expression in wildtype embryos is set to 1 and expression levels in *Creld1KO* embryos are presented as fold change compared to the wildtype. Data are presented as mean ± SEM; n = 3. Aldoa: aldolase A, Car9: carbonic anhydrase 9, Epo: erythropoietin, EpoR erythropoietin receptor, Glut-1: glucose transporter-1, Hk1: hexokinase 1, Hmbs: hydroxymethylbilane synthase, Ldha: lactate dehydrogenase A, Vegfa: vascular endothelial growth factor A.

Gene	Fold expression *Creld1KO*
Aldoa	4.3 ± 1.8
Car9	17.2 ± 4.1
Epo	2.2 ± 0.7
EpoR	3.1 ± 0.6
Glut-1	6.8 ± 2.0
Hk1	2.1 ± 0.4
Hmbs	1.5 ± 0.3
Ldha	2.8 ± 0.6
Vegfa	14.0 ± 3.1

Endocardial cushions are the precursors of the mature heart valves. To investigate whether the lack of *Creld1* affects heart-valve development, cushion formation was examined (Fig. 4-8). To minimize the possibility of the defects in cushion formation being secondary to the growth retardation observed at E11.0, wildtype and *Creld1KO* hearts were compared at E10.5. Hearts of wildtype and *Creld1KO* embryos were stained with hematoxylin/eosin and analyzed for cushion formation.

Creld1KO embryos displayed severe hypocellular AVCs (Fig. 4-8b). Quantitative analysis of mesenchymal cell number revealed that *Creld1KO* embryos had significantly fewer cells in the AVC compared to wildtype controls (Fig. 4-8c). To investigate whether the low cell number was due to a defect in EMT, an EMT assay was performed (Fig. 4-8d)[61]. No significant difference could be observed in the number of migrating mesenchymal cells between wildtype and *Creld1KO* AVC explants (Fig. 4-8e). Thus, a defect in EMT does not seem to be responsible for the hypocellular AVCs. Another explanation for the reduced mesenchymal cell number could be a defect in cell proliferation. Proliferation is crucial during a growth period between E10.5 and E13.5 in mesenchymal and endothelial cells[64–66]. To visualize proliferating cells, tissue sections from embryonic hearts at E10.5 were stained with an antibody against p-Histone H3. In the AVCs of wildtype embryos, the endocardial and mesenchymal cells positive for the proliferation marker p-Histone H3 could be detected, whereas in sections from *Creld1KO* embryos, p-Histone H3-positive cells were lacking (Fig. 4-8f). These results demonstrate that at E10.5 the proliferation in the AVC of *Creld1KO* embryos is absent.

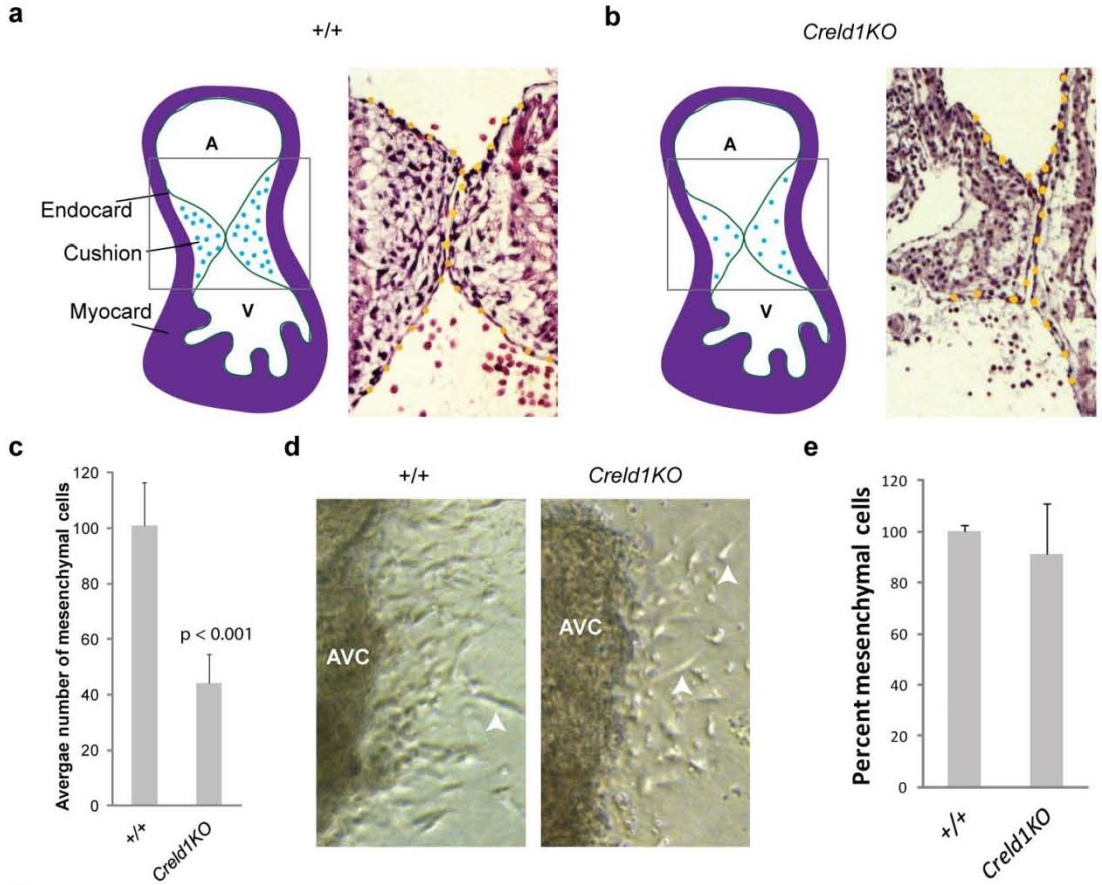
a
+/+
b
Creld1KO
A
V
Endocard
Cushion
Myocard
c
Avergae number of mesenchymal cells
120
100
80
60
40
20
0
p < 0.001
+/+
Creld1KO
d
+/+
Creld1KO
AVC
AVC
e
Percent mesenchymal cells
120
100
80
60
40
20
0
+/+
Creld1KO

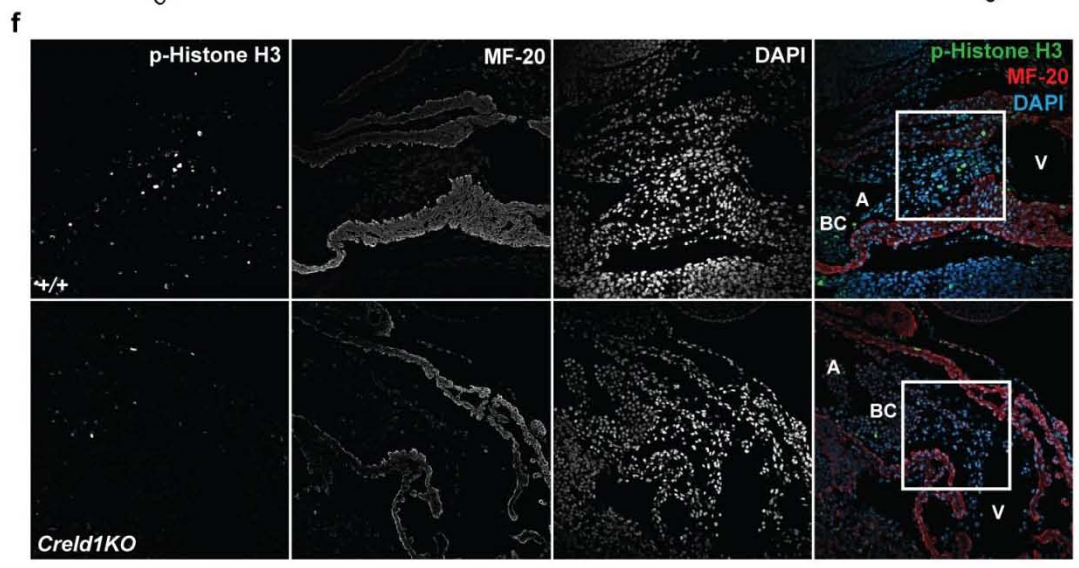
f
p-Histone H3
MF-20
DAPI
p-Histone H3
MF-20
DAPI
V
A
BC
+/+
A
BC
V
Creld1KO

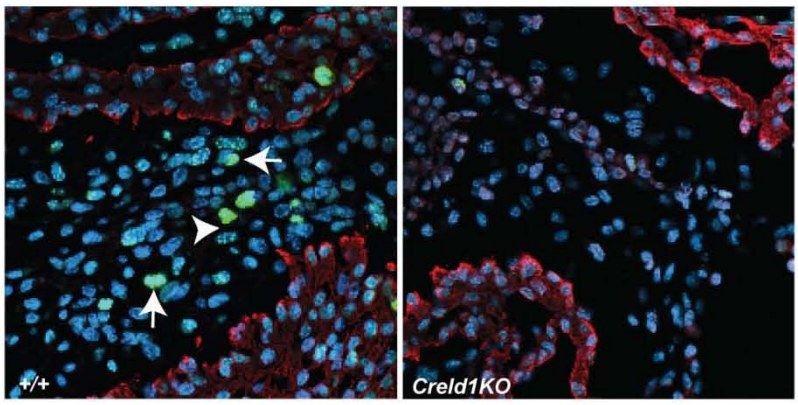
+/+
Creld1KO

Fig. 4-8 *Creld1KO* embryos display hypocellular AVCs. (a, b) Representative sections of wildtype (+/+) (a) and *Creld1KO* (b) hearts at E10.5 stained with hematoxylin/eosin. Dotted orange lines indicate the area of the AVC. Grey boxes in the diagram indicate area magnified in the staining. **(c)** Quantitative analysis of mesenchymal cell number in the AVC at E10.5. Sections presented in (a) and (b) were used for the analysis. Cell numbers were significantly reduced in *Creld1KO* embryos ($p = 0.001$). Data are presented as mean ± SEM; n = 3. **(d)** EMT assay, showing AVC heart explants of +/+ and *Creld1KO* embryos. Arrowheads indicate migrating mesenchymal cells. **(e)** Percentage of migrating mesenchymal cells observed after EMT assay. No significant difference could be detected between +/+ and *Creld1KO*. Data are presented as mean ± SEM; n = 3. **(f)** Expression of the proliferation marker p-Histone H3 in the AVC of E10.5 wildtype (top) and *Creld1KO* (bottom) embryos. Myocardium is stained with an antibody against MF-20. Nuclei are stained with DAPI. Magnification of AVC is indicated as a white box. In wildtype cells (+/+), p-Histone H3 (green) is visible in endocardial (arrowhead) and mesenchymal cells (arrows). In *Creld1KO* hearts, a staining is absent. A minimum of n = 3 has been analyzed for each genotype. A: atrium, BC: blood cells, AVC: atrioventricular cushion, V: ventricle.

4.1.4 The role of Creld1 in calcineurin/NFATc1 signaling during heart-valve formation

It has been shown that calcineurin/NFAT signaling is crucial for cardiac cushion formation and, thereby, for proper septation of the heart[67,68]. VEGFA-dependent activation of NFATc1 in endocardial cells at E10.5 initiates proliferation of endocardial and mesenchymal cells in the AVC[66]. *Creld1KO* embryos fail to proliferate at E10.5 and septation of the heart is lacking. Therefore, the interaction of Creld1 with the calcineurin/NFATc1 signaling pathway was analyzed *in vivo* and *in vitro*.

To induce expression of its downstream targets, NFATc1 needs to be dephosphorylated by calcineurin and consequently translocate to the nucleus[28,29,60]. Thus, the expression pattern of NFATc1 in the AVC of wildtype and *Creld1KO* embryos was examined. At E10.5, NFATc1 is solely expressed in endocardial cushion cells (ECC) of the AVC. In wildtype embryos, NFATc1 was mainly localized in the nucleus (Fig. 4-9a). In contrast, in *Creld1KO* embryos, NFATc1 was exclusively localized in the cytoplasm (Fig. 4-9a). Thus, lack of Creld1 abolishes nuclear translocation of NFATc1 in the ECCs of the AVC at

E10.5

To investigate whether the lack of NFATc1 nuclear translocation affects downstream signaling, the expression levels of NFATc1 downstream targets were analyzed by qRT-PCR and Western blot in isolated hearts of E10.5 embryos. The main NFATc1 target genes, namely *NFATc1* and *Regulator of calcineurin 1* (*Rcan1*)[69,70] were significantly downregulated in *Creld1KO* hearts (Fig. 4-9b). In line with this finding, Rcan1 protein-levels were diminished in *Creld1KO* hearts at E10.5 (Fig. 4-9c).

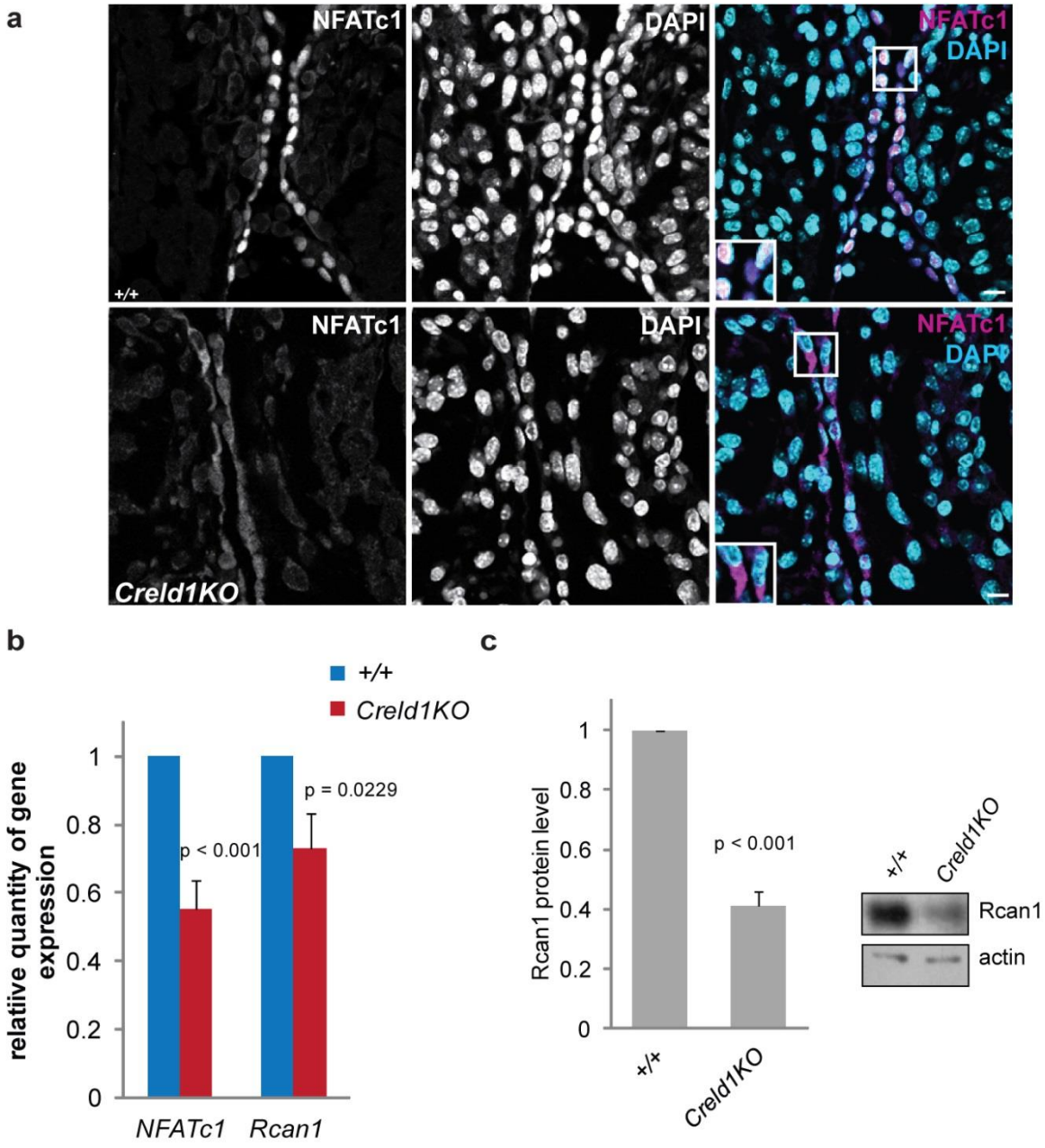

Fig. 4-9 NFATc1 activity is decreased in *Creld1KO* hearts. (a) NFATc1 expression in the endocardium of the AVC of E10.5 wildtype (+/+, top) and *Creld1KO* (bottom) embryos. In wildtype cells, NFATc1 (magenta) is mainly localized in the nucleus (stained with DAPI, cyan), whereas in *Creld1KO*, NFATc1 is predominantly found in the cytoplasm. Scale bar indicates 20 µm. **(b)** Gene expression in *Creld1KO* hearts at E10.5. Expression levels of wildtype hearts were set to 1. Two target genes of NFATc1, namely *NFATc1* itself and *Rcan1* were significantly downregulated. Data are presented as mean ± SEM; n = 6 for *Rcan1* and n = 8 for *NFATc1*. **(c)** Representative Western blot of wild-type (+/+) and *Creld1KO* isolated hearts at E10.5. Protein expression levels were quantified by setting expression of +/+ hearts to 1. Data are presented as mean ± SEM; n = 6.

4.1.5 Creld1 function in calcineurin/NFATc1 signaling *in vitro*

To investigate the effect of Creld1 on calcineurin/NFATc1 signaling in more detail *in vitro*, a fluorescently tagged NFATc1 (NFATc1-GFP) was used to study its localization in NIH3T3 cells by live-cell imaging. Without any stimuli, NFATc1 remained in the cytoplasm. When cells were treated with thapsigargin (Tg) to stimulate Ca^{2+} release from intracellular stores, thereby activating calcineurin, NFATc1 translocated to the nucleus (Fig. 4-10a, c). In the presence of heterologously expressed Creld1, NFATc1 translocated to the nucleus even in the absence of Ca^{2+} release from intracellular stores (Fig. 4-10b, c). The effect was diminished using the calcineurin inhibitor cyclosporine A (CsA) (Fig. 4-10b, c), demonstrating that Creld1 affects NFATc1 translocation through calcineurin.

Translocation of NFATc1 into the nucleus is dependent on its dephosphorylation by calcineurin. Thus, the phosphorylation state of NFATc1 was analyzed by Western blot. Phosphorylated NFATc1 was visualized as a slower migrating band and, thereby, with an apparent higher molecular weight compared to the faster migrating, dephosphorylated protein with a lower molecular weight (Fig. 4-10d). In control cells, NFATc1 was mainly phosphorylated (Fig. 4-10d). However, co-expression of Creld1 augmented the dephosphorylation of NFATc1, whereas addition of CsA reversed the effect, resulting in NFATc1 being mainly phosphorylated (Fig. 4-10d).

In the nucleus, NFATc1 acts as transcription factor by binding to the NFAT consensus-sequence 5'-GGAAA-3' [71,72]. To investigate whether Creld1 controls

NFATc1-dependent transcription, NFATc1 luciferase assays were performed with the luciferase gene being under the control of an NFAT-specific promoter (Fig. 4-10e, assays were performed by Dagmar Wachten). Creld1 overexpression increased the luciferase activity to 290 % (Fig. 4-10e). Treatment with phorbol myristate acetate (PMA) and ionomycin was used as a positive control to increase the intracellular Ca^{2+} concentration[60]. This treatment increased the luciferase activity to 343 % (Fig. 4-10e). In the presence of Creld1, the effect of PMA and ionomycin was even further enhanced (945 %, Fig. 4-10e). Presence of CsA reduced the action of Creld1 on luciferase activity (218 %, Fig. 4-10e).

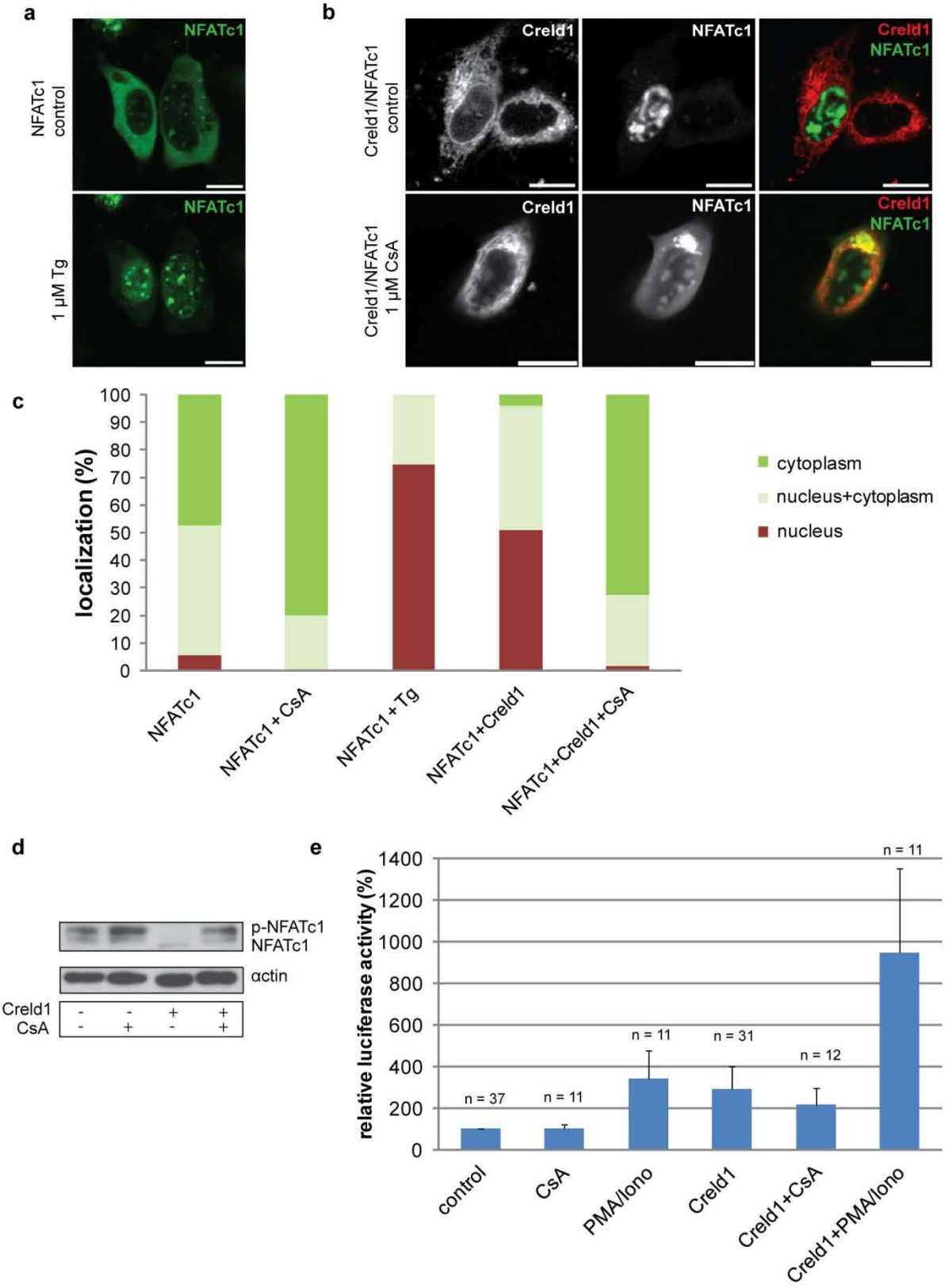
a
NFATc1
control
NFATc1
1 µM Tg
NFATc1
b
Creld1/NFATc1
control
Creld1
NFATc1
Creld1
NFATc1
Creld1/NFATc1
1 µM CsA
Creld1
NFATc1
Creld1
NFATc1
c
localization (%)
100
90
80
70
60
50
40
30
20
10
0
NFATc1
NFATc1+CsA
NFATc1+Tg
NFATc1+Creld1
NFATc1+Creld1+CsA
cytoplasm
nucleus+cytoplasm
nucleus
d
p-NFATc1
NFATc1
actin
Creld1
CsA
e
relative luciferase activity (%)
1400
1200
1000
800
600
400
200
0
n = 37
n = 11
n = 11
n = 31
n = 12
n = 11
control
CsA
PMA/Iono
Creld1
Creld1+CsA
Creld1+PMA/Iono

Fig. 4-10 Creld1 activates calcineurin/NFATc1 signaling. (a) Live-cell imaging of NIH3T3 cells overexpressing NFATc1-GFP. Upon addition of 1 µM thapsigargin (Tg), NFATc1 (green) translocates to the nucleus. **(b)** Live-cell imaging of NIH3T3 cells overexpressing NFATc1-GFP and Creld1-RFP. The presence of Creld1 (red) is sufficient to drive NFATc1 into the nucleus. Addition of the calcineurin inhibitor cyclosporine A (CsA, 1 µM) inhibits the effect of Creld1 on NFATc1 translocation. Scale bar: 10 µm. **(c)** Quantification of NFATc1 localization in NIH3T3 cells. NFATc1 is predominantly localized in the cytoplasm. Stimulation with Tg (1 µM) or overexpression of Creld1 drives NFATc1 into the nucleus. The presence of CsA reverses the effect and NFATc1 stays in the cytoplasm. Chi square test for nuclear localization for NFATc1 vs. NFATc1+Creld1 is p = 5.7354E-14. The relative distribution was determined according to the absolute cell number per condition. At least n = 198 cells were counted for each condition. **(d)** Phosphorylation state of NFATc1. In NIH3T3 cells, overexpressed NFATc1 is mainly phosphorylated. Addition of 1 µM CsA further enhances this effect. In the presence of Creld1, NFATc1 is mainly dephosphorylated. The effect can be blocked by addition of 1 µM CsA. **(e)** Luciferase assay. HEK239 cells were transfected with a NFAT-luciferase plasmid possessing NFAT binding-sites upstream of a *luciferase* gene. As a control, cells were transfected with an empty pcDNA3.1 vector and treated with 0.3 % DMSO (ctrl); the resulting luciferase activity was set to 100%. Activation of NFAT was induced by treatment with 20 ng/ml PMA and 1 µM ionomycin (iono) and blocked by the addition of 1 µM CsA. To study the function of Creld1, Creld1-RFP was co-expressed with the luciferase plasmid and the luciferase activity was measured. Data are presented as mean ± SEM; n numbers are indicated.

To reveal whether Creld1 controls calcineurin activation and NFATc1 localization across species and different tissues, NFATc1 localization and its phosphorylation state were also analyzed in human HEK293 (performed by Dagmar Wachten, not shown) and Jurkat T cells (Fig. 4-11). The results were similar as observed in murine cells: 1) Creld1 promotes the translocation of NFATc1 to the nucleus in a calcineurin-dependent manner, as shown by treatment with CsA (Fig. 4-10a). 2) Presence of Creld1 mainly caused dephosphorylation of NFATc1, indicating that Creld1 controls the phosphatase activity of calcineurin (Fig. 4-10b). These data strongly imply that Creld1 is directly involved in the translocation of NFATc1 into the nucleus by controlling the function of calcineurin. In addition, Creld1 function seems to be conserved across species, representing a unified mechanism to control calcineurin/NFATc1 signaling.

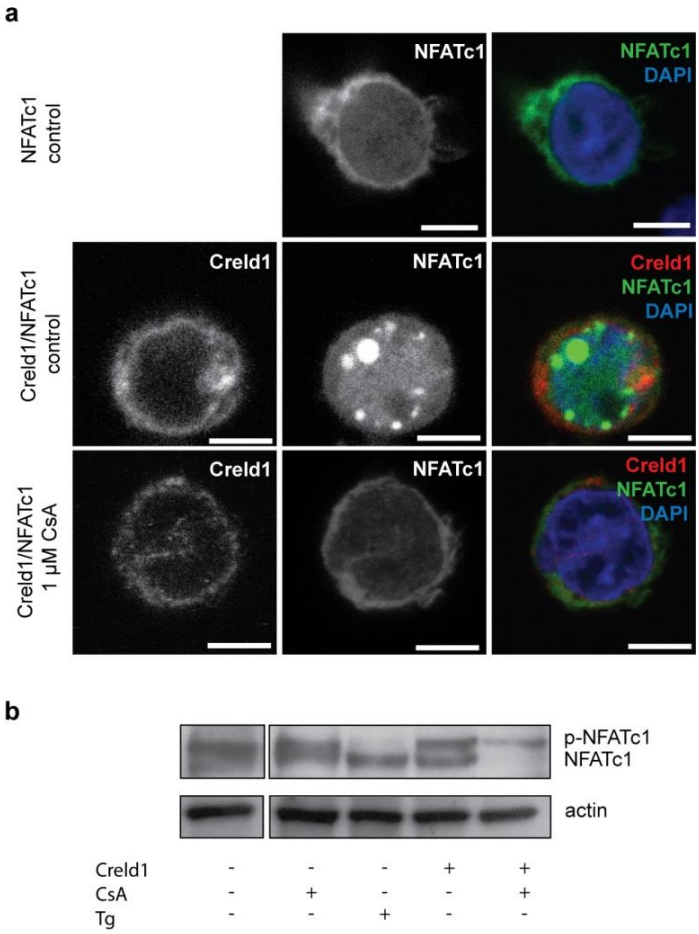

Fig. 4-11 NFATc1 activation in Jurkat E6.1 T cells. (a) Immunofluorescent analyses of Jurkat E6.1 T cells transfected with NFATc1-GFP alone or additionally with Creld1-RFP. Overexpression of Creld1 drives NFATc1-GFP (green) to the nucleus. Addition of 1 µM CsA inhibits the effect of Creld1 on NFATc1 translocation. Scale bars: 5 µm. **(b)** Phosphorylation state of NFATc1. In Jurkat E6.1 T cells, overexpressed NFATc1 is mainly phosphorylated. Treatment with 1 µM Tg causes dephosphorylation of NFATc1, which is blocked by addition of 1 µM CsA. In the presence of Creld1, NFATc1 dephosphorylation is more pronounced than in the untreated cells. The effect can be blocked by addition of 1 µM CsA.

Data from a Yeast-2-Hybrid screening in *D. melanogaster* indicated that the fly orthologs of Creld1 and the regulatory calcineurin subunit, CnB, directly interact with each other[73]. Therefore, interaction between the murine proteins was studied by co-localization and co-immunoprecipitation (Fig. 4-12). CnB from NIH3T3 protein lysates was used as bait by binding the protein to sepharose

beads with a CnB specific antibody. The control was performed only with the corresponding immunoglobulin G (IgG). Indeed, Creld1 and CnB co-immunoprecipitate, suggesting that they are contained within a joint protein complex (Fig. 4-12b). Further indication to support the interaction between these two proteins comes from partial co-localization of endogenously expressed Creld1 and CnB in NIH3T3 cells (Fig. 4-12a).

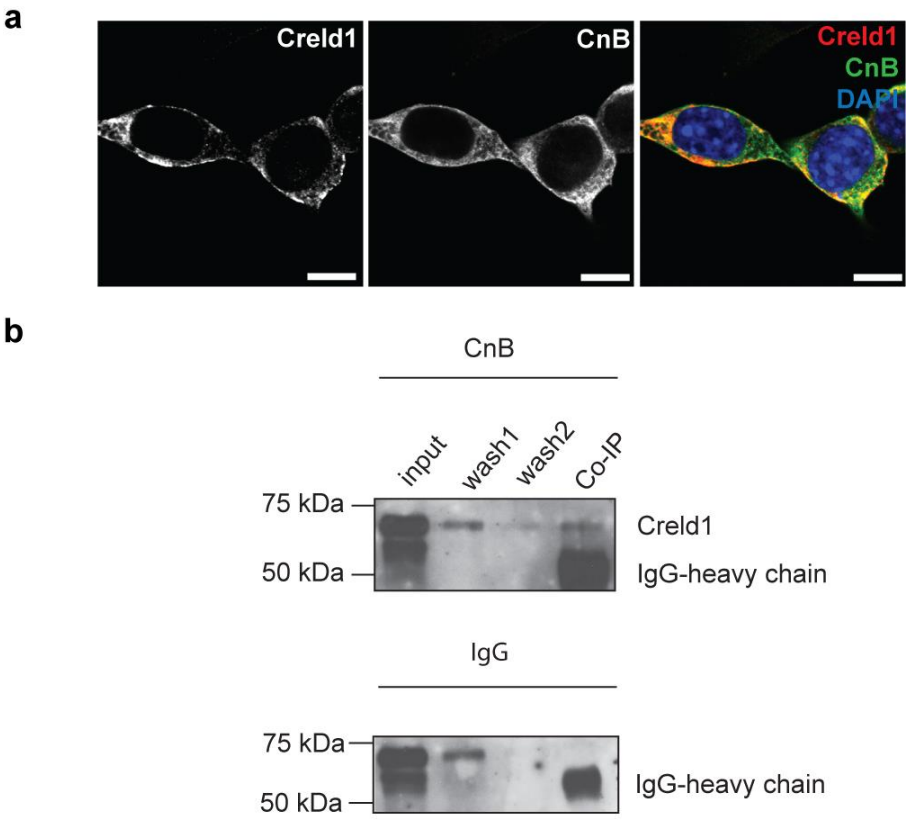

Fig. 4-12 Creld1 and calcineurin B interaction. (a) Immunofluorescent analysis of endogenously expressed Creld1 and calcineurin B (CnB) in NIH3T3 cells. Cells were labeled with a Creld1-specific antibody (red) and a CnB-specific antibody (green). Scale bars indicate 10 µm. **(b)** Co-immunoprecipitation of CnB and Creld1. NIH3T3 total lysates were incubated with a CnB-specific antibody, proteins in the Western blot were labeled with a Creld1-specific antibody. IgG was used as control.

4.1.6 Functional analysis of Creld1 domains

Creld1 contains three distinct protein domains: the WE domain, the EGF-like domains, and the cbEGF-like domains. However, their functional role is unknown. Therefore, I different deletion mutants and Creld1 variants with point mutations corresponding to the mutations found in AVSD patients were generated (Fig. 4-13)[11,12,74,75].

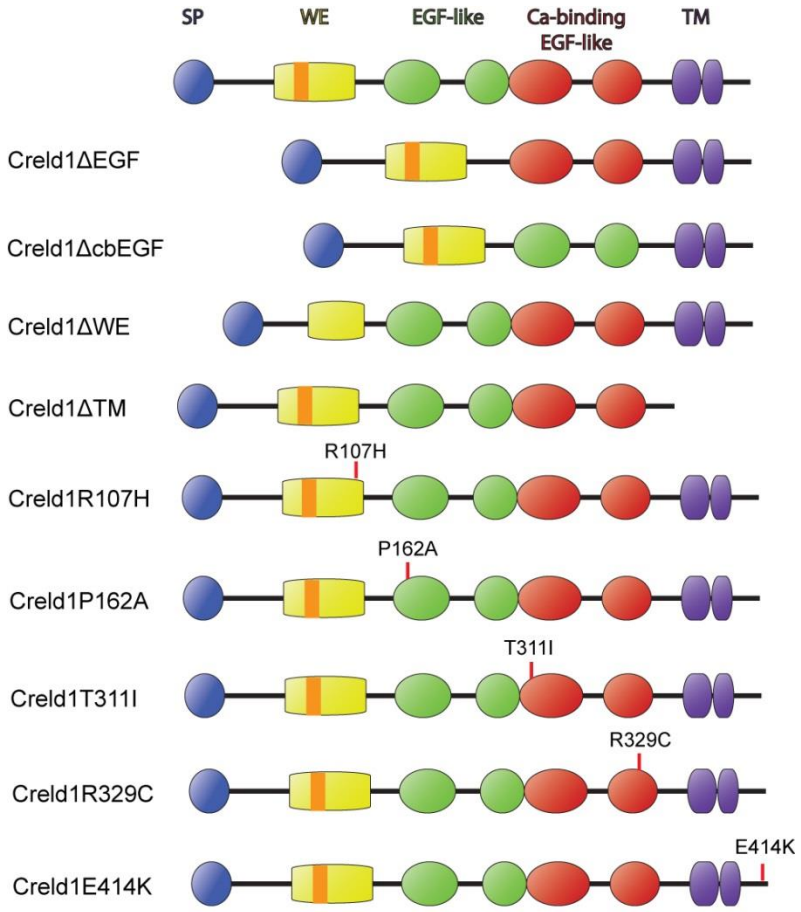

Fig. 4-13 Primary protein structure of Creld1 mutants. Either the EGF-like (Creld1ΔEGF), the cbEGF-like (Creld1ΔcbEGF), the nonapeptide GGNTAWEEE in the WE domain (Creld1ΔWE), or the transmembrane domains (Creld1ΔTM) were deleted. *CRELD1* mutations found in human patients with AVSD that were introduced into *Creld1* are indicated.

All Creld1 mutants were analyzed in the NFATc1-GFP translocation and the luciferase assay. Deletion of either the EGF-like (Creld1ΔEGF) or the cbEGF-like (Creld1ΔcbEGF) domains did not affect the translocation of NFATc1 into the

nucleus. The subcellular distribution was similar to the full length Creld1 protein (Fig. 4-14a). In contrast, deletion of the highly conserved nonapeptide (GG(N/D)TAWEE(E/K), Creld1ΔWE)[1] within the WE domain reduced NFATc1 translocation to the nucleus to 19 % (43 % with full length Creld1). Thus, the WE domain seems to be important for regulation calcineurin function and thereby, also for translocation of NFATc1 to the nucleus. For the luciferase assay, the relative NFAT-luciferase activity of the deletion mutants was normalized to the activity in the presence of Creld1. Here, all three deletion mutants (Creld1ΔEGF, Creld1ΔcbEGF, and Creld1ΔWE) showed a decrease of luciferase activity down to 64 %, 74 %, and 52 %, respectively (Fig. 4-14b, luciferase assays were performed by Dagmar Wachten). Taken together, these results indicate that the WE domain is important for nuclear translocation of NFATc1, whereas the EGF-like and cbEGF-like domains seem to play a role in the subsequent activation of NFATc1 in the nucleus.

To examine whether the localization of Creld1 at the ER is important for calcineurin/NFATc1 signaling, a Creld1 deletion-mutant was generated that lacked the two transmembrane domains (Creld1ΔTM). The localization of Creld1ΔTM was different to the wildtype protein (Fig. 4-14c): ER localization was lost and Creld1ΔTM was rather distributed throughout the whole cell, including the nucleus. Accordingly, NFATc1 translocation to the nucleus was reduced to 26 % and NFAT-luciferase activity was decreased to 52 % (Fig. 4-14a, b).

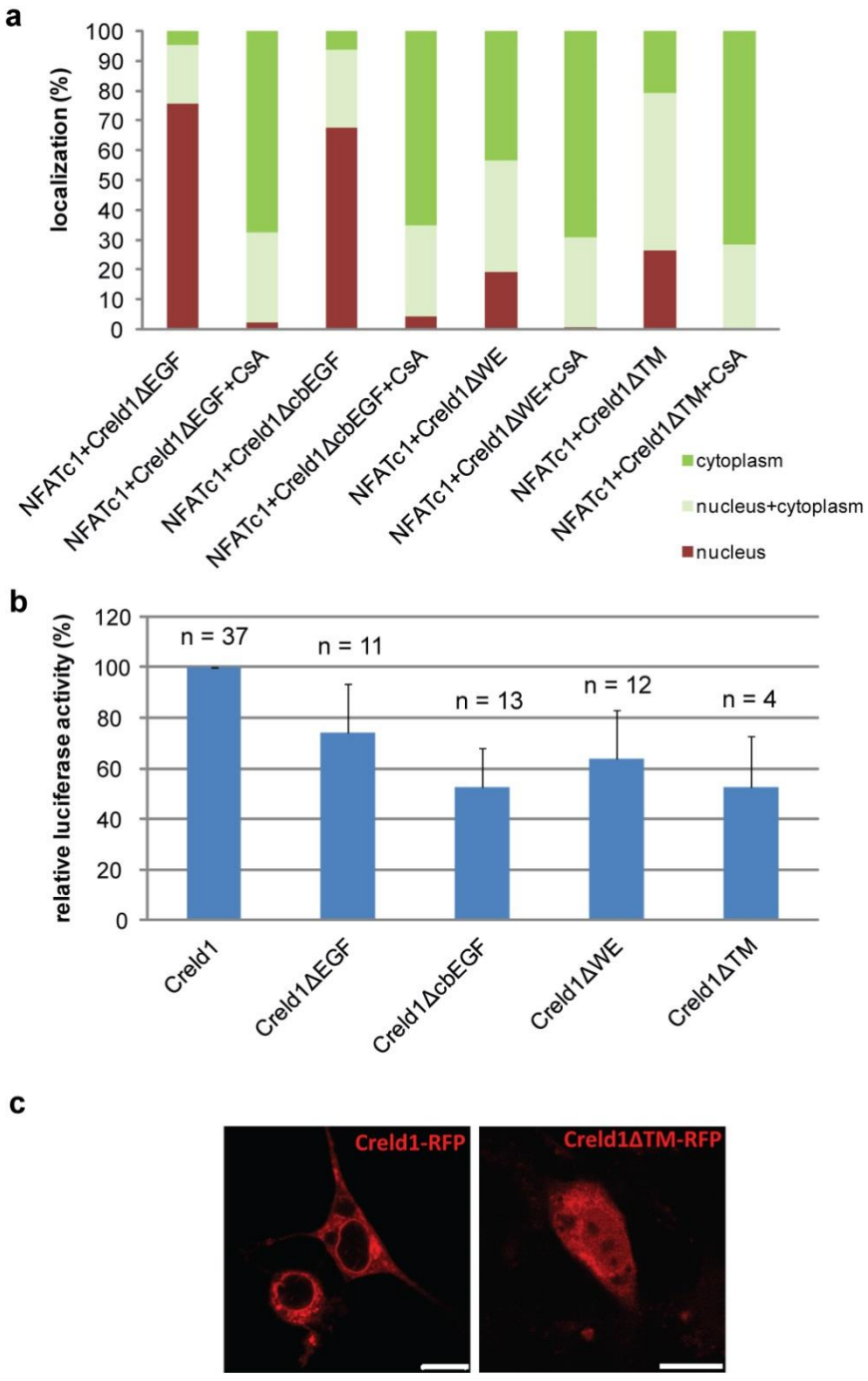

Fig. 4-14 Impact of Creld1 deletion-mutants on NFATc1 activation. (a) Quantification of NFATc1 localization in NIH3T3 cells expressing Creld1 mutants. Deleting the EGF-like (Creld1ΔEGF) or cbEGF-like (Creld1ΔcbEGF) domain had no effect on NFATc1 translocation to the nucleus. Deletion of the highly conserved nonapeptide in the WE domain (Creld1ΔWE) or the transmembrane domains (Creld1ΔTM) severely reduced NFATc1 translocation. The relative distribution was determined according to the absolute cell number per condition. Nuclear translocation of NFATc1 co-expressed with either of the deletion

mutants could be abolished by addition of 1 µM CsA. At least n = 329 cells were counted for each condition. **(b)** Luciferase assay. HEK239 cells were transfected with a NFAT-luciferase plasmid possessing NFAT binding-sites upstream of a *luciferase* gene. The relative luciferase activity of cells transfected with the full length Creld1 protein was set to 1. To study the function of the Creld1 domains, Creld1-RFP, Creld1ΔEGF, Creld1ΔcbEGF, Creld1ΔWE and Creld1ΔTM were co-expressed with the luciferase plasmid and the luciferase activity was measured. Data are presented as mean ± SD; n numbers are indicated. **(c)** Subcellular distribution of the Creld1ΔTM mutant. Scale bar indicates 10 µm.

To further investigate the function of the Creld1 domains, various point mutations were introduced: Creld1R107H, Creld1P162A, Creld1T311I, Creld1R329C, and Creld1E414K (Fig. 4-13). These mutations were chosen, because they were found in AVSD patients[11,12,74,75]. Creld1R107H is located in the WE domain and changes the positively charged amino acid arginine (R) to the neutral histidine (H). The R107H mutation significantly reduced the translocation of NFATc1 to the nucleus (12 %, Fig. 4-15a). Subsequently, NFAT-luciferase activity also dropped to 64 % (Fig. 4-15b). The Creld1P162A mutation is located in the first EGF-like domain. Here, the non-polar and neutral proline (P) was changed to a neutral alanine (A). In turn, this mutation neither affected the translocation of NFATc1 to the nucleus (42 %), nor the NFAT-luciferase activity (110 %, Fig. 4-15a, b). Two different amino acids in the cbEGF-like domains were mutated (Fig. 4-15c). The point mutation in the first cbEGF-like domain changed the polar amino acid threonine (T) to the non-polar isoleucine (I) (Creld1T311I). However, NFATc1 translocation (45 %) and NFAT-luciferase activity (99 %) remained unaltered (Fig. 4-15a, b). The missense mutation Creld1R329C in the second cbEGF-like domain affects one of the six cysteines that form three disulfide bonds and thereby, account for the typical secondary structure of cbEGF-like domains (Fig. 4-15c). The R329C mutation diminished both, the NFAT translocation (15 %) and the luciferase activity (57 %, Fig. 4-15a, b). This indicates that disruption of disulfide-bond formation impairs Creld1 function, probably by causing misfolding of the protein. The mutation Creld1E414K is located at the C terminus of the protein downstream of the transmembrane domains. The change of the negatively charged side chain of glutamic acid (E) to the positively charged lysine (K) slightly affected the translocation of NFATc1 to the nucleus (30 %), but did not significantly

change the NFAT-luciferase activity (95 %, Fig. 4-15a, b).

Taken together, these results demonstrate that 1) the WE domain is important for the action of Creld1 on calcineurin phosphatase activity and 2) the structural integrity of the cbEGF-like domain is crucial for Creld1 function.

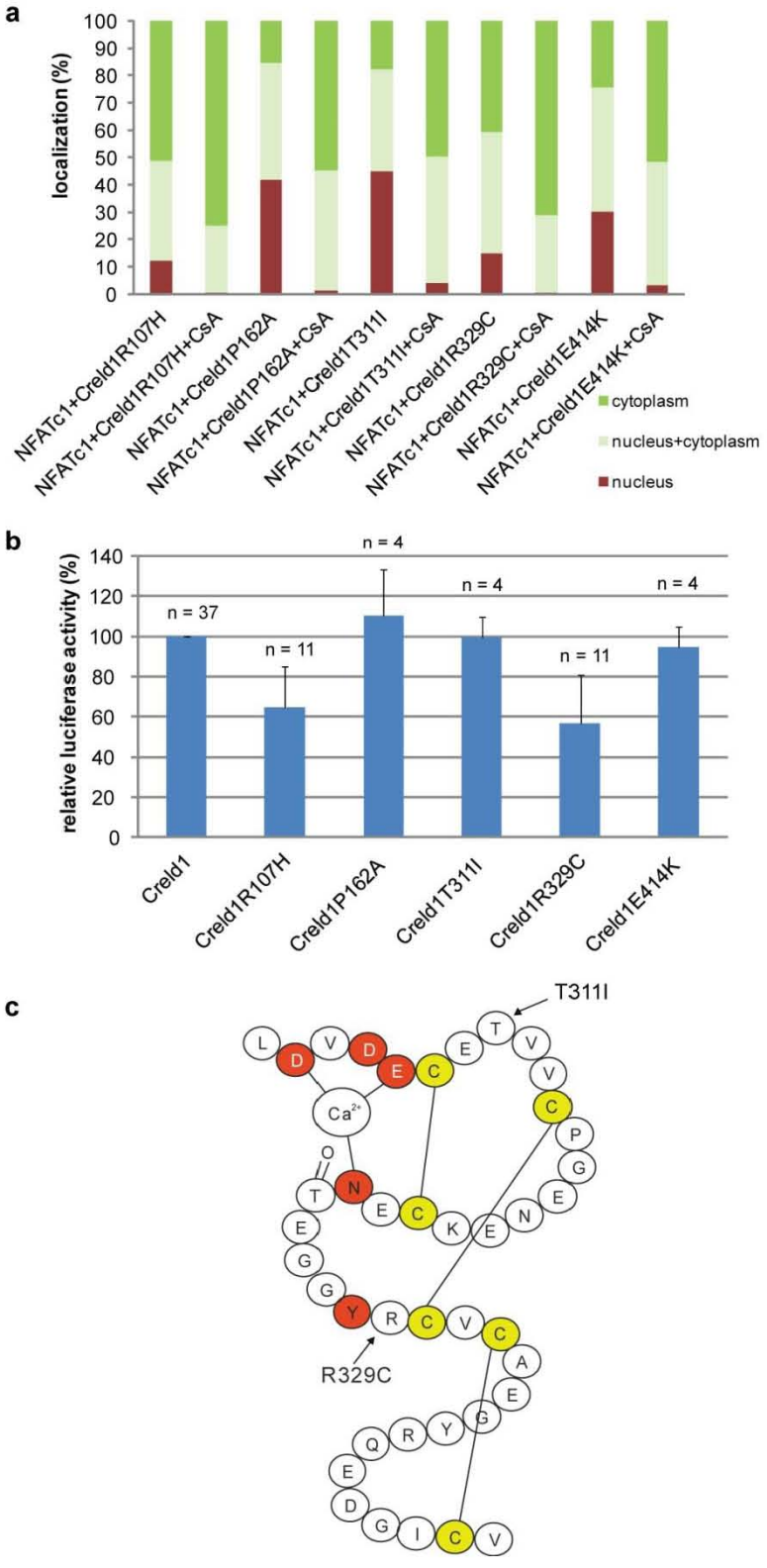

Fig. 4-15 Point mutations in Creld1 affect NFATc1 activation. (a) Quantification of NFATc1 localization in NIH3T3 cells expressing Creld1 mutants. The mutations P162A (EGF-like domain), T311I (cbEGF-like domain), and E414K (C terminus) had no effect on NFATc1 translocation to the nucleus. The change of arginine to cysteine (R329C) in the cbEGF-like domain and a point mutation in the WE domain (R107H) diminished NFATc1 translocation. The relative distribution was determined according to the absolute cell number per condition. At least n = 249 cells were counted for each condition. **(b)** Luciferase assay. For experimental details see Fig. 4-14c. Point mutations that diminished NFATc1 translocation (R107H and R329C) also decreased luciferase activity. Data are presented as mean ± SD; n numbers are indicated. **(c)** Schematic representation of the second cbEGF-like domain of Creld1. Amino acids that have been shown to be important for Ca^{2+}-binding in other cbEGF-like domains are highlighted in red. Cysteines and the corresponding disulfide bonds are labeled in yellow. The point mutations T311I and R329C are indicated.

4.2 Creld2

4.2.1 Non-conditional *Creld2KO* mouse

To analyze the physiological function of Creld2, a conventional *Creld2KO* mouse was generated by homologous recombination. The open reading frame (ORF) of *Creld2* was replaced by an enhanced GFP (eGFP) and a neomycin resistance-cassette (neoR) flanked by two FRT sites. The neoR cassette was used to screen for homologous recombination in ES cells. The endogenous 5' and 3' untranslated regions (UTR) of Creld2 were fused to the eGFP ORF. Furthermore, a diphtheria toxin A (DTA) cassette was introduced after the 3' homologous region to exclude false positive ES-cell clones (Fig. 4-16a). ES-cell clones were first screened by PCR (Fig. 4-16b, primer indicated in Fig. 4-16a). 45 positive clones were identified. Out of these, 18 clones were tested by Southern blot (Fig. 4-16c). Clones positive for the internal and the 5' external probe were tested by karyotyping and all showed a normal number of 40 chromosomes. ES-cell clone number 9 was used for blastocyst injection.

Heterozygous *Creld2KO*$^{w/neo}$ mice were crossed with mice that ubiquitously express the FLP recombinase to excise the neoR cassette (Fig. 4-16a). The deletion was confirmed by PCR (Fig. 4-16d). Absence of Creld2 protein was analyzed by Western blot (Fig. 4-16e). *Creld2KO* heterozygous matings resulted in birth of wildtype, heterozygous, and knockout pups in a ratio according to Mendel (Fig. 4-16f). *Creld2KO* animals were viable and fertile and therefore indistinguishable from wildtype animals.

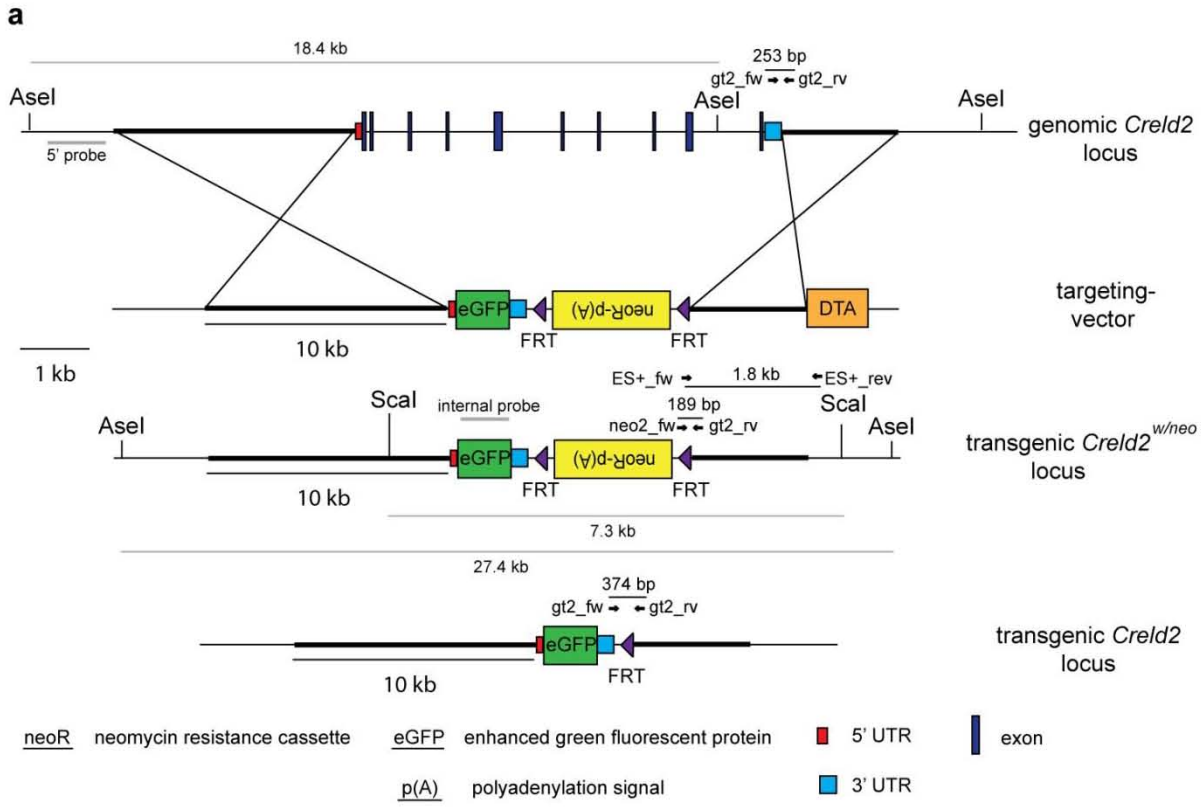
a
18.4 kb
253 bp
gt2_fw gt2_rv
AseI
AseI
AseI
5' probe
genomic Creld2 locus
eGFP
neoR-p(A)
DTA
targeting-vector
FRT
FRT
10 kb
1 kb
ES+_fw
1.8 kb
ES+_rev
ScaI
internal probe
189 bp
neo2_fw
gt2_rv
ScaI
AseI
AseI
transgenic Creld2 w/neo locus
10 kb
FRT
FRT
7.3 kb
27.4 kb
374 bp
gt2_fw
gt2_rv
transgenic Creld2 locus
eGFP
10 kb
FRT
neoR neomycin resistance cassette
eGFP enhanced green fluorescent protein
p(A) polyadenylation signal
5' UTR
3' UTR
exon

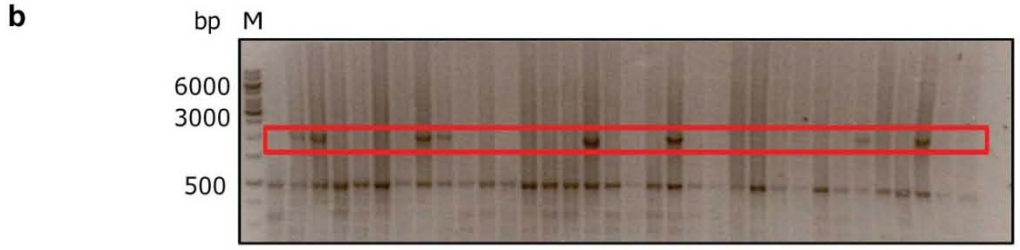
b
bp M
6000
3000
500

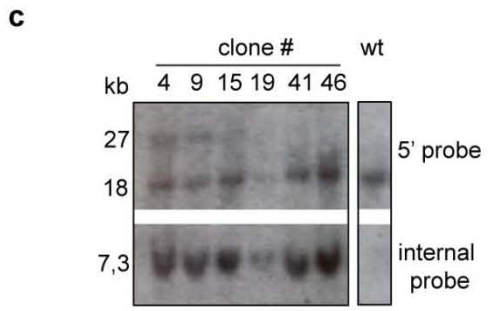
c
clone #
wt
kb
4 9 15 19 41 46
27
18
7,3
5' probe
internal probe

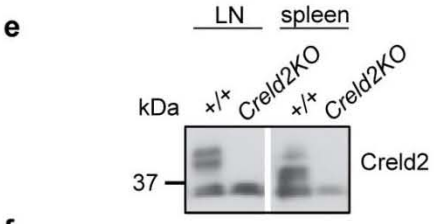
e
LN
spleen
kDa
+/+
Creld2KO
+/+
Creld2KO
37
Creld2

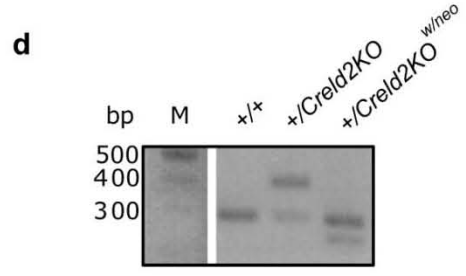
d
bp
M
+/+
+/Creld2KO
+/Creld2KO w/neo
500
400
300

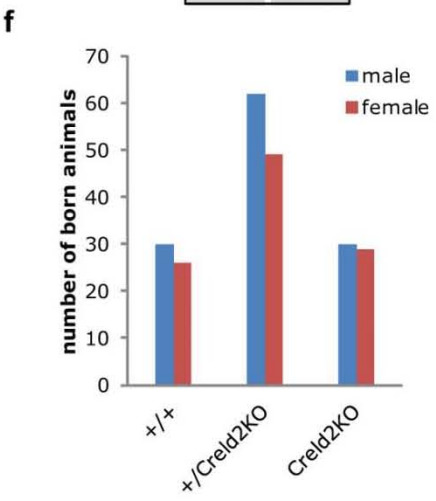
f
number of born animals
70
60
50
40
30
20
10
0
male
female
+/+
+/Creld2KO
Creld2KO

Fig. 4-16 Non-conditional *Creld2KO*. (a) Murine genomic *Creld2* locus was replaced by homologous recombination with *eGFP* and a neoR cassette flanked with FRT sites. Primers used for screening of the ES cells and for genotyping PCR are indicated. Genomic DNA of PCR-positive ES cells was cut with AseI for detection with the 5' probe. For the internal probe, the DNA was cut with ScaI. Lengths of the resulting bands in the Southern blot are indicated. **(b)** Representative PCR analysis of ES cells screened after homologous recombination. The red box shows the band that occurs after successful homologous recombination. **(c)** Southern blot analysis of ES cells that were positive in the PCR. For screening, the 5' and internal probe were used. **(d)** PCR analysis of wildtype (+/+), heterozygous with (+/*Creld2KO*$^{w/neo}$), and heterozygous animals without neoR (*Creld2KO*). **(e)** Western-blot analysis of +/+ and *Creld2KO* total lysates from the lymph node (LN) and spleen using a Creld2-specific antibody. **(f)** Animals born from heterozygous matings. UTR: untranslated region.

4.2.2 Creld2 expression pattern

Creld2 is rather ubiquitously expressed (Fig. 4-17a). Organs with high expression levels are secretory and digestive organs such as pancreas, stomach, foregut, and salivary gland. Moreover, white adipose tissue (WAT) and testis express high amounts of Creld2. In the pancreas, Creld2 is not expressed in the insulin secreting beta-cells, but rather in the ER of acinar cells, which are the functional units of the exocrine pancreas (Fig. 4-17b). In the salivary gland, Creld2 seems to be expressed in the excretory duct (Fig. 4-17). It is noteworthy that organs important for the immune system, namely thymus and spleen, also express Creld2 (Fig. 4-18a). To investigate whether Creld2 plays a role in immune cells, FACS analysis was performed with cells from spleen and thymus (Fig. 4-18b, c). As a marker for Creld2 expression, GFP that is replacing the ORF of Creld2 was used. Wildtype cells were used as negative control, because they lack GFP expression. In heterozygous and homozygous knockout animals, GFP was detected in all cell types that were analyzed: B-cells, T-cells, dendritic cells, natural killer cells (Fig. 4-18b, c), macrophages, and granulocytes (not shown). There is one population of double-negative T cells in the thymus that does not express GFP (Fig. 4-18b). Some cells within the populations of double-positive T cells in the thymus and B cells in the spleen seem to express more GFP than others (Fig. 4-18d).

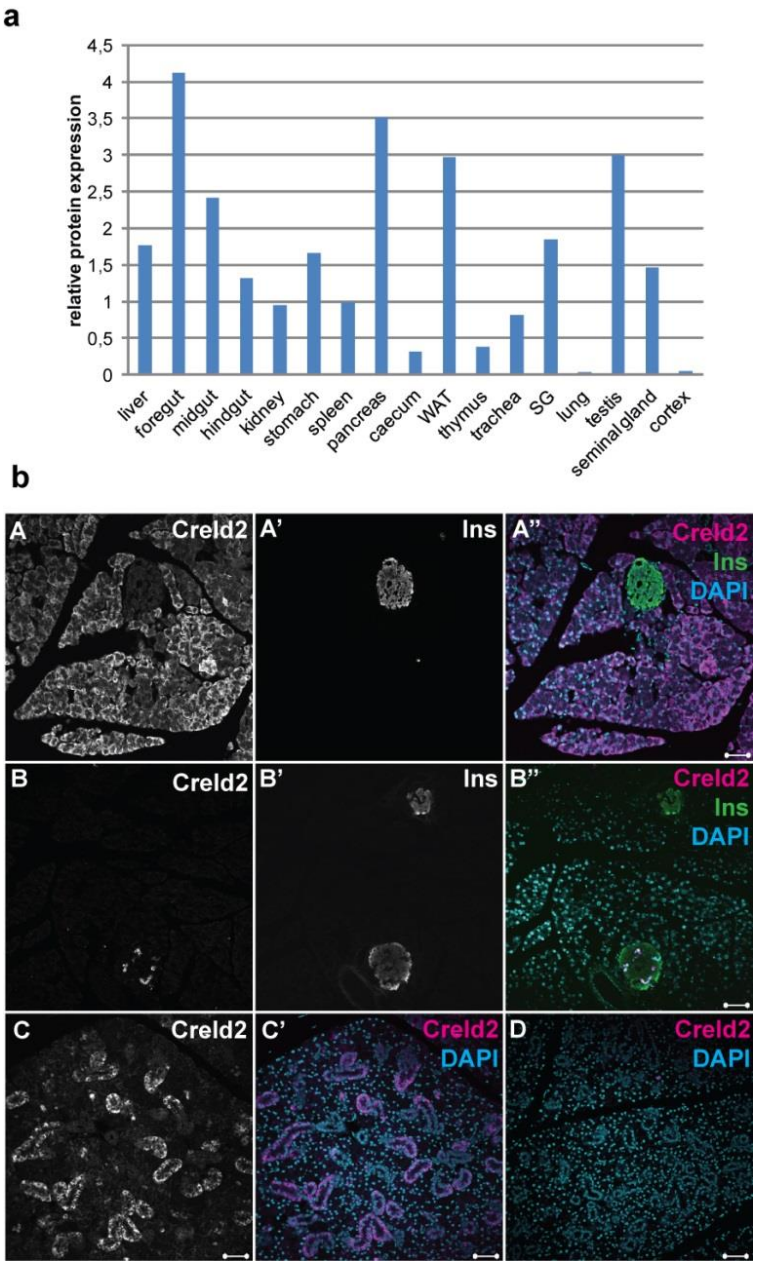

Fig. 4-17 Creld2 expression pattern. (a) Comparison of Creld2 expression in different tissues by Western blot using a Creld2-specific antibody. Organs with the highest expression levels are the foregut, the pancreas, white adipose tissue (WAT), salivary gland (SG), and testis. **(b)** Immunofluorescent analyses of the pancreas (A, B) and salivary gland (C, D). In the pancreas, Creld2 is detected in every acinar cell (A), but not in the beta cells that are stained with an anti-insulin (Ins) antibody (A'). B-B'' represent the control staining of a *Creld2KO* pancreas. In the salivary gland, Creld2 seems to be expressed in the excretory ducts (C, C'). D represents the control staining of a *Creld2KO* salivary gland. Scale bars indicate 100 µm.

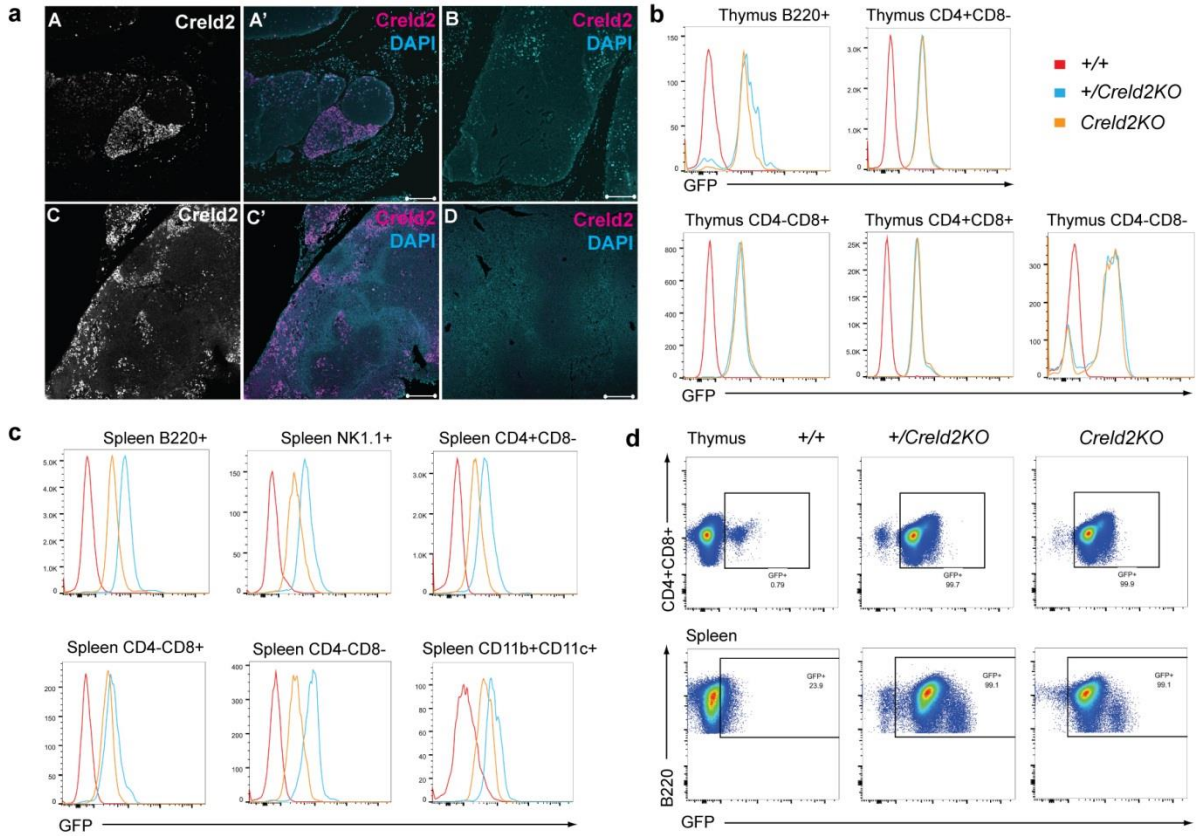

Fig. 4-18 Creld2 expression in immune cells. (a) Immunofluorescent analyses of thymus (A, B) and spleen (C, D). B and D represent the control staining of the corresponding *Creld2KO* organs. **(b)** Histograms of the FACS analysis of B (B220) and T (CD4 CD8) cells in the thymus of wildtype (+/+), heterozygous (*+/Creld2KO*), and homozygous (*Creld2KO*) animals. Almost all cells of *+/Creld2KO* and *Creld2KO* animals are GFP positive, indicating a broad Creld2 expression pattern. **(c)** Histograms of FACS analysis from B (B220), natural killer (NK1.1), dendritic (CD11b CD11c) and T (CD4 CD8) cells in the spleen. All cells of *+/Creld2KO* and *Creld2KO* animals express GFP. **(d)** FACS analysis of thymic double-positive T cells and splenic B cells. Within the GFP-positive populations of *+/Creld2KO* and *Creld2KO* animals are cells that display a more intensive expression of GFP. Scale bars indicate 200 µm.

4.2.3 Phenotype analysis of *Creld2KO* mice

Young *Creld2KO* mice show no apparent phenotype under normal growth conditions. Therefore, *Creld2KO* mice were aged and histologically analyzed when they were one year old. All knockout animals showed signs of liver steatosis (also known as "fatty liver"). They displayed impaired tissue integrity due to microvesicular steatosis (Fig. 4-19). To visualize lipid accumulation in the liver, an Oil-red-O staining was performed, which stains neutral

triacylglycerol (TAG) and lipids. *Creld2KO* showed accumulations of bigger lipid droplets in the area of damaged tissue (Fig. 4-19).

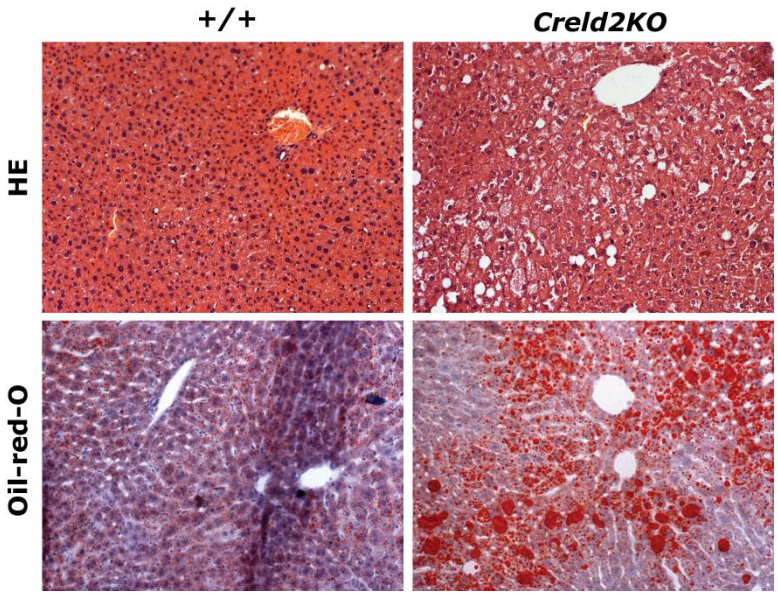

Fig. 4-19 Histological analysis of *Creld2KO* liver sections. One year old *Creld2KO* animals suffer from liver steatosis, which is visualized by a hematoxylin/eosin (HE) staining. Cells in the area around the vessel harbor vesicles that were identified as lipid droplets using an Oil-red-O staining.

In the liver, TAGs are synthesized from acylation of glycerol-3-phosphate using acyl-CoA. Acyl-CoA is formed when coenzyme A (CoA) is attached to the end of a long-chain fatty acid. Fatty acid levels are tightly regulated by four different mechanisms: uptake, export, synthesis, and catabolism (β-oxidation)[76–78]. To determine which of these processes was affected in the liver of *Creld2KO* mice, gene expression patterns in one year old wildtype and *Creld2KO* females were analyzed (Fig. 4-20). First, different transcriptional regulators that are involved in lipid metabolism were examined (Fig. 4-20a). Peroxisome proliferator-activated receptor alpha (Pparα), which regulates lipid metabolism and gluconeogenesis, was significantly downregulated. In contrast, the expression levels of other transcription factors like Pparγ (controls fatty-acid storage and synthesis), CCAAT/enhancer binding protein alpha (C/ebpα, controls gluconeogenesis and lipogenesis), estrogen-related receptor alpha (Errα, controls fatty-acid oxidation and glucose metabolism[79]), sterol regulatory element-binding protein 1 (Srebp1) and Srebp2 (both regulators of lipogenesis)

did not display significant differences in expression level between wildtype and *Creld2KO* animals. Consistent with these results, the expression of Pparα targets, acyl-CoA oxidase 1 (Acox1), carnitine palmitoyltransferase 1a (Cpt1a), and hepatic lipase (Lipc)[80] were downregulated (Fig. 4-20b). Acox1 and Cpt1a proteins are involved in fatty acid β-oxidation. Lipc is considered to be a lipase of the vascular compartment, where it hydrolyzes both TAGs and phospholipids in the very low density lipoproteins[78]. The expression levels of two known Ppparα targets remained unchanged in *Creld2KO*: fatty acid binding protein 1 (Fabp1) and fatty acid synthase (Fasn). Fabp1 has been shown to be important for fatty-acid activation, whereas, Fasn controls lipid synthesis. However, both genes are regulated by various other transcription factors like Hnf4α and Srebp1[81,82], so that diminished Ppparα function could be compensated.

Furthermore, two other proteins involved in lipid metabolism were significantly downregulated in *Creld2KO* mice: diacylglycerol acyltransferase 2 (Dgat2) and NADH-ubiquinone oxidoreductase (Ndufs1) (Fig. 4-20d). Dgat2 is an enzyme that catalyzes the *de novo* synthesis of TAGs. Ndufs1 is part of the respiratory chain in mitochondria and important for oxidative phosphorylation.

Pparα has been shown to regulate hepatic glycogen metabolism. Hence, the expression levels of proteins involved in gluconeogenesis and glycolysis were examined (Fig. 4-20c): phosphoenolpyruvate carboxykinase 1 (Pck1), pyruvate carboxylase (Pcx), and glucose-6-phosphatase (G6pc). G6pc hydrolyses D-glucose 6-phosphate to D-glucose and orthophosphate. Its expression was significantly downregulated in *Creld2KO* animals (Fig. 4-20c). Glycokinase (Gck) catalyzes the reverse reaction, namely phosphorylation of glucose to glucose-6-phosphate. Its expression in *Creld2KO* remained unchanged. Pck1 and Pcx have been shown to be suppressed in Pparα knockout animals[83], but in *Creld2KO* there was no change in the expression of both the genes.

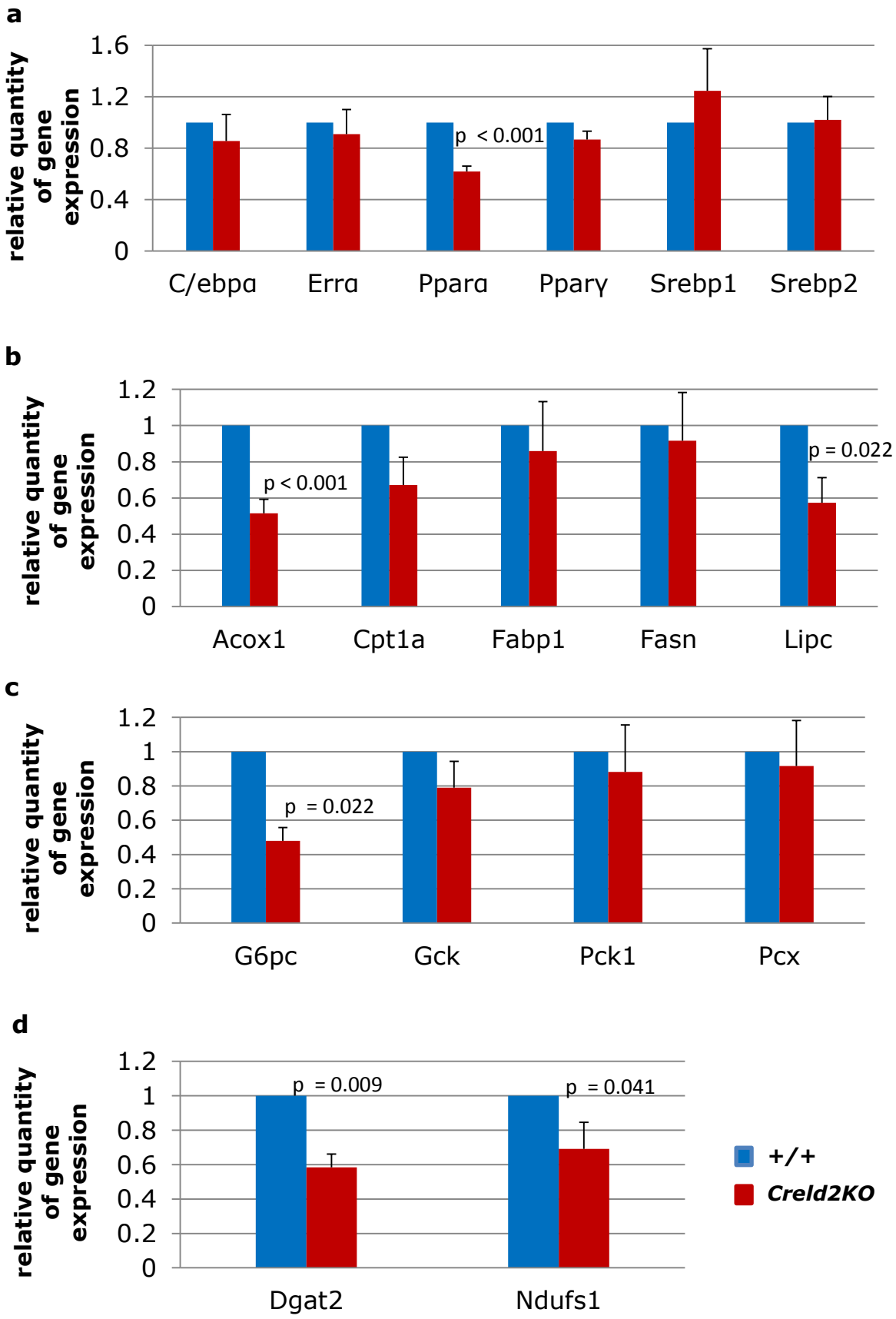
a
relative quantity of gene expression
1.6
1.2
0.8
0.4
0
p < 0.001
C/ebpα
Errα
Pparα
Pparγ
Srebp1
Srebp2
b
relative quantity of gene expression
1.2
1
0.8
0.6
0.4
0.2
0
p < 0.001
p = 0.022
Acox1
Cpt1a
Fabp1
Fasn
Lipc
c
relative quantity of gene expression
1.2
1
0.8
0.6
0.4
0.2
0
p = 0.022
G6pc
Gck
Pck1
Pcx
d
relative quantity of gene expression
1.2
1
0.8
0.6
0.4
0.2
0
p = 0.009
p = 0.041
Dgat2
Ndufs1
+/+
Creld2KO

Fig. 4-20 Expression analysis of metabolic genes in *Creld2KO* livers. (a) Expression of transcriptional regulators. **(b)** Expression of Pparα gene targets. **(c)** Expression of genes involved in gluconeogenesis and glycolysis. **(d)** Expression of genes important for *de novo* synthesis of TAGs and oxidative phosphorylation. One year old litter mates were analyzed. The gene expression of wildtype animals was set to one. Data are presented as mean ± SEM; n = 4.

Taken together, analysis of *Creld2KO* animals indicates that 1) fatty acid oxidation is diminished due to decreased Pparα expression[77] and 2) that D-glucose 6-phosphate is accumulated and can subsequently be metabolized to Acetyl-CoA[83], which in turn can be utilized for lipogenesis. Both mechanisms provide an explanation for the liver steatosis observed in *Creld2KO* animals.

4.2.4 Functional analysis of Creld2 protein

Creld2 is localized in the ER and subsequently undergoes secretion to the extracellular matrix[9]. In the ER lumen and outside the cell, Ca^{2+} concentrations are higher than in the cytosol. Thereby, the two cbEGF-like domains of Creld2 constantly face high Ca^{2+} concentration. To analyze whether the cbEGF-like domains bind Ca^{2+} ions, a native gel-shift assay was performed. Protein lysates were incubated with 10 mM $CaCl_2$ or 10 mM EGTA before running them on native gels containing either 50 µM $CaCl_2$ or 1 mM EGTA, respectively. Indeed, in the presence of Ca^{2+}, Creld2 migrated more slowly in the gel compared to the Ca^{2+}-free condition due to Ca^{2+} bound to Creld2 (Fig. 4-21a).

In protein lysates of the spleen, an additional Creld2 band of >545 kDa was detected (Fig. 4-21a). Similarly, in other organs like the stomach (not shown) and the pancreas, a band of about 300 kDa appeared in the presence of Ca^{2+} (Fig. 4-21a). This implies that Creld2 is part of multi-protein complexes. To investigate this further, 2D-PAGE was used. In the first dimension, the protein lysate was run in a native gradient gel to separate proteins and protein complexes according to their size in a native state. The second dimension is a SDS-PAGE in a 90 degrees angle from the first dimension. Using stomach protein lysates of a wildtype animal, Creld2 was detected as several dots in the second dimension (Fig. 4-21b), representing different protein complexes that

contained Creld2 in the native state.

In some tissues like the lymph node and spleen, two distinct bands for Creld2 appear (Fig. 4-16e). This could be due to splice variants or post-translational modifications. To examine possible modifications, NIH3T3 protein lysates were treated with a phosphatase and different glycosidases. In the untreated sample, only one band was detected at around 42 kDa, corresponding to the upper band seen before (Fig. 4-21c). After treatment with peptide-*N*-glycosidase F (PNGase F), this band shifted down to about 40 kDa (Fig. 4-21c). PNGase F cleaves the link between asparagine and N-acetylglucosamines, thereby releasing N-linked oligosaccharides. When protein lysates were treated with O-glycosidase or calf intestinal alkaline phosphatase (CIP), no change was observed in the band pattern for Creld2 (Fig. 4-21c). Therefore, I conclude that Creld2 is an N-glycosylated protein.

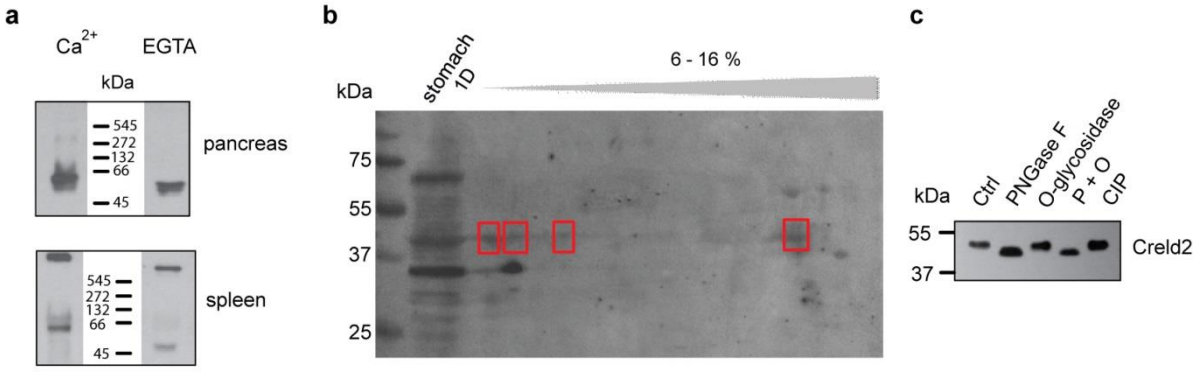

Fig. 4-21 Characteristics of Creld2 protein. (a) Creld2 binds to Ca^{2+} as visualized by a native gel shift assay. **(b)** 2D-PAGE of a stomach protein lysate. The presence of native Creld2 in protein complexes before the second dimension is indicated by red boxes. **(c)** Analysis of post-translational modifications of Creld2. P+O: combined treatment of PNGase F and O-glycosidase. CIP: calf intestinal alkaline phosphatase.

Creld2 expression has been described to be induced by ER stress[9,38]. In murine Neuro2a cells, addition of thapsigargin (Tg) increased Creld2 expression 3- to 4-fold after 4 or 8 hours, respectively[9,38]. Moreover, overexpression of ATF6, which represents one of the three axes of the UPR, induced *Creld2* expression[9].

To verify these results and analyze Creld2 function, ER stress was induced with Tg in NIH3T3 cells and Creld2 mRNA expression was quantified (Fig. 4-22a). Upregulation of Chop and Grp78 served as a positive control for ER stress[84], Creld1 was used as a negative control (Fig. 4-22a). Creld2 mRNA expression in NIH3T3 cells increased 20-fold after 4 hours and over 30-fold after 8 and 24 hours treatment with Tg (Fig. 4-22a). Consequently, Creld2 protein levels also increased upon Tg treatment (Fig. 4-22b).

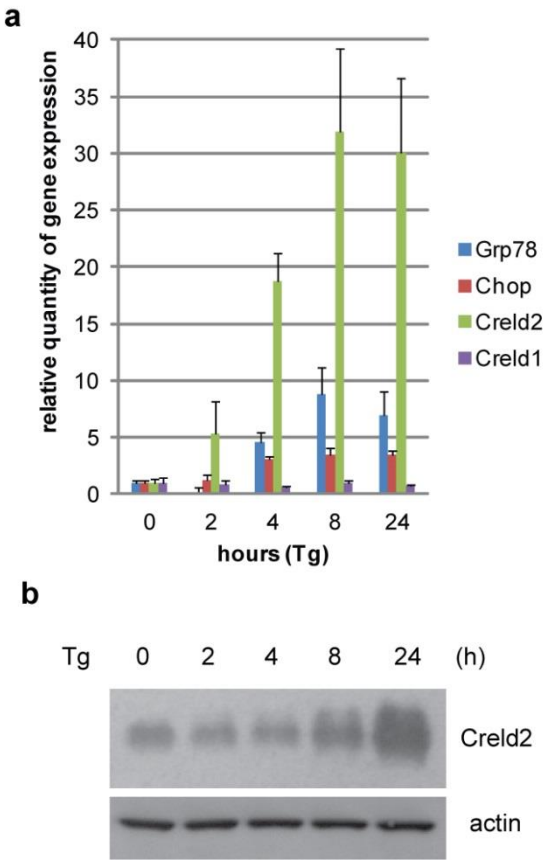

Fig. 4-22 Creld2 is upregulated upon ER stress. (a) qRT-PCR analysis of NIH3T3 cells treated with 1 µM Tg for different time periods to induce ER stress. Creld2 induction occurs already after 2 hours and increases with time. Data are presented as mean ± SD; n = 3. **(b)** Protein lysates of cells used in (a) were analyzed by Western blotting using a Creld2-specific antibody. In line with the increase in mRNA expression, also Creld2 protein levels increased over time.

To examine, whether increased Creld2 expression affects the UPR, Creld2 was overexpressed in NIH3T3 cells. 24 hours after transfection, an increase in Creld2 protein expression could be detected (Fig. 4-23b). However, markers for UPR were not upregulated (Fig. 4-23a). Only after 48 hours, when Creld2 expression was still high, splicing of Xbp1 (sXbp1) was augmented and expression of *Chop* and *Gadd34* were increased (Fig. 4-23a). *Atf6* expression was unchanged. *Grp78* was slightly downregulated on the transcriptional level, but protein levels remained similar compared to untransfected cells (Fig. 4-23b).

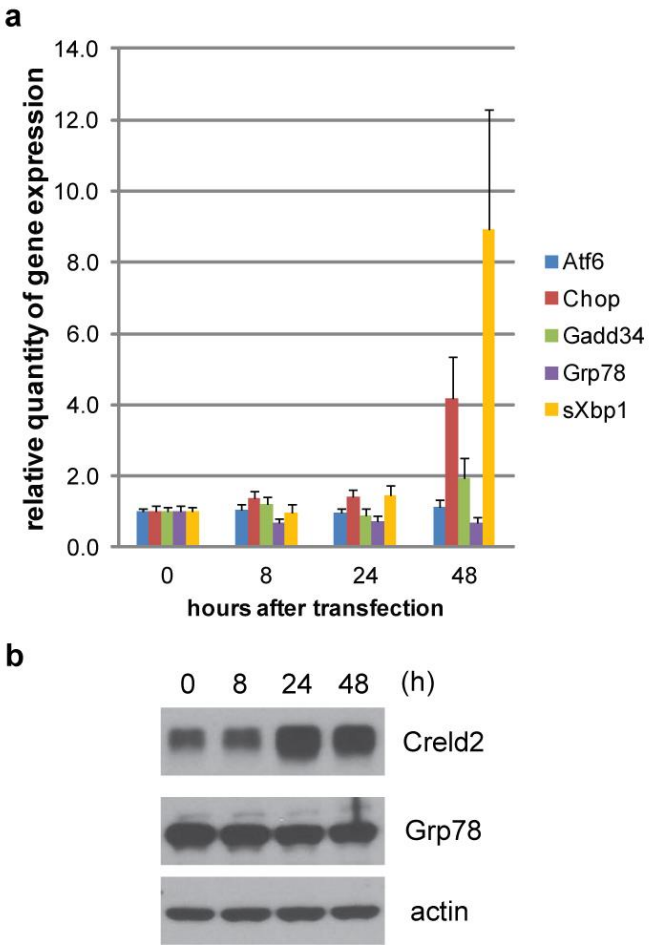

Fig. 4-23 Creld2 overexpression in NIH3T3 cells. (a) qRT-PCR analysis of NIH3T3 cells transfected with Creld2 for different time periods. After 48 hours, expression of *Chop* and *Gadd34* is increased and splicing of Xbp1 (sXbp1) is augmented. Data are presented as mean ± SD; n = 2. **(b)** Protein lysates of cells used in (a) were analyzed by Western blotting using antibodies against Creld2 and Grp78.

5 Discussion

In my PhD thesis, I investigated the physiological function of the two members that belong to the murine Creld protein-family: Creld1 and Creld2. Using knockout mice for both genes, I investigated their function in murine development. Interestingly, even though Creld1 and Creld2 proteins share many of their domain structures, they fulfill different physiological functions *in vivo*.

5.1 Creld1

5.1.1 Creld1 regulates heart valve development

My data revealed that Creld1 plays an important role during embryonic development. *Creld1KO* embryos die at embryonic day E11.5, because they fail to undergo normal cardiac development. At E11.0, the wildtype embryos already show a four-chambered heart, whereas, the mutants display only one common atrium. This arrest in heart developmental is mainly due to the lack of endocardial cushion formation and remodeling.

Endocardial cushions are the precursors of the heart valves, which are critical for heart septation, and thereby for the formation of the four-chambered heart. This mechanism is tightly regulated by several pathways, epigenetic regulators, and cell adhesion/migration molecules that are sequentially activated[17,35]. Formation of the heart valves is initiated by the delamination of endocardial cells within the endocardial cushion. This process, termed EMT, is triggered by the first wave of calcineurin/NFAT signaling: myocardial NFATc2/3/4 repress the EMT inhibitor VEGF. After the EMT, the second wave of calcineurin/NFAT signaling occurs: NFATc1 is activated in the endocardium and promotes proliferation to support endocardial growth needed for cushion elongation and remodeling[17,35].

EMT in *Creld1KO* hearts is normal, indicating that lack of Creld1 does not affect calcineurin/NFATc2/3/4 signaling. However, hearts from *Creld1KO* embryos

display a diminished number of mesenchymal cells in the cardiac jelly of the AVC due to lack of proliferation. There are different factors known that are important for endocardial and mesenchymal proliferation during heart valve formation, like Gata4[85], Smad4[86], and Wnt2[87]. Loss of these factors is not only associated with diminished proliferation, but additionally with a defect in EMT[85–87]. However, loss of NFATc1 leads to decreased proliferation, but EMT is normal[88], resembling the *Creld1KO* phenotype. At E10.5, when NFATc1 is normally recruited to the nucleus[31], endocardial and mesenchymal cells in *Creld1KO* hearts showed a lack of proliferation. NFATc1 failed to translocate to the nucleus in the absence of Creld1. This resulted in the reduced transcriptional activity of NFATc1 in the heart of *Creld1KO* embryos. Thus, my data suggest that Creld1 is an upstream regulator of NFATc1 in the endocardium and that it controls proliferation in the cells of the AVC. In the absence of Creld1, NFATc1 signaling fails, preventing normal heart development in *Creld1KO* embryos. This results in a decrease of cardiac output as seen in the reduction of heart-beat frequency. Therefore, the heart is not able to maintain the blood circulation, leading to hypoxia. Consequently, not only the heart but also the whole *Creld1KO* embryo arrested in development. Eventually, *Creld1KO* embryos died at E11.5 due to heart failure.

5.1.2 Creld1 regulates NFATc1 activation via calcineurin

With respect to Creld1 function, the main question is how Creld1 controls the activation of NFATc1. NFATc1 is expressed in the endocardium of the AVC at E10.5, where it is activated through dephosphorylation by calcineurin[32,67,68,89]. Therefore, we hypothesized that Creld1 activates NFATc1 through controlling the function of calcineurin. This hypothesis was underlined by a yeast-2-hybrid screen in *D. melanogaster*, where dCRELD was found to be a potential interaction partner of the calcineurin regulatory subunit CnB[73]. Indeed, I could show that murine Creld1 interacts with CnB. Through this interaction, it regulates calcineurin function and promotes translocation of NFATc1 into the nucleus.

In future studies it would be of interest to investigate if CnA is needed for the interaction between CnB and Creld1 or if it is even the primary binding site for Creld1. So far, there are two CnA docking sites described for calcineurin interactors and substrates: PxIxIT and LxVP[90]. Creld1 does not possess either of these consensus sequences. However, there are calcineurin interactors such as RCANs that show substitutions for three residues of the PxIxIT motif (PSVVVH) and still display a strong binding to calcineurin[37,91,92]. Thus, the mapping of binding sites for calcineurin, especially in the WE domain of Creld1 should be performed in the future (see 4.2.1).

When Creld1 was described for the first time, it was reported to be a plasma-membrane protein with its functional domains facing the extracellular space[1]. This prediction was made according to other transmembrane proteins with EGF-like and cbEGF-like domains, such as selectins and fibrillins[2,7]. However, no experimental data was reported to support this conclusion.

My data suggest that Creld1 is rather localized at the ER and not at the plasma membrane. A fluorescence protease protection (FPP) assay underlined the localization at the ER and demonstrated that both the N and C terminus of Creld1 are facing the cytoplasm. This topology and localization provides the basis for the interaction with CnB through at least one of the cytoplasmic domains. The requirement of Creld1 localization at the ER membrane is further underlined by results from the Creld1ΔTM mutant: deletion of the transmembrane domains leads to a broad distribution of Creld1 throughout the cell, which is accompanied by a decreased NFATc1 activation. Therefore, ER-resident Creld1 is important for calcineurin activity. The function of the regulatory CnB subunit is directly controlled by Ca^{2+} binding[93]. Calcineurin has been found to localize in ER-microdomains, where proteins are exposed to high Ca^{2+} concentrations[94]. My *in vitro* results hint to a model, in which Creld1 serves as an anchor for localizing calcineurin to the ER, where it experiences high local Ca^{2+} concentrations and becomes activated (Fig. 5-1). Creld1 could serve as a Ca^{2+} sensor, which measures Ca^{2+} release from the ER. This could trigger the recruitment of calcineurin to locally high Ca^{2+} concentrations at the ER membrane. A similar mechanism has been shown for calcineurin in skeletal muscle. Here, FKBP12 interacts via FK506 indirectly with calcineurin in a Ca^{2+}-

dependent manner. FKBP12 is an accessory subunit of a Ca^{2+}-release channel, the ryanodine receptor (RyR). Thus, interaction with FKBP12 brings calcineurin close to the Ca^{2+}-release site[95]. However, the interaction between Creld1 and calcineurin could also be independent of Ca^{2+} release from the ER. Creld1 could serve as a stabilizing and activating component of the calcineurin complex by tethering the proteins to the ER membrane.

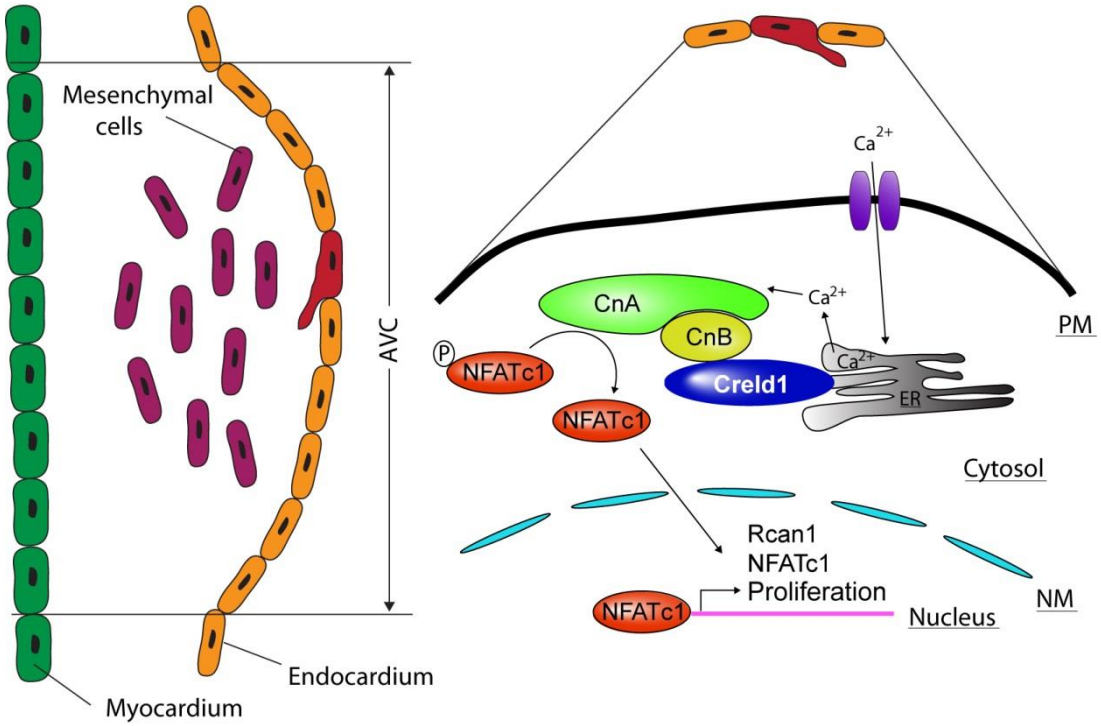

Fig. 5-1 Creld1 function in the calcineurin/NFATc1 signaling pathway. After delamination into the cardiac jelly, endocardial cells of the AVC mature into mesenchymal cells. During this process endocardial cells undergo calcineurin/NFATc1 dependent proliferation. In detail, Creld1 is located at the ER membrane, where it interacts with the regulatory subunit of calcineurin (CnB), thereby, promoting dephosphorylation of NFATc1 by the catalytic subunit of calcineurin (CnA). Translocation of dephosphorylated NFATc1 to the nucleus leads to the transcription of NFATc1 target genes, and thus, to proliferation in the AVC. AVC: atrioventricular cushion, ER: endoplasmic reticulum, ERM: endoplasmic reticulum membrane, NM: nuclear membrane, PM: plasma membrane.

5.1.3 The WE domain is important for regulation of calcineurin

Instead of serving solely as an anchor for calcineurin at the ER and facilitating its activation by Ca^{2+}, Creld1 might as well have a functional domain for the positive regulation of calcineurin/NFAT signaling. So far, only the RCAN family has been described to positively, but also negatively regulate calcineurin[96–98]. Whether RCANs exert their regulative activity by inhibiting or facilitating calcineurin function is dependent on their phosphorylation status[90,99]. The inhibitory action of unphosphorylated RCAN on calcineurin/NFAT signaling is not only due to the phosphatase activity inhibition, but also due to the competition between NFAT and RCAN for binding to the same residues on calcineurin[36,37]. However, the molecular mechanism by which calcineurin/NFAT signaling is facilitated after phosphorylation of RCAN remains unclear[99].

In order to analyze, which Creld1 domain is important for the regulation of calcineurin/NFATc1 signaling, various deletions and point mutations were introduced into the protein. These mutants were analyzed in the NFATc1 translocation and the luciferase activity assay. This approach enabled the analysis of both, the calcineurin phosphatase and NFATc1 activity, respectively.

Deletion of the highly conserved nonapeptide (Creld1ΔWE) and the point mutation in the WE domain (R107H) diminished NFATc1 translocation and activation. This indicates that this unique domain, which is only found in members of the Creld protein-family is important for calcineurin regulation. To investigate whether the WE domain directly interacts with calcineurin it would be necessary to examine if the Creld1ΔWE or Creld1R107H still co-immunoprecipitate with CnB. However, also the EGF-like and cbEGF-like domains might be involved in calcineurin regulation (see 4.3). As mentioned above, a detailed mapping of the calcineurin binding-site in the Creld1 protein sequence is required. To analyze whether calcineurin phosphatase activity is directly dependent on Creld1, a calcineurin activity assay could be performed. This could be either done with protein lysates of whole *Creld1KO* embryos, provided the fact that Creld1 is not only regulating calcineurin in the endocardium, or with protein lysates from cells overexpressing the full length protein of Creld1. The latter should lead to an increased activity as suggested by the augmented NFATc1 translocation.

5.1.4 Creld1 in the nucleus

Interestingly, deleting either the EGF-like or the cbEGF-like domains did not affect the translocation of NFATc1 to the nucleus. This indicates that both domains are not crucial for Creld1 to control calcineurin activity. However, both deletion mutations decreased NFAT-dependent luciferase activity, demonstrating that NFATc1 activation was diminished. These data support the idea of Creld1 not only controlling calcineurin function in the cytosol, but also fulfilling a role in the nucleus by directly regulating the activity of NFATc1 as a transcription factor. But being a transmembrane protein at the ER, how can Creld1 exhibit a role in the nucleus? One possibility would be that a part of the protein, containing the EGF-like and cbEGF-like domains, is cleaved off and enters the nucleus through an import mechanism. Evidence for Creld1 being truncated was revealed by Western-blot analyses of protein lysates from adult tissues. Here, the Creld1-specific antibody recognized smaller proteins between 25 and 37 kDa in size. Whether these are indeed truncated variants of Creld1 protein has yet to be analyzed in the conditional *Creld1KO*, when embryonic lethality is circumvented by a tissue specific knockout. An additional way to determine the identity of these bands is by mass spectrometry.

Creld1 could also regulate NFATc1 activity in the nucleus, when it is localized in the nucleoplasmic reticulum (NR, Fig. 5-2). The NR is formed by a complex network of nuclear invaginations of the ER[100]. Here, Creld1 as an ER transmembrane protein could enter the nucleus through the nuclear pore, thereby promoting NFATc1 activity in the nucleus.

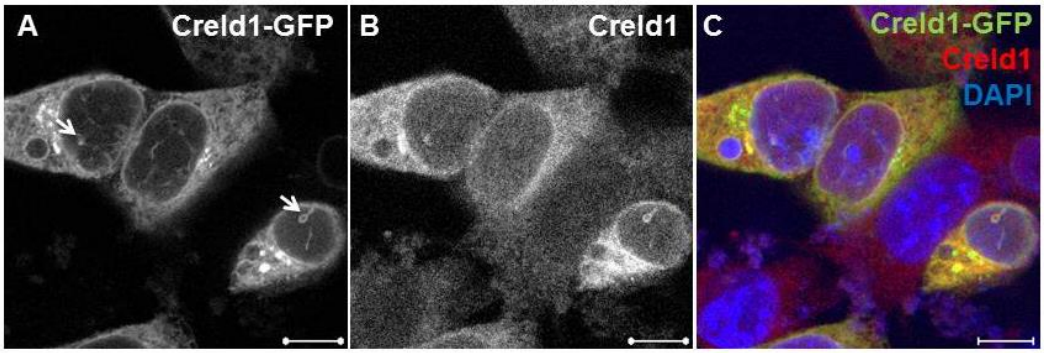

Fig. 5-2 Creld1 expression in the nucleoplasmic reticulum. Heterologous expression of Creld1-GFP in NIH3T3 cells (A) stained with a Creld1-specific antibody (B). Arrows indicate nuclear invaginations of the ER. Scale bar represents 10 µm.

5.1.5 The role of human CRELD1 in AVSD

The human *CRELD1* has been identified as a risk gene factor for atrioventricular septal defects (AVSD)[11,12], a prevalent heart disease, occurring in about 5 % of all recognized congenital heart diseases.

It has been proposed that *CRELD1* mutations predispose the human Down syndrome (DS) patients to AVSD[12,101,102]. Another gene that has been associated with AVSD in DS patients is the *RCAN1* gene, which is encoded on the human chromosome 21. During cardiac development, Rcan1 is also expressed in the endocardium of the developing heart valves and its expression is dependent on NFATc1 function[69]. The DS patients contain three copies of chromosome 21, which increases the levels of *RCAN1* up to 1.5-fold. In line with this finding, in a murine DS model, augmented Rcan1 expression reduces calcineurin activity, and thereby impairs activation of NFATc1[103].
The phenotype observed in our *Creld1KO* mouse model supports the idea of *CRELD1* contributing to the dysfunction of NFATc1 in DS patients, who are more susceptible to AVSD if the CRELD1 function is impaired.

Indeed, mutations that have been identified in the human *CRELD1* locus diminish the action of Creld1 on calcineurin/NFATc1 signaling. Beside the mutation in the WE domain (R107H), one other mutation in the cbEGF-like domain (R329C) caused a decrease of NFATc1 translocation and activity. This mutation probably results in a misfolded protein, because it affects the formation of the characteristic disulfide bonds of the cbEGF-like domain[11].

Although a major impact of the other mutations on calcineurin/NFATc1 signaling *in vitro* could not be observed, it cannot be excluded that they affect NFATc1 activity *in vivo*. Creld1 undergoes posttranslational modifications, such as phosphorylation, and N- and O-glycosylation (not shown). Moreover, cbEGF-like domains contain amino acids that need to be β-hydroxylated and fucosylated for proper Ca^{2+} binding[104]. However, none of the mutated amino acids is predicted to be modified in the Creld1 protein. It is most likely that the mutations lead to an allosteric change of the Creld1 protein structure, which hinders activation by an upstream stimulus. In case of the calcineurin/NFATc1 signaling pathway, this stimulus could be VEGF[66]. VEGF binding could e.g. promote phosphorylation of Creld1 and only then Creld1 would be activated. *In*

vivo, NFATc1 activation would be affected by a lack of Creld1 activation. In cell culture, however, this effect is probably overcome by an excess of Creld1 protein when heterologously expressed.

In order to analyze the effects of Creld1 mutations on heart development in more detail *in vivo,* knock-in mouse models could be generated, containing individual mutations that are found in AVSD patients. This will allow elucidating, why mutations in *CRELD1* increase the risk of developing heart defects.

5.1.6 Creld1 – part of other signaling pathways?

Creld1KO mice die at E11.5, two to three days earlier than mice with endocardial-specific deletion of calcineurin[32] or NFATc1[88], which die between E13.5-14.5. As Creld1 is also expressed in the myocardium, it might have additional functions, which could explain the earlier lethality. From E9.0 on, the formation of the AVC is initialized by NFATc2/3/4 in the myocardium, where they are activated by calcineurin[17]. Thus, Creld1 could also regulate calcineurin function in the myocardium, thereby controlling activity of NFATc2/3/4. However, preliminary data suggest that Creld1 predominantly controls the function of NFATc1 and to a barely low extent the function of NFATc2 (personal communication with D. Wachten). Moreover, EMT and the migration of mesenchymal cells requried to form the AVC is unaffected in *Creld1KO* embryos, indicating that calcineurin/NFATc2/3/4 signaling is not controlled by Creld1. Thus, it would be of great interest to analyze a myocardium-specific conditional knockout of *Creld1* to investigate its function in this tissue.

Taken together, this study identifies Creld1 as a new regulator of calcineurin/NFATc1 signaling using *in vivo* and *in vitro* analyses, providing a new key player in heart-valve formation.

5.2 Creld2 is a new key player of the UPR

Analysis of *Creld2KO* mice suggests that Creld2 expression is not only induced upon ER stress, but that it belongs to one of the three axes of the UPR. Its molecular function is probably important to maintain or restore healthy cell homeostasis under or after stress conditions. This idea is supported by my results, showing that only the aging as an additive effect on the mutant background led to liver steatosis in *Creld2KO* animals.

This resembles the phenotype of Atf6α knockout mutants. They show no phenotype under unchallenged conditions. But when they are injected with the ER-stress inducing agent tunicamycin (Tm), the animals display persistent ER stress in liver and kidneys[105]. To support this hypothesis, young *Creld2KO* could be stimulated with Tm in order to induce ER stress. If the resulting phenotype would be similar to *Atf6α*-null mice, it would support the idea of Creld2 playing are role during UPR.

This model is further supported by the fact that Creld2 overexpression is sufficient to induce the transcription of *Gadd34* and *Chop*. These are genes known to be induced during UPR by Perk activation[40], suggesting an activation of Perk through Creld2. The augmented splicing of Xbp1 upon increased Creld2 protein-levels indicates that Ire1 is also activated by Creld2.

Upon enhanced Creld2 protein levels, there is no increase of *Grp78* expression, which is the marker for broad ER stress. Therefore, the effects on *Gadd34* and *Chop* expression are not due to a Creld2-protein overload of the ER, but they are Creld2 dependent. Moreover, *Atf6α* expression remains unaffected upon high Creld2 levels, underlining a selective regulation of a subset of UPR gene expression by Creld2.

It is noteworthy that Creld2 has been shown to possess an ER-stress response element (ERSE) in its promoter, which is the recognition sequence for Atf6α[9]. This *in vitro* study supports the idea of Creld2 being a downstream target of Atf6α, which then induces the activity of both the Perk and Ire1 pathways. Creld2 could be a ‘cross-link’ between the three axes of the UPR, enabling the additive activation of Perk and Ire1 in an Atf6α-dependent manner. The

following data support this model: after injection of Tm, the Perk-dependent phosphorylation of eIF2α remains as under unstressed conditions in Atf6α-null animals[105]. Therefore, there should be signaling events in the Atf6α axis that promote activation of Perk. Creld2 could be one of these signaling proteins. To strengthen this hypothesis, it would be necessary to perform stress-inducing experiments with *Creld2KO* animals and analyze the phosphorylation status of eIF2α and splicing of Xbp1 in the liver.

Taking the expression data into account, Creld2 is most likely expressed in all cells, at least at a very low level. Only during an UPR, cells might increase Creld2 expression via Atf6α. Highly secretory cells of organs such as the pancreas and salivary gland are known to undergo permanent ER stress[106]. The ER protein load is quite high in these cells during secretion, which is why they depend on UPR. Other cells that undergo large fluctuations in ER protein load are cells of the immune system[39]. Here, Creld2 is also highly expressed, hinting to a rather universal function during UPR. Hence, Creld2 could maintain chronic ER stress in cells that need a high ER capacity, without resulting in a maladaptive response and apoptosis[43]. In line with this hypothesis, only prolonged heterologous expression of Creld2 over more than 24 hours induced the expression of *Chop*, *Gadd34*, and sXbp1.

Interestingly, all analyzed *Creld2KO* cells of the spleen and thymus had the same or even lower intensity of the GFP signal as the heterozygous animals. These results hint towards a tissue-specific enhancer within the ORF of Creld2. Possibly, regulating elements such as non-coding RNA (ncRNA) are located in the introns, which, however are replaced by GFP in the knockout mouse. Thus, analysis of the enhancer elements located not only in the promoter region, but also in the ORF should be taken into account when planning the generation of a conditional *Creld2KO* mouse line.

Certainly, further analyses are needed to investigate Creld2 function during ER stress. A good model for that would be the induction of ER stress in *Creld2KO* animals and also usage of *Creld2KO* mouse embryonic fibroblasts (MEFs) as a model system. Moreover, with this *in vitro* tool at hand, the impact of Creld2 secretion[10] could be analyzed. It would be important to know under what conditions cells would take up Creld2, which can be easily analyzed with

Creld2KO MEFs.

Taken together, Creld2 is a promising candidate for playing a key role in the UPR.

6 Summary

In my thesis, I investigated the physiological function of the two members that belong to the murine Cysteine-rich with EGF-like domain (Creld) family: Creld1 and Creld2.

Using Creld1 knockout-mice (*Creld1KO*), Creld1 was identified as an important regulator of the calcineurin/nuclear factor of activated T-cells c1 (NFATc1) signaling pathway during heart valve formation. *Creld1KO* embryos die at embryonic day E11.5 due to cardiac dysfunction. At E10.5, *Creld1KO* embryos display defects in the formation of the atrioventricular cushion, the precursor of the heart valve. Heart-valve formation crucially relies on the calcineurin/NFATc1 signaling cascade. My results showed that in the *Creld1KO* endocardium, from where the heart valves originate, nuclear translocation of NFATc1 is impaired. This results in a decrease of NFATc1 target-gene expression thereby, proliferation within the atrioventricular cushions is impaired. I could demonstrate that Creld1 directly interacts with calcineurin B, the regulatory subunit of calcineurin, thus controlling NFATc1 translocation to the nucleus. In a heterologous system, expression of Creld1 is sufficient to endorse NFATc1 translocation to the nucleus. Sequential deletion of the different functional domains or the introduction of various point mutations indicate that the conserved WE domain of Creld1 is important for regulating the calcineurin phosphatase activity.

To analyze the physiological function of Creld2, Creld2 knockout-mice (*Creld2KO*) were generated. Young *Creld2KO* mice do not show any gross phenotype. However, one year old animals show indications of liver steatosis. A gene-expression study of liver tissue indicates that regulators of the lipid metabolism, especially the β-oxidation, are downregulated in *Creld2KO* mice. This resembles the phenotype shown by activating transcription factor 6 (Atf6) knockout mice, which have been exposed to chronic ER stress. Creld2 expression is upregulated upon ER stress, which is known to be possible via Atf6. My results indicate that Creld2 plays an essential role during ER-stress conditions. Thereby, *Creld2KO* liver cells cannot cope with the given ER stress over time, resulting in liver steatosis.

7 References

1. Rupp, P. A. *et al.* Identification, genomic organization and mRNA expression of CRELD1, the founding member of a unique family of matricellular proteins. *Gene* **293,** 47–57 (2002).

2. Davis, C. G. The many faces of epidermal growth factor repeats. *The New biologist* **2,** 410–9 (1990).

3. Ley, K. The role of selectins in inflammation and disease. *Trends in Molecular Medicine* **9,** 263–268 (2003).

4. Kansas, G. S. *et al.* A role for the epidermal growth factor-like domain of P-selectin in ligand recognition and cell adhesion. *The Journal of cell biology* **124,** 609–18 (1994).

5. Phan, U. T., Waldron, T. T. & Springer, T. A. Remodeling of the lectin-EGF-like domain interface in P- and L-selectin increases adhesiveness and shear resistance under hydrodynamic force. *Nature immunology* **7,** 883–9 (2006).

6. Zhou, T. *et al.* Anti-P-selectin lectin-EGF domain monoclonal antibody inhibits the maturation of human immature dendritic cells. *Experimental and molecular pathology* **80,** 171–6 (2006).

7. Yáñez, M., Gil-Longo, J. & Campos-Toimil, M. Calcium binding proteins. *Advances in experimental medicine and biology* **740,** 461–82 (2012).

8. Ortiz, J. A. *et al.* The cysteine-rich with EGF-like domains 2 (CRELD2) protein interacts with the large cytoplasmic domain of human neuronal nicotinic acetylcholine receptor alpha4 and beta2 subunits. *Journal of neurochemistry* **95,** 1585–96 (2005).

9. Oh-hashi, K. *et al.* CRELD2 is a novel endoplasmic reticulum stress-inducible gene. *Biochemical and biophysical research communications* **387,** 504–10 (2009).

10. Oh-hashi, K., Kunieda, R., Hirata, Y. & Kiuchi, K. Biosynthesis and secretion of mouse cysteine-rich with EGF-like domains 2. *FEBS letters* **585,** 2481–7 (2011).

11. Robinson, S. W. *et al.* Missense mutations in CRELD1 are associated with cardiac atrioventricular septal defects. *American journal of human genetics* **72,** 1047–52 (2003).

12. Maslen, C. L. *et al.* CRELD1 mutations contribute to the occurrence of cardiac atrioventricular septal defects in Down syndrome. *American journal of medical genetics. Part A* **140,** 2501–5 (2006).

13. Sarkozy, A. *et al.* CRELD1 and GATA4 gene analysis in patients with nonsyndromic atrioventricular canal defects. *American journal of medical genetics. Part A* **139,** 236–8 (2005).

14. Zatyka, M. *et al.* Analysis of CRELD1 as a candidate 3p25 atrioventicular septal defect locus (AVSD2). *Clinical genetics* **67,** 526–8 (2005).

15. Posch, M. G. *et al.* Mutations in GATA4, NKX2.5, CRELD1, and BMP4 are infrequently found in patients with congenital cardiac septal defects. *American journal of medical genetics. Part A* **146A,** 251–3 (2008).

16. Zhian, S., Belmont, J. & Maslen, C. L. Specific association of missense mutations in CRELD1 with cardiac atrioventricular septal defects in heterotaxy syndrome. *American journal of medical genetics. Part A* **158A,** 2047–9 (2012).

17. Armstrong, E. J. & Bischoff, J. Heart valve development: endothelial cell signaling and differentiation. *Circulation research* **95,** 459–70 (2004).

18. Aanhaanen, W. T. J., Moorman, A. F. M. & Christoffels, V. M. Origin and development of the atrioventricular myocardial lineage: insight into the development of accessory pathways. *Birth defects research. Part A, Clinical and molecular teratology* **91,** 565–77 (2011).

19. Person, A. D., Klewer, S. E. & Runyan, R. B. Cell biology of cardiac cushion development. *International review of cytology* **243,** 287–335 (2005).

20. Barnett, J. V & Desgrosellier, J. S. Early events in valvulogenesis: a signaling perspective. *Birth defects research. Part C, Embryo today : reviews* **69,** 58–72 (2003).

21. Butcher, J. T. & Markwald, R. R. Valvulogenesis: the moving target. *Philosophical transactions of the Royal Society of London. Series B, Biological sciences* **362,** 1489–503 (2007).

22. De la Cruz, M. V *et al.* Living morphogenesis of the ventricles and congenital pathology of their component parts. *Cardiology in the young* **11,** 588–600 (2001).

23. Gittenberger-de Groot, A. C., Bartelings, M. M., Deruiter, M. C. & Poelmann, R. E. Basics of cardiac development for the understanding of congenital heart malformations. *Pediatric research* **57,** 169–76 (2005).

24. Schroeder, J. A., Jackson, L. F., Lee, D. C. & Camenisch, T. D. Form and function of developing heart valves: coordination by extracellular matrix and growth factor signaling. *Journal of molecular medicine (Berlin, Germany)* **81,** 392–403 (2003).

25. Wagner, M. & Siddiqui, M. A. Q. Signal transduction in early heart development (II): ventricular chamber specification, trabeculation, and heart valve formation. *Experimental biology and medicine (Maywood, N.J.)* **232,** 866–80 (2007).

26. Crabtree, G. R. & Olson, E. N. NFAT signaling: choreographing the social lives of cells. *Cell* **109 Suppl,** S67–79 (2002).

27. Klee, C. B., Ren, H. & Wang, X. Regulation of the calmodulin-stimulated protein phosphatase, calcineurin. *The Journal of biological chemistry* **273,** 13367–70 (1998).

28. Beals, C. R., Clipstone, N. A., Ho, S. N. & Crabtree, G. R. Nuclear localization of NF-ATc by a calcineurin-dependent, cyclosporin-sensitive intramolecular interaction. *Genes & development* **11,** 824–34 (1997).

29. Flanagan, W. M., Corthésy, B., Bram, R. J. & Crabtree, G. R. Nuclear association of a T-cell transcription factor blocked by FK-506 and cyclosporin A. *Nature* **352,** 803–7 (1991).

30. Crabtree, G. R. Contingent genetic regulatory events in T lymphocyte activation. *Science (New York, N.Y.)* **243,** 355–61 (1989).

31. Lambrechts, D. & Carmeliet, P. Sculpting heart valves with NFATc and VEGF. *Cell* **118,** 532–4 (2004).

32. Chang, C.-P. *et al.* A field of myocardial-endocardial NFAT signaling underlies heart valve morphogenesis. *Cell* **118,** 649–63 (2004).

33. Dor, Y. *et al.* A novel role for VEGF in endocardial cushion formation and its potential contribution to congenital heart defects. *Development (Cambridge, England)* **128,** 1531–8 (2001).

34. Yang, J. *et al.* Independent Signals Control Expression of the Calcineurin Inhibitory Proteins MCIP1 and MCIP2 in Striated Muscles. *Circulation Research* **87,** e61–e68 (2000).

35. Lin, C.-J., Lin, C.-Y., Chen, C.-H., Zhou, B. & Chang, C.-P. Partitioning the heart: mechanisms of cardiac septation and valve development. *Development (Cambridge, England)* **139,** 3277–99 (2012).

36. Martínez-Martínez, S. *et al.* Blockade of NFAT activation by the second calcineurin binding site. *The Journal of biological chemistry* **281,** 6227–35 (2006).

37. Mehta, S., Li, H., Hogan, P. G. & Cunningham, K. W. Domain architecture of the regulators of calcineurin (RCANs) and identification of a divergent RCAN in yeast. *Molecular and cellular biology* **29,** 2777–93 (2009).

38. Oh-Hashi, K. *et al.* Role of an ER stress response element in regulating the bidirectional promoter of the mouse CRELD2 - ALG12 gene pair. *BMC genomics* **11,** 664 (2010).

39. Todd, D. J., Lee, A.-H. & Glimcher, L. H. The endoplasmic reticulum stress response in immunity and autoimmunity. *Nature reviews. Immunology* **8,** 663–74 (2008).

40. Walter, P. & Ron, D. The unfolded protein response: from stress pathway to homeostatic regulation. *Science (New York, N.Y.)* **334,** 1081–6 (2011).

41. Zhao, L. & Ackerman, S. L. Endoplasmic reticulum stress in health and disease. *Current opinion in cell biology* **18,** 444–52 (2006).

42. Ron, D. & Walter, P. Signal integration in the endoplasmic reticulum unfolded protein response. *Nature reviews. Molecular cell biology* **8,** 519–29 (2007).

43. Szegezdi, E., Logue, S. E., Gorman, A. M. & Samali, A. Mediators of endoplasmic reticulum stress-induced apoptosis. *EMBO reports* **7,** 880–5 (2006).

44. Bertolotti, A., Zhang, Y., Hendershot, L. M., Harding, H. P. & Ron, D. Dynamic interaction of BiP and ER stress transducers in the unfolded-protein response. *Nature cell biology* **2,** 326–32 (2000).

45. Harding, H. P., Zhang, Y. & Ron, D. Protein translation and folding are coupled by an endoplasmic-reticulum-resident kinase. *Nature* **397,** 271–4 (1999).

46. Shi, Y. *et al.* Identification and characterization of pancreatic eukaryotic initiation factor 2 alpha-subunit kinase, PEK, involved in translational control. *Molecular and cellular biology* **18,** 7499–509 (1998).

47. Harding, H. P. *et al.* Regulated translation initiation controls stress-induced gene expression in mammalian cells. *Molecular cell* **6,** 1099–108 (2000).

48. Novoa, I., Zeng, H., Harding, H. P. & Ron, D. Feedback inhibition of the unfolded protein response by GADD34-mediated dephosphorylation of eIF2alpha. *The Journal of cell biology* **153,** 1011–22 (2001).

49. Marciniak, S. J. *et al.* CHOP induces death by promoting protein synthesis and oxidation in the stressed endoplasmic reticulum. *Genes & development* **18,** 3066–77 (2004).

50. Haze, K., Yoshida, H., Yanagi, H., Yura, T. & Mori, K. Mammalian transcription factor ATF6 is synthesized as a transmembrane protein and activated by proteolysis in response to endoplasmic reticulum stress. *Molecular biology of the cell* **10,** 3787–99 (1999).

51. Chen, X., Shen, J. & Prywes, R. The luminal domain of ATF6 senses endoplasmic reticulum (ER) stress and causes translocation of ATF6 from the ER to the Golgi. *The Journal of biological chemistry* **277,** 13045–52 (2002).

52. Ye, J. *et al.* ER stress induces cleavage of membrane-bound ATF6 by the same proteases that process SREBPs. *Molecular cell* **6,** 1355–64 (2000).

53. Yoshida, H., Haze, K., Yanagi, H., Yura, T. & Mori, K. Identification of the cis-acting endoplasmic reticulum stress response element responsible for transcriptional induction of mammalian glucose-regulated proteins. Involvement of basic leucine zipper transcription factors. *The Journal of biological chemistry* **273,** 33741–9 (1998).

54. Okada, T., Yoshida, H., Akazawa, R., Negishi, M. & Mori, K. Distinct roles of activating transcription factor 6 (ATF6) and double-stranded RNA-activated protein kinase-like endoplasmic reticulum kinase (PERK) in transcription during the mammalian unfolded protein response. *The Biochemical journal* **366,** 585–94 (2002).

55. Wang, X. Z. *et al.* Cloning of mammalian Ire1 reveals diversity in the ER stress responses. *The EMBO journal* **17,** 5708–17 (1998).

56. Tirasophon, W., Lee, K., Callaghan, B., Welihinda, A. & Kaufman, R. J. The endoribonuclease activity of mammalian IRE1 autoregulates its mRNA and is required for the unfolded protein response. *Genes & development* **14,** 2725–36 (2000).

57. Yoshida, H., Matsui, T., Yamamoto, A., Okada, T. & Mori, K. XBP1 mRNA is induced by ATF6 and spliced by IRE1 in response to ER stress to produce a highly active transcription factor. *Cell* **107,** 881–91 (2001).

58. Lee, A.-H., Iwakoshi, N. N. & Glimcher, L. H. XBP-1 regulates a subset of endoplasmic reticulum resident chaperone genes in the unfolded protein response. *Molecular and cellular biology* **23,** 7448–59 (2003).

59. Lorenz, H., Hailey, D. W., Wunder, C. & Lippincott-Schwartz, J. The fluorescence protease protection (FPP) assay to determine protein localization and membrane topology. *Nature protocols* **1,** 276–9 (2006).

60. Clipstone, N. A. & Crabtree, G. R. Identification of calcineurin as a key signalling enzyme in T-lymphocyte activation. *Nature* **357,** 695–7 (1992).

61. Xiong, Y., Zhou, B. & Chang, C.-P. Analysis of the endocardial-to-mesenchymal transformation of heart valve development by collagen gel culture assay. *Methods in molecular biology (Clifton, N.J.)* **843,** 101–9 (2012).

62. Lorenz, H., Hailey, D. W. & Lippincott-Schwartz, J. Fluorescence protease protection of GFP chimeras to reveal protein topology and subcellular localization. *Nature methods* **3,** 205–10 (2006).

63. Keith, B., Johnson, R. S. & Simon, M. C. HIF1α and HIF2α: sibling rivalry in hypoxic tumour growth and progression. *Nature reviews. Cancer* **12,** 9–22 (2012).

64. Lincoln, J., Alfieri, C. M. & Yutzey, K. E. Development of heart valve leaflets and supporting apparatus in chicken and mouse embryos. *Developmental dynamics : an official publication of the American Association of Anatomists* **230,** 239–50 (2004).

65. Hinton, R. B. *et al.* Extracellular matrix remodeling and organization in developing and diseased aortic valves. *Circulation research* **98,** 1431–8 (2006).

66. Combs, M. D. & Yutzey, K. E. Heart valve development: regulatory networks in development and disease. *Circulation research* **105,** 408–21 (2009).

67. De la Pompa, J. L. *et al.* Role of the NF-ATc transcription factor in morphogenesis of cardiac valves and septum. *Nature* **392,** 182–6 (1998).

68. Ranger, A. M. *et al.* The transcription factor NF-ATc is essential for cardiac valve formation. *Nature* **392,** 186–90 (1998).

69. Lange, A. W., Molkentin, J. D. & Yutzey, K. E. DSCR1 gene expression is dependent on NFATc1 during cardiac valve formation and colocalizes with anomalous organ development in trisomy 16 mice. *Developmental biology* **266,** 346–60 (2004).

70. Crabtree, G. R. & Schreiber, S. L. SnapShot: Ca2+-calcineurin-NFAT signaling. *Cell* **138,** 210, 210.e1 (2009).

71. Rao, A., Luo, C. & Hogan, P. G. Transcription factors of the NFAT family: regulation and function. *Annual review of immunology* **15,** 707–47 (1997).

72. Hogan, P. G., Chen, L., Nardone, J. & Rao, A. Transcriptional regulation by calcium, calcineurin, and NFAT. *Genes & development* **17,** 2205–32 (2003).

73. Giot, L. *et al.* A protein interaction map of Drosophila melanogaster. *Science (New York, N.Y.)* **302,** 1727–36 (2003).

74. Guo, Y. *et al.* Novel CRELD1 gene mutations in patients with atrioventricular septal defect. *World journal of pediatrics : WJP* **6,** 348–52 (2010).

75. Kusuma, L. *et al.* A maiden report on CRELD1 single-nucleotide polymorphism association in congenital heart disease patients of Mysore, South India. *Genetic testing and molecular biomarkers* **15,** 483–7

76. Bradbury, M. W. Lipid metabolism and liver inflammation. I. Hepatic fatty acid uptake: possible role in steatosis. *American journal of physiology. Gastrointestinal and liver physiology* **290,** G194–8 (2006).

77. Reddy, J. K. & Rao, M. S. Lipid metabolism and liver inflammation. II. Fatty liver disease and fatty acid oxidation. *American journal of physiology. Gastrointestinal and liver physiology* **290,** G852–8 (2006).

78. Duval, C., Müller, M. & Kersten, S. PPARalpha and dyslipidemia. *Biochimica et biophysica acta* **1771,** 961–71 (2007).

79. Giguère, V. Transcriptional control of energy homeostasis by the estrogen-related receptors. *Endocrine reviews* **29,** 677–96 (2008).

80. Rakhshandehroo, M. *et al.* Comprehensive analysis of PPARalpha-dependent regulation of hepatic lipid metabolism by expression profiling. *PPAR research* **2007,** 26839 (2007).

81. Guzmán, C. *et al.* The human liver fatty acid binding protein (FABP1) gene is activated by FOXA1 and PPARα; and repressed by C/EBPα: Implications in FABP1 down-regulation in nonalcoholic fatty liver disease. *Biochimica et biophysica acta* **1831,** 803–18 (2013).

82. Jakobsson, A., Westerberg, R. & Jacobsson, A. Fatty acid elongases in mammals: their regulation and roles in metabolism. *Progress in lipid research* **45,** 237–49 (2006).

83. Peeters, A. & Baes, M. Role of PPARα in Hepatic Carbohydrate Metabolism. *PPAR Research* **2010,** (2010).

84. Hetz, C. The unfolded protein response: controlling cell fate decisions under ER stress and beyond. *Nature reviews. Molecular cell biology* **13,** 89–102 (2012).

85. Rivera-Feliciano, J. *et al.* Development of heart valves requires Gata4 expression in endothelial-derived cells. *Development (Cambridge, England)* **133,** 3607–18 (2006).

86. Moskowitz, I. P. *et al.* Transcription factor genes Smad4 and Gata4 cooperatively regulate cardiac valve development. [corrected]. *Proceedings of the National Academy of Sciences of the United States of America* **108,** 4006–11 (2011).

87. Tian, Y. *et al.* Characterization and in vivo pharmacological rescue of a Wnt2-Gata6 pathway required for cardiac inflow tract development. *Developmental cell* **18,** 275–87 (2010).

88. Wu, B. *et al.* Nfatc1 coordinates valve endocardial cell lineage development required for heart valve formation. *Circulation research* **109,** 183–92 (2011).

89. Liberatore, C. M. & Yutzey, K. E. Calcineurin signaling in avian cardiovascular development. *Developmental dynamics : an official publication of the American Association of Anatomists* **229,** 300–11 (2004).

90. Li, H., Rao, A. & Hogan, P. G. Interaction of calcineurin with substrates and targeting proteins. *Trends in cell biology* **21,** 91–103 (2011).

91. Vega, R. B., Yang, J., Rothermel, B. A., Bassel-Duby, R. & Williams, R. S. Multiple domains of MCIP1 contribute to inhibition of calcineurin activity. *The Journal of biological chemistry* **277,** 30401–7 (2002).

92. Chan, B., Greenan, G., McKeon, F. & Ellenberger, T. Identification of a peptide fragment of DSCR1 that competitively inhibits calcineurin activity in vitro and in vivo. *Proceedings of the National Academy of Sciences of the United States of America* **102,** 13075–80 (2005).

93. Rusnak, F. & Mertz, P. Calcineurin: form and function. *Physiological reviews* **80,** 1483–521 (2000).

94. Higazi, D. R. *et al.* Endothelin-1-stimulated InsP3-induced Ca2+ release is a nexus for hypertrophic signaling in cardiac myocytes. *Molecular cell* **33,** 472–82 (2009).

95. Shin, D. W. *et al.* Ca(2+)-dependent interaction between FKBP12 and calcineurin regulates activity of the Ca(2+) release channel in skeletal muscle. *Biophysical journal* **83,** 2539–49 (2002).

96. Sanna, B. *et al.* Modulatory calcineurin-interacting proteins 1 and 2 function as calcineurin facilitators in vivo. *Proceedings of the National Academy of Sciences of the United States of America* **103,** 7327–32 (2006).

97. Liu, Q., Busby, J. C. & Molkentin, J. D. Interaction between TAK1-TAB1-TAB2 and RCAN1-calcineurin defines a signalling nodal control point. *Nature cell biology* **11,** 154–61 (2009).

98. Martínez-Høyer, S. *et al.* Protein kinase CK2-dependent phosphorylation of the human Regulators of Calcineurin reveals a novel mechanism regulating the calcineurin-NFATc signaling pathway. *Biochimica et biophysica acta* **1833,** 2311–21 (2013).

99. Shin, S.-Y., Yang, H. W., Kim, J.-R., Heo, W. Do & Cho, K.-H. A hidden incoherent switch regulates RCAN1 in the calcineurin-NFAT signaling network. *Journal of cell science* **124,** 82–90 (2011).

100. Malhas, A., Goulbourne, C. & Vaux, D. J. The nucleoplasmic reticulum: form and function. *Trends in cell biology* **21,** 362–73 (2011).

101. Li, H. *et al.* Genetic modifiers predisposing to congenital heart disease in the sensitized Down syndrome population. *Circulation. Cardiovascular genetics* **5,** 301–8 (2012).

102. Ghosh, P. *et al.* Polymorphic haplotypes of CRELD1 differentially predispose Down syndrome and euploids individuals to atrioventricular septal defect. *American journal of medical genetics. Part A* **158A,** 2843–8 (2012).

103. Arron, J. R. *et al.* NFAT dysregulation by increased dosage of DSCR1 and DYRK1A on chromosome 21. *Nature* **441,** 595–600 (2006).

104. Wouters, M. A. *et al.* Evolution of distinct EGF domains with specific functions. *Protein science : a publication of the Protein Society* **14,** 1091–103 (2005).

105. Wu, J. *et al.* ATF6alpha optimizes long-term endoplasmic reticulum function to protect cells from chronic stress. *Developmental cell* **13,** 351–64 (2007).

106. Marciniak, S. J. & Ron, D. Endoplasmic reticulum stress signaling in disease. *Physiological reviews* **86,** 1133–49 (2006).

107. High, F. A. & Epstein, J. A. The multifaceted role of Notch in cardiac development and disease. *Nature reviews. Genetics* **9,** 49–61 (2008).